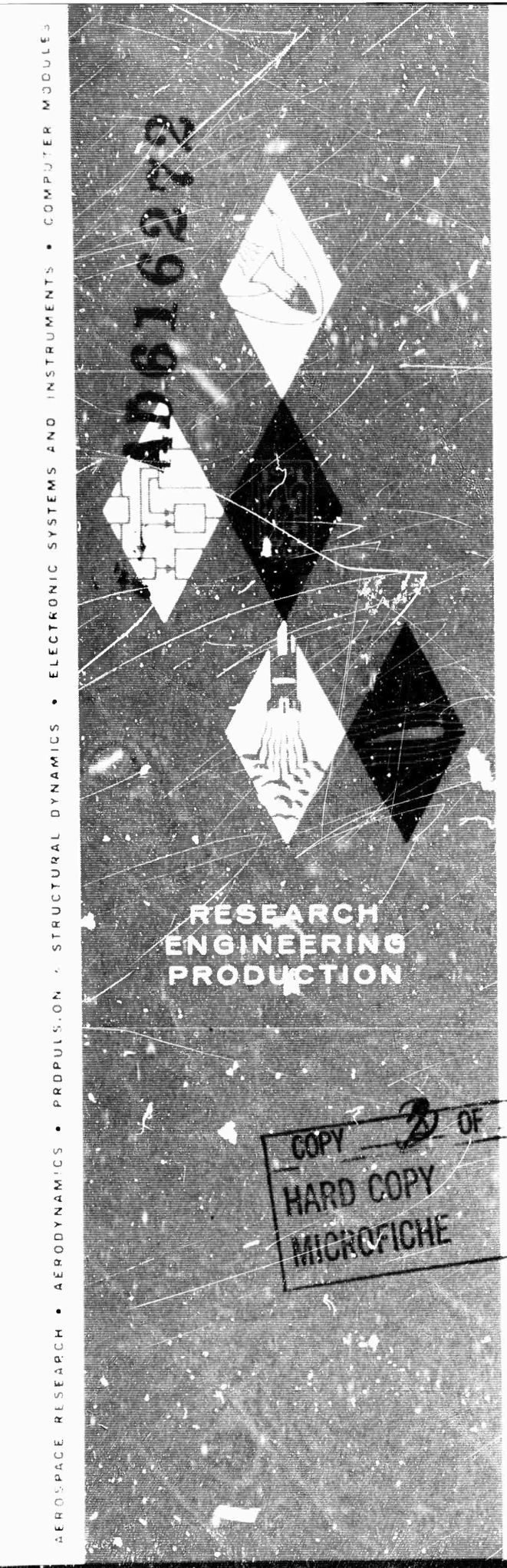

TECHNICAL REPORT NO. 519

ELECTROMAGNETIC STUDIES IN SHOCK PRODUCED PLASMAS

(FINAL REPORT)

By R. Tomboulian

April 15, 1965

GENERAL APPLIED SCIENCE LABORATORIES, INC.
MERRICK and STEWART AVENUES, WESTBURY, L.I., N.Y. · (516) ED 3-6960

Project 5246

Total No. of Pages - vi & 174

Copy No. 106 of 380

TECHNICAL REPORT NO. 519

ELECTROMAGNETIC STUDIES IN SHOCK PRODUCED PLASMAS*

(FINAL REPORT)

By R. Tomboulian

Prepared for

Advanced Research Projects Agency
Department of Defense
Washington, D.C.

ARPA ORDER No. 207-62
Project Code No. 4740
Project Scientist:
Dr. Manlio Abele
516-333-6960
516-694-5500

Contract No. Nonr-3475(00)
Date of Contract 4/1/61
Contract Expiration Date 3/14/65

"Electromagnetic Properties of Non-uniform Plasmas"

Prepared by

General Applied Science Laboratories, Inc.
Merrick and Stewart Avenues
Westbury, L. I., New York

April 15, 1965

Approved by: _____
Antonio Ferri
President

*This work has been sponsored by the Advanced Research Projects Agency (Ballistic Missile Defense Office) and technically administered by the Fluid Dynamics Branch of the Office of Naval Research.

TABLE OF CONTENTS

TABLE OF CONTENTS (Continued)

LIST OF FIGURES

LIST OF FIGURES (Continued)

INDEX OF PUBLICATIONS AND PRESENTATIONS

TR
No.

255 Abele, M., Napolitano, L., Caldirola, P., Lane, F., Tomboulian, R., Wecker, M., Moretti, G., Studies of the Electromagnetic Characteristics of Moving Ionized Gases, First Semiannual Technical Summary Report, November 1961.

290 Wecker, M., Abele, M., Caldirola, P., Tomboulian, R., Napolitano, L., Medecki, H., Studies of the Electromagnetic Characteristics of Moving Ionized Gases, Second Semiannual Technical Summary Report, April 1962.

316 Gavril, B., Abele, M., Albertoni, S., Cercignani, C., Tomboulian, R., Medecki, H., Studies of the Electromagnetic Properties of Nonuniform Plasmas, Third Semiannual Technical Summary Report, October 1962.

348 Abele, M., Medecki, H., Tomagno, J., Tomboulian, R., Fourth Semiannual Technical Summary Report, Studies of Electromagnetic Properties of Nonuniform Plasmas, April 1963.

388 Abele, M., Medecki, H., Tomboulian, R., Electromagnetic Studies in Shock Produced Plasmas, Third Annual Report, April 1964.

Presentations at Meetings

Measurement of Electron Density Profiles, Using a Microwave Technique, Presented at the Fifth Shock Tube Symposium, Washington, D.C., April 1965.

Fast Acting Mechanical Valve to Replace Shock Tube Diaphragm, Presented at the American Physical Society Meeting, Washington, D.C., 1964.

Measurement of Electron Density Profiles, Using a Microwave Technique, Presented at the American Physical Society Meeting, Washington, D.C., 1963.

CHAPTER I

INTRODUCTION

This report represents a compilation of the important aspects of an analytical and experimental study concerned with non-uniform plasmas. The information presented in this report will not necessarily represent the chronological development of the experimentation, but rather a summary of the physical problem and the methods of solutions.

The experimental work was done using a shock tube to produce the plasma. A detailed description of the shock tube facility is presented in Chapter II. Of particular interest is a description of a mechanical valve which has been successfully used to replace the conventional driver and diaphragm sections of the shock tube. In addition a description is given of a thin film resistance gauge and amplifier circuit which has been found to be a useful trigger under a wide variety of conditions.

An integral part of the work performed on this contract has been the development of a spatially resolving electron density microwave diagnostic technique useful in a range of electron densities infrequently explored by other investigators. This technique permits accurate spatial resolution in plasma gradients

for electron densities, orders of magnitude below that possible, using a conventional microwave interferometer. After an initial calibration phase in which argon was the driven gas in the shock tube, this microwave technique has been used to measure electron densities and electron density profiles behind normal air shocks in the range of Mach number 8.5-11 and initial pressure conditions of ~ 1 mm Hg.

The microwave instrumentation for this technique is described in detail in Chapter III. The analytical formulation correlating the measured properties to ascertain the electron density is shown in Chapter IV. Included in this discussion are the details of a data processing program used to convert the raw data taken from the microwave instrumentation into a usable form for computation.

When the results of the measurements were compared with the values of electron densities predicted on the basis of the accepted semi-analytical rate chemistry program, an order of magnitude discrepancy was found. Specifically, the measurements indicate an electron density behind the shock which tends to the equilibrium value at a rate which is about an order of magnitude faster than the one predicted by the numerical calculations. Since the shock conditions where the measured

discrepancy exists are relevant to the 150,000 ft altitude range aerodynamic calculations, it was deemed pertinent to explore the reasons for the observed discrepancy. To this effect an extensive program of measurements was initiated with different gas compositions and the sources of errors in the measuring technique.

Chapter V presents a summary of the theoretical work conducted in conjunction with the experimental program. A brief description of the generalized properties of non-uniform plasmas is given and referenced to the detailed formulations. A section is presented where the diffusion effects in a non-uniform plasma are outlined quantitatively. On the basis of the diffusion calculation, the electromagnetic properties of the plasma contained in the shock tube where radial non-uniformity exists are discussed.

CHAPTER II

THE FACILITY

A-1 INTRODUCTION

The explicit purpose of the following detailed description of the GASL combined shock tube and waveguide facility is to enable other investigators to duplicate any or all parts of this highly successful experimental arrangement. Since it is the details rather than the basic principles that are time consuming in the fabrication of such a facility, great effort will be made to present all salient features.

A-2 BASIC SHOCK TUBE

In this experimental facility, the driven section of the shock tube is also used as a circular waveguide. Because of this duplicity, some precautions must be taken as to the choice of material, the surface finish, and the method of connecting tubing sections.

A compromise material for the tube is seamless stainless steel pipe. While this material is certainly not the best electrical conductor as would be desirable from the waveguide point of view, it offers the advantages of strength machinability, corrosion resistance and availability. The stock material used for the driven sections of the shock tube were commercially available, extra heavy, three-inch stainless steel pipe. This tube has a nominal inside diameter of 2.9" and outside diameter of 3.5".

Highly desirable from the waveguide aspect is that the tube's inner diameter be constant. For use as a shock tube, the inner surface should be smooth with no wall discontinuities at the tube section junctions. To satisfy these conditions, each ten foot length of pipe was reamed and honed by a specialist in this field. The resultant inside diameter for all four driven sections was measured to be 2.917" ± .001".

The problem of coupling the tube sections is summarized as follows: for use as a waveguide, good and complete electrical contact must be maintained at each junction, the sections should join with a minimum angle between their axes, discontinuities in the wall should be minimized, and the junction must be pressure and vacuum tight and mechanically strong. Also desirable is a connection that can be easily removed and reassembled, since the insertion of various test sections may be required at any junction. In addition, each section, should be able to be rotated and be locked independently. This requirement originates from the fact that the microwave radiation is polarized and both parallel and perpendicular measurements are sometimes desirable.

To satisfy these requirements, the coupling assembly shown in Fig. A-2.1 was devised. In this scheme, one end of each tube section is machined with a right hand thread and cylindrical surface concentric with the inner axis. On the other end of each section, a left hand thread, an identical cylindrical surface and a partical "O" ring groove are machined. This "O" ring forms the seal between sections, and is held in place by the inner surface of the coupling nut. These are relatively simple machining operations, and if done in the order stated,

concentricity and diametric tolerances are maintained without the usual distortion problems associated with weld type coupling structures.

Bronze is used for the coupling nut to prevent galling of the surfaces, and is available as standard unfinished bronze bearing stock. If the tolerances of the cylindrical surfaces are held to .002", the maximum angular deviation between sections, excluding bending, is approximately .1 degree. Great care and patience should be exercised in the assembly of tube sections in order to prevent bending.

This coupling arrangement satisfies all of the conditions previously mentioned. However, in order to assemble and disassemble the tubes, the downstream sections must be able to slide on their mounting pads. Since the reaction forces on the shock tube exert only axial stresses, there is no need to rigidly restrain the tube along its length, so long as the main reactionary forces are absorbed at the diaphragm location. Since this is not only feasible but desirable from the point of view of simple electrical isolation from ground, the supports for the driven section need carry only the compressional weight load of the tube. This being the case, no extensive foundations or structure are required. Since perfect alignment

of these supports to the accuracy dictated by the coupling is not practically attainable, an adjustable set of "vee" jaws can be mounted on simple "I" beam structures to support the entire driven tube. Such a set of jaws are shown in Fig. A-2.2.

These jaws allow independent adjustment of height and horizontal position. The vertical adjustment is achieved by rotating the central screw which has right and left hand threads operating through the respective threads in the "V" jaws. The vertical load on the jaws is transmitted directly to the mounting plate on which they slide. Horizontal adjustment is made by moving the angle bracket, containing the center slot guide bearing, in the range provided by the slots in the bracket. The jaws are finally clamped to the angle bracket which is also slotted in the horizontal direction. Satisfactory support is accomplished with two sets of jaws for each ten foot section of tube. With this basic mounting and coupling arrangement the entire driven tube can be assembled in one day with the help of a precision level, an inexpensive transit, suitable "vee" blocks which will fit on the cylindrically machined part of the tube section, and a little patience and luck.

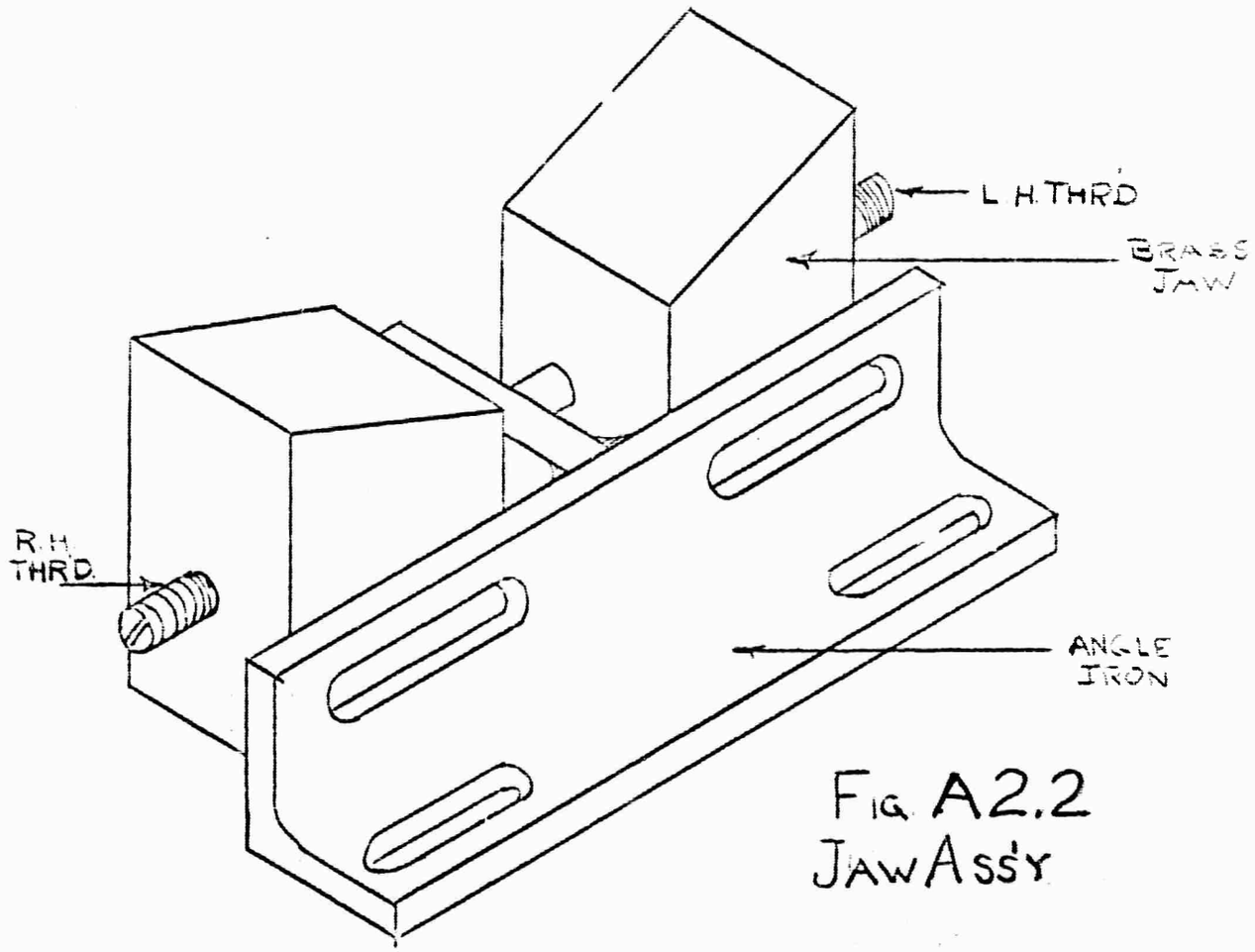

FIG. A2.2
JAW ASS'Y

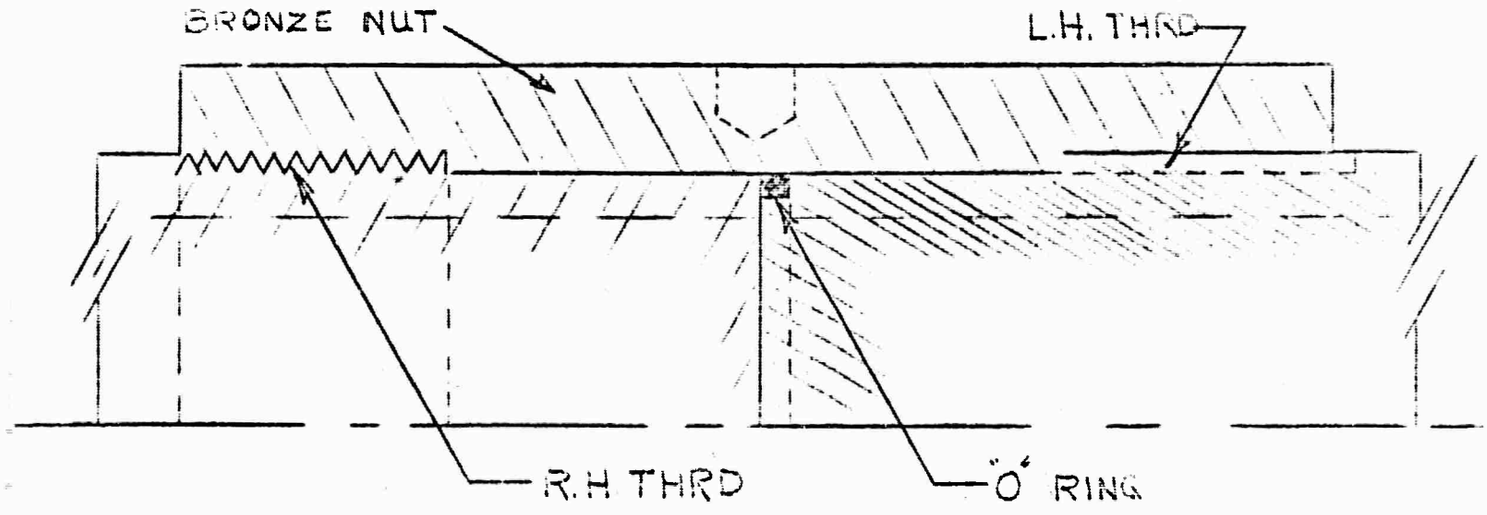

TYPICAL JOINT ASS'Y
FIG A2.1

A-3 FAST OPENING MECHANICAL VALVE

General Characteristics

This valve has been developed and constructed to replace the diaphragm in a small shock tube.

The conditions of operation are:

Driver pressure:	100 to 500 psi
Driver temperature:	up to 200°C
Opening area:	7 sq. inches
Seal:	vacuum tight

Additional conditions which should be satisfied are remote operation and minimum of adjustment or replacement of parts. The adopted solution has only one moving part, a piston, that provides two types of seal: an "O" ring seal for vacuum and a sleeve valve for fast action.

Sequence of Operations

This sequence is shown in Fig. A-3.1.

(a) The valve is closed. Pressure in chamber A is equal to pressure in chamber B (driver). The resulting force pushes the piston towards the seal.

(b) Venting: Pressure in chamber A goes down towards atmospheric; the driver pressure remains constant. The resulting force pushing the piston drops and then reverses.

(c) Vacuum seal opening: When the piston starts to move towards the left the force pushing it increases suddenly because the pressure starts acting over the surface between vacuum seal and sleeve seal.

(d) Fast opening: When the sleeve goes out of the driver chamber the gas starts to flow from driver to driven. The piston has been accelerated along a distance equal to the length of the sleeve.

(e) Stopping: The piston compresses the gas left in chamber A, stopping and oscillating around a position which is a function of the final pressure of the tube.

(f) Closing: After firing, the driver and driven are evacuated; the gas left in chamber A expands and closes the valve.

(g) Charging: The gas is fed first into chamber A, closing the valve if step (f) fails to do so, and then the gas goes into the driver through a check valve.

The two main facts to be considered in the action of the valve are:

FIG. A-3.1

SEQUENCE OF OPERATIONS OF THE FAST OPENING VALVE

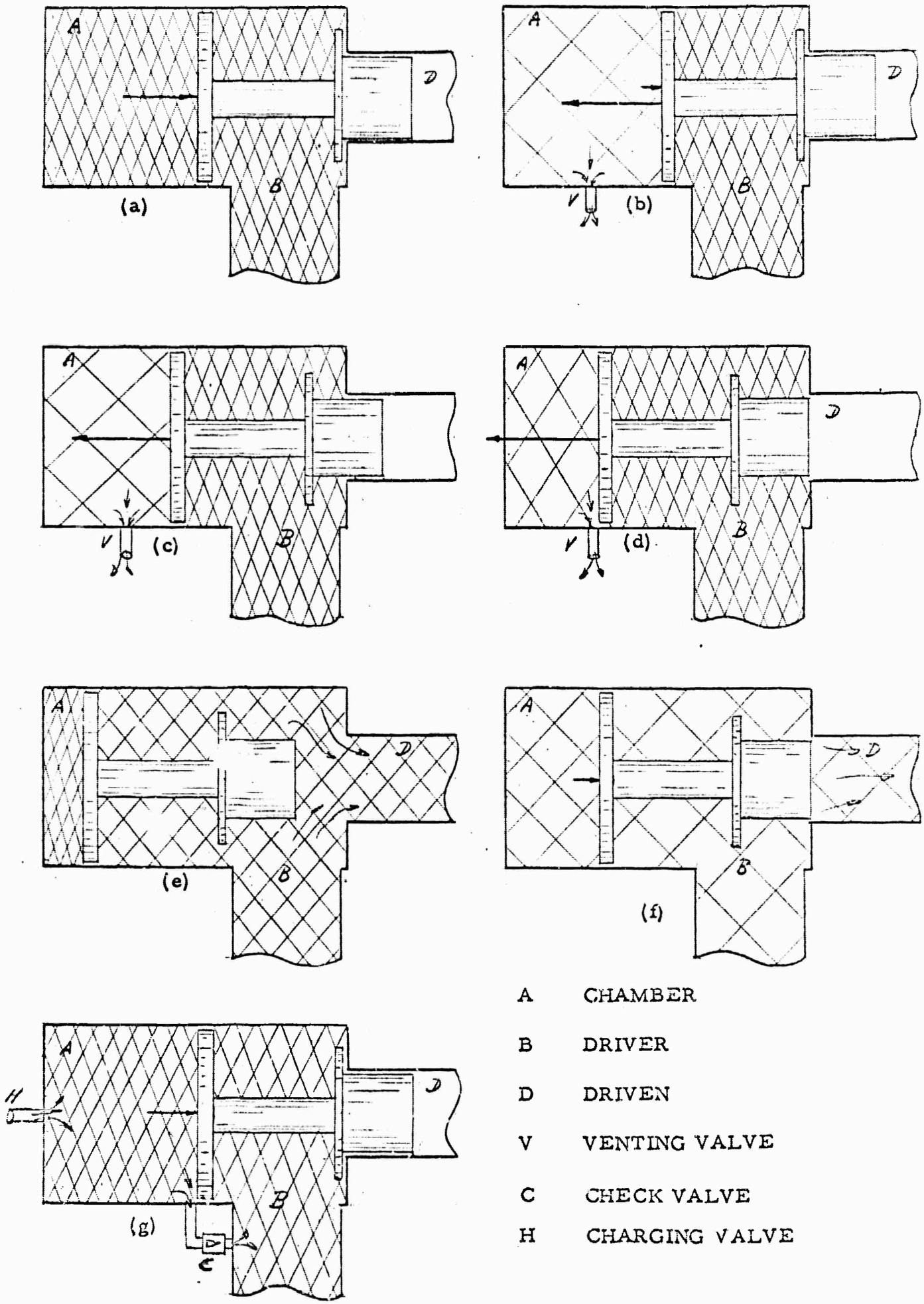

A	CHAMBER
B	DRIVER
D	DRIVEN
V	VENTING VALVE
C	CHECK VALVE
H	CHARGING VALVE

(1) The valve behaves as an unstable system near the firing pressure. The force pushing the piston jumps from zero to a maximum value in a very short time ($< 10^{-4}$ sec). This fast action cannot be obtained by controlling the flow of gas with conventional valves.

(2) The fast seal: Only after the piston receives its maximum velocity is the communication between driver and driven established. For a given acceleration of the piston the opening time goes down with the square root of the length of the sleeve.

The fast seal is not tight and the possible leakage between the opening of both seals establishes a compromise between length of sleeve, acceleration and quality of seal.

Computation of the Main Characteristics

The calculations are very easy if we disregard secondary effects.

The main parameters are:

S_A area of piston

S_B area of the vacuum tight seal

S_D transversal section of driven

P_A pressure in the chamber A

P_B pressure in the driver

W weight of the piston

e length of the sleeve

The pressure in the driven is, in normal working conditions, on the order of a few millimeters of mercury and we disregard it in the calculations. When charged it is $P_A = P_B$, and the force closing the seal is $F = P_B S_B$. The chamber A is vented towards atmospheric; P_B remains constant and P_A goes down reaching the firing pressure P_f corresponding to zero force acting on the piston; $P_f = P_B \left(1 - \frac{S_B}{S_A}\right)$; if P_f is equal to atmospheric pressure, the corresponding P_B is the minimum at which the valve can operate for a given ratio $\frac{S_B}{S_A}$.

When the piston starts to move, the force pushing it back jumps to $F_f = P_B(S_A - S_D) - P_A S_A$; because of the volume of the chamber A we can assume that $P_A = P_f$ during the fast seal opening of the valve, so $F_f = P_B(S_B - S_D)$. With this force we can compute the acceleration, velocity and opening time.

We consider that the valve is open when the passage area of the gas through the fast seal equals the transversal area of the driven.

The corresponding values for the valve in operation are:

P_f = 60 psi

P_B = 300 psi

S_A = 16 in^2

S_B = 13 in^2

S_D = 7 in^2

F_f = 1800 pounds

opening speed = 120 ft/sec

opening time = 300 microseconds

Figure A-3.2 presents the calculated shock Mach numbers as a function of the pressure ratio between driver and driven for air. This calculation assumes an infinitely fast opening diaphragm and no energy loss mechanisms occurring in the flow. Experimental points (+) have been superimposed on the plot indicating the behavior obtained using the mechanical valve. The agreement equals or exceeds that obtainable using a bursting diaphragm.

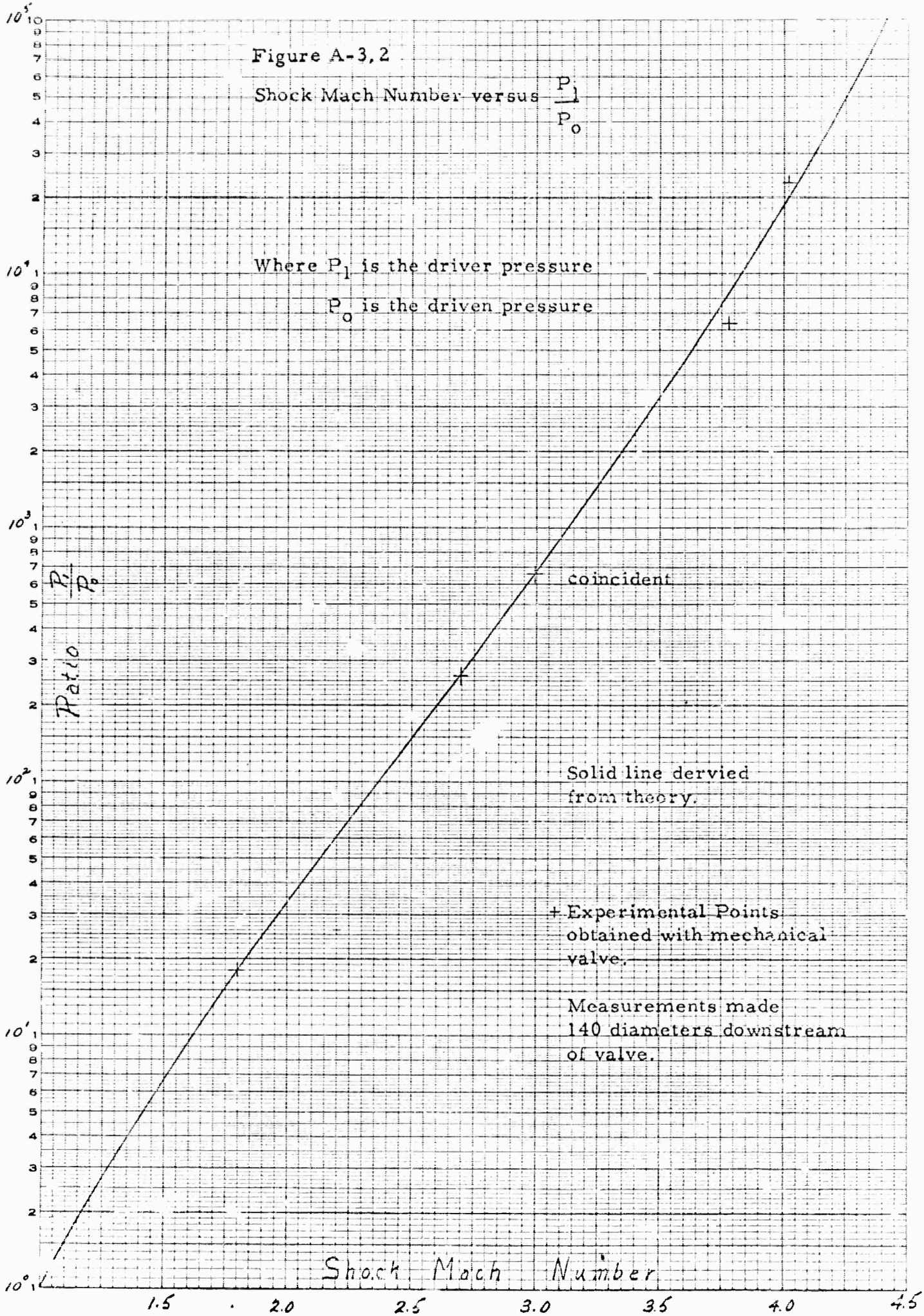
Figure A-3,2
Shock Mach Number versus $\frac{P_1}{P_o}$
Where P_1 is the driver pressure
P_o is the driven pressure
P_1/P_o Ratio
coincident
Solid line dervied from theory.
+ Experimental Points obtained with mechanical valve.
Measurements made 140 diameters downstream of valve.
Shock Mach Number
1.5
2.0
2.5
3.0
3.5
4.0
4.5

A-4 SHOCK TUBE PLUMBING

The governing factor in the engineering of the shock tube plumbing is safety. Since the driver gas normally used in the facility is hydrogen, the possibility of explosion either internally or externally due to a leak is omnipresent. While the basic tube is rated for over 1000 psi, the various detectors and fittings are in general not designed for these pressures. Hence, even a limited internal explosion is serious.

The replacing of the conventional diaphragm system with the mechanical valve has considerably reduced the hazards of operation. With the valve the use of the shock tube has become a closed operation. Since the tube need not be opened, the only air entering the system is introduced during the controlled filling cycle of the driven. This air charging can only be performed if the driver is not charged, the driven previously evacuated, and then the air charge cannot exceed one atmosphere. The driver cannot be filled until the pressure in the driven is again reduced below 50 mm Hg. Once the driver has been filled the only operation that can be performed is either "fire" or "purge". After firing, a pressure switch in the driven starts the purging cycle automatically, venting excess pressure over atmospheric to the atmosphere. Then the vacuum system is

opened and the tube evacuated. While it is possible to bypass these automatic operations to obtain unusual conditions, it is generally during the routine operation of such a system that a careless error is serious. Specific details of the plumbing system are not warranted here due to the fact that the use of the mechanical valve instead of a diaphragm has permitted additional simplifications. The basic system to be installed is outlined below.

The combined driver-mechanical valve as previously discussed need have only one solenoid type filling valve, and one small mechanical vacuum valve to be used only if the assembly is to be opened for cleaning or servicing. Another small solenoid valve may be used if the possibility of a high pressure dump is desired. The driven tube is equipped with two semi-automatic valves. The first is an over pressure valve which will seal vacuum but will open a two-inch port if the static pressure in the driven exceeds one atmosphere absolute. This valve mechanically interlocks to the vacuum valve so that if the over-pressure valve is open, the vacuum valve must be closed. The vacuum valve is pneumatically operated.

With this system a typical operating cycle would be as follows. The driven tube is pumped down by opening the pneumatic vacuum valve. The tube is filled with the desired test

gas which is limited in pressure by the over-pressure valve. The tube is now evacuated to the desired pressure. The driver is then filled. It may be noted that if the driver had been inadvertently filled and fired during any of the above operations all systems including the vacuum pump would have been protected by the over-pressure valve. When the firing sequence is started, a relay is locked so that the next pressure rise occurring in the driven will open the driven vacuum valve. After firing, if the pressure exceeds one atmosphere, the operation of the vacuum valve is blocked until a safe pressure in the driven is reached, after which the system will be evacuated leaving it in a safe condition and ready for the next test. For the above operation, it was assumed that the main mechanical valve operating in place of the diaphragm closed after firing. In the event that a malfunction occurs, no further operation of the shock tube is possible until the trouble is corrected, but neither are any safety problems present.

Two basic static pressure gauges have been found to be adequate in the system. To monitor the driver pressure a standard 250 psi Heiss gauge is used without valves or restricting orifices. An effective and accurate gauge for measurement of pre-firing pressure in the driven is the Alphatron gauge. This gauge (an old model) has three linear ranges, 0-100 microns.

0-1 mm Hg, and 0-10 mm Hg, with a zero shift raising the upper range to 20 mm Hg. Supplementing the Alphatron gauge is a standard thermocouple gauge with one probe in the driven tube and another monitoring the pressure at the vacuum pump. Neither gauge system is electrically damaged by operating at atmospheric pressure. So far, it has not been necessary to protect any gauge systems by isolation during firing. This is important from a safety standpoint, as well as an aid in avoiding possible readout errors.

A-5 VACUUM SYSTEM

A satisfactory range of initial pressures in the driven tube was deemed to be from 50 microns to 10 mm Hg. To avoid the additional complication of a diffusion pump, a high quality, high capacity mechanical pump is used. Though pumping speed is slow near ultimate pressure, this range is seldom used for decontaminating the tube during firing. With the tube clean enough to avoid excessive gassing in the operating pressure ranges, the simplest and quickest way to achieve a contamination-free test gas is by repeated filling with test gas and evacuating. For instance, with the tube at atmospheric and full of hydrogen after firing, only two or three minutes' pumping will evacuate it to .1 mm Hg. By refilling with test gas and evacuating to test pressure, remaining hydrogen contamination is approximately only one part in ten thousand.

With the addition of a liquid nitrogen trap, the gassing contaminants important at low pressures (including pump oil) are removed. However, if the trap is used, a bypass system should also be employed since when pumping at high pressures, severe and wasteful boiling occurs in the trap. With the system tight, pumping for twelve hours with only the mechanical pump will reduce the pressure to a few microns. Using the trap, one micron can be obtained in two hours.

A-6 INSTRUMENTATION

The instrumentation discussed below are those devices and recording instruments pertinent to the general operation of the shock tube. The microwave instrumentation is discussed in Section A.7. The specific problem under study requires a high degree of accuracy in all measuring and recording instruments. Three specific areas will be discussed; accurate location of the aerodynamic shock, measurement of dynamic pressures and recording of fast rise, small amplitude electrical signals.

Location of Shock Front

Accurate estimates of the equilibrium properties of the gas behind the incident shock can be made if the initial pressure and the shock velocity are known, the latter parameter being the most sensitive. Measurement of the shock velocity can be made by measuring the time interval between two points along the tube where an observable property associated with the shock front can be detected. The difficulty in this problem is the measurement of a property directly attributed to the shock front. Basically only three fundamental parameters are implicitly associated with the shock; a temperature change, a pressure change or a density change. Measurement of parameters induced, such as electron density and light radiation to locate

the shock front, assumes that these properties abruptly change across the front. This assumption is never strictly valid but may be satisfactory at high Mach numbers, when the use of ionization gauges or photomultipliers may be acceptable.

If it is desirable to detect the actual aerodynamic shock front, one of the fundamental property changes must be observed. A direct measurement of the density change can be made optically by measuring the deflection of a light beam. However, even for moderate strength shocks, this method is very delicate.

A direct measurement of pressure is possible except that the response time of the detector strongly limits the possible resolutions. That is, using a good quality crystal detector, a rise time of three microseconds is typical. If the shock velocity is on the order of 3 mm/μsec (~M9), the spatial resolution is about 1 cm. Assuming the rise time is consistent for two gauges and the shock pressure profile is constant during the interval of the measurement, a velocity measurement is possible with a spatial resolution of .5 cm. Hence, to measure velocity to 1%, the distance between gauges should be .5 meters. It is clear however that for the purpose of locating the shock as a method of correlating events, the gauges have limitations. In addition, if measurements are to be made over a wide range of

conditions, continual adjustment of sensitivity must be made. A more serious difficulty is the isolation of the gauge from the mechanical shock generated wher the diaphragm breaks (valve opens). If the mechanical shock reaches the gauge prior to the arrival to the aerodynamic shock, a spurious signal may render the measurement useless. A discussion of pressure gauges and measurements will be made in a following subsection.

Heat Transfer Gauges

A satisfactory solution to a detector for locating the shock front has been found to be a heat transfer gauge. The basic gauge is a thin film resistance thermometer element bonded to a glass slug. The gauge response is a function of not only the temperature, but also the density. This combined response allows the useful operation from M~4 to~14 in this facility. The gauge is fabricated by painting a thin strip of metallic silver coating less than 1 micron thick and 1 mm wide on a glass disk ¼ inch in diameter. This film is then baked, and connecting leads are fed through two holes in the glass disc and soldered to the film. The entire front surface is then given a thin coating of magnesium fluoride, which aids in preventing the collection of the charge diffused in front of the shock (Ref. 1). Unsatisfactory measurements are obtained without

the coating. In operation, a steady current of 10-50 ma is passed through the resistance element (thin film). The temperature change as the shock passes, creates a change in resistance which generates a change in voltage if the current is nearly constant.

An extremely simple method of generating an essentially constant current is to use a large voltage with a large series resistor to the gauge as shown in Fig. A-6.1. To be sure, this system is wasteful of power, but its simplicity over a suitable transistor stabilized constant current supply for each gauge is obvious.

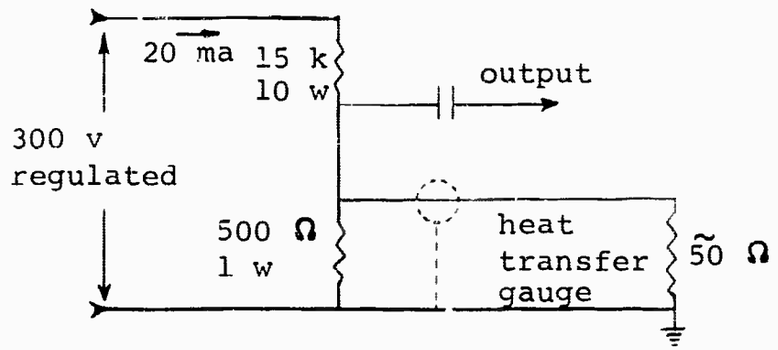

Fig. A-6.1. HTG Power Supply

To obtain a significant pulse (20 volts) from this circuit, very large amplification (20×10^3) of the voltage pulse must follow. If the fast response of the gauge is to be fully utilized, the amplifier should have a rise time of .3 μsec.

To make the gauge useful as a standard and reliable shock front detector the circuit shown in Fig. A-6.2 has been designed and built. The circuit is intended to generate a sharp pulse and no attempt is made to preserve the long term (10 μsec or more) variations occurring at the gauge. That is, all the time constants are made conveniently small. The grounded grid first stage utilizes the low impedance character of the gauge to simultaneously provided a very stable first amplifier and the required bias current for the gauge element. The following two stages of amplification are conventional RC pentode amplifiers utilizing an extremely high transconductance tube. The output cathode follower allows extended cabling without loss of response time which is typically .3 microsec. The combination of series condensers and the normally closed relay in the final output provides a simple method of avoiding spurious trigger signals which occur from the various switching operations performed in the firing sequence. Because of poor grounding practices in other nearby facilities, a common failing in many laboratories, minor power line noises generated by switching transients are amplified by the high gain amplifiers. To minimize this problem, the first step in the firing sequence disconnects all unnecessary ac components from the system (fans, heaters, pumps, etc).

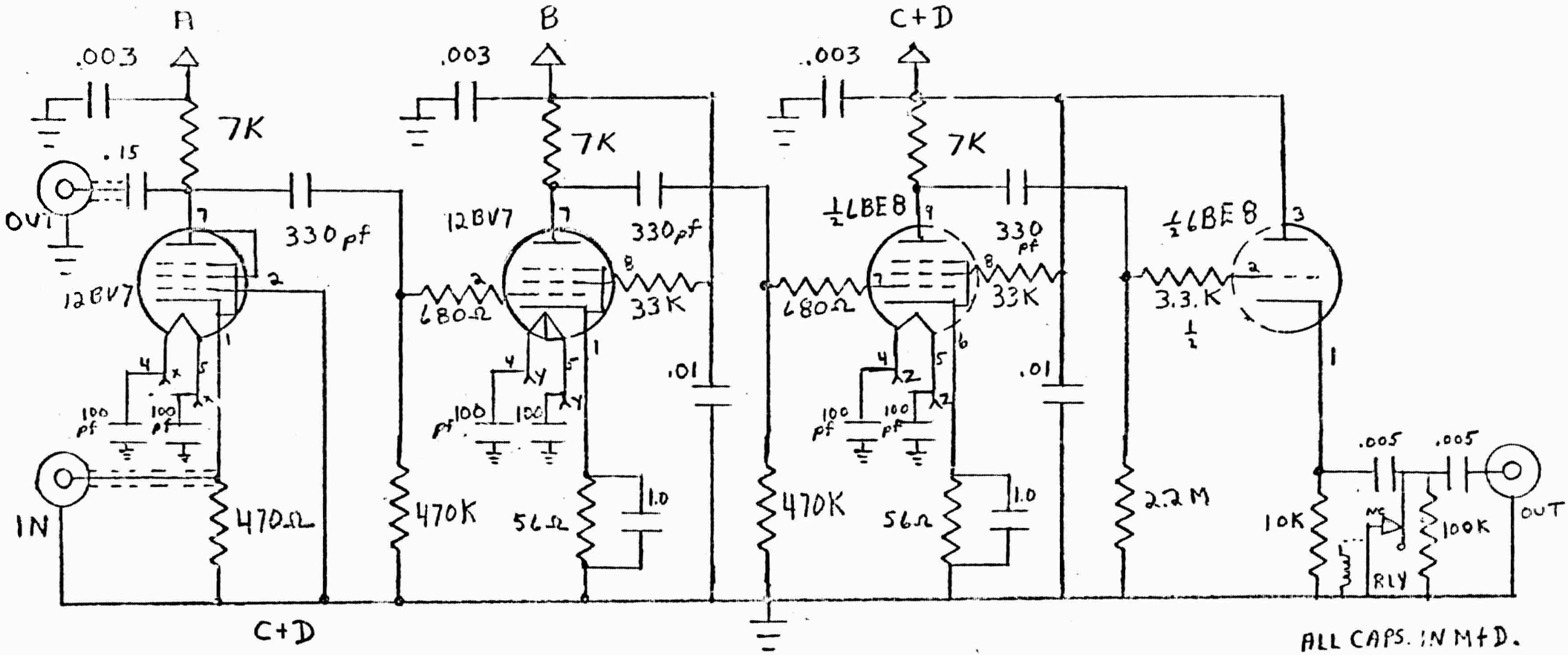
A
B
C+D
.003
7K
.15
OUT
330 pf
12BV7
680Ω
33K
.01
100 pf
470Ω
470K
56Ω
1.0
½6BE8
3.3K
2.2M
10K
100K
.005
RLY
IN
OUT
ALL CAPS. IN M+D.

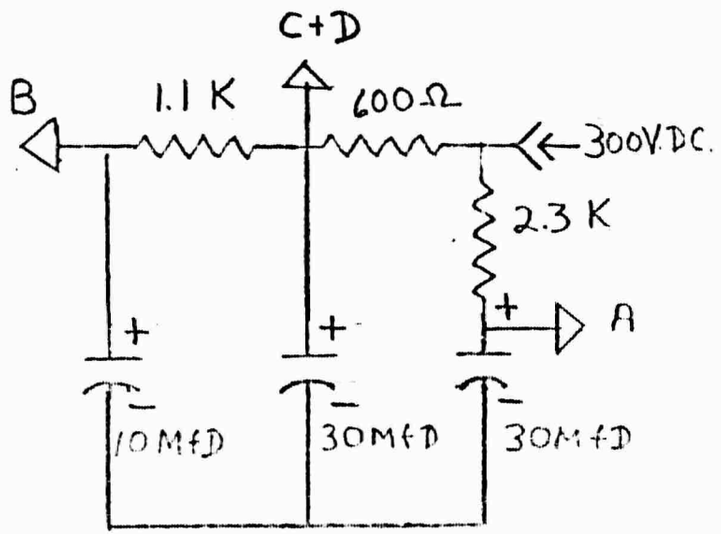
C+D
B
1.1K
600Ω
300V.DC.
2.3K
A
10MFD
30MFD
30MFD

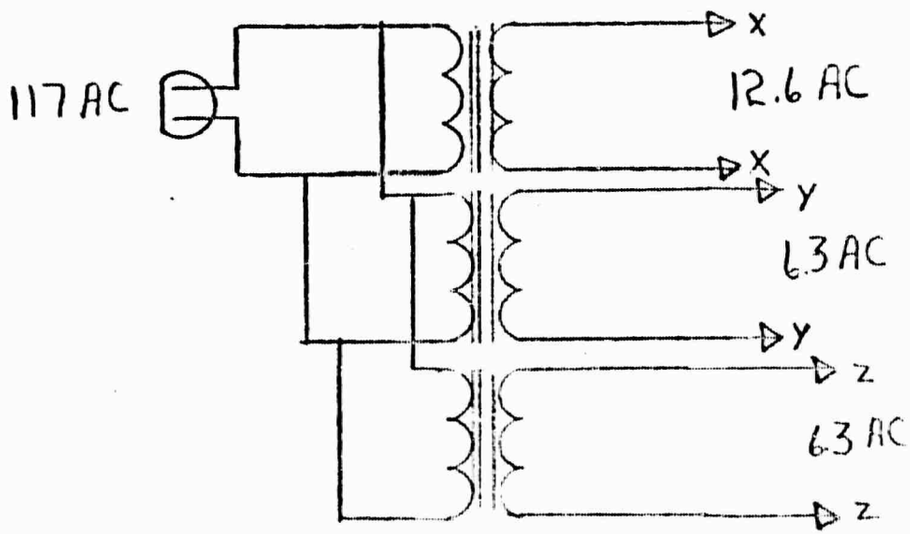
117 AC
X
12.6 AC
X
Y
6.3 AC
Y
Z
6.3 AC
Z

The first step also applies a dc voltage to the time delay circuit of the output relay which opens a few seconds later. This system is not a replacement for proper grounding procedures but rather an insurance to avoid 60 cycle pickup and line transients.

Care must be taken in the general circuit construction because of the high gain. The general circuit construction utilizes vector turret type sockets. Separate filament supplies are used as a precaution against high frequency oscillation. The separate transformers are practical if multiple units are to be constructed on the same chassis. For one amplifier unit one supply is probably adequate. The B+ supply can be unregulated with minor filtering. At 300 volts, the current consumption is about 70 ma per amplifier. No gain control is used since in general the purpose is to provide a fast, large trigger. For most of the shock conditions shown in Fig. B-4.5, the amplifier is saturated, thus generating a 60 volt, .2 μsec rise time pulse, independent of shock conditions.

With this heat transfer gauge and amplifier, spatial resolution of the location of the front is comparable to the actual discontinuity in physical parameters occurring across the shock. Typically, this resolution is 1 mm, indicating that for a shock velocity of 3 mm/μsec the required distance between

detectors in order to determine velocity to 1% is about 10 cm, assuming the timer can resolve .3 μsec or better.

Pressure Detectors

Measurement of pressures or pressure variations behind the shock is extremely difficult if accuracy and space resolution are required. The only suitable gauge elements for this purpose are piezoelectric crystals. The basic problem in the design of a gauge for shock tube use is that the requirements of high natural resonant frequencies and high sensitivities are contradictory. The second problem is the design of the crystal mounting in the gauge so that the output is insensitive to external stresses at right angles to the measured stress.

If one considers that the useful pressure information in the shock tube occurs for an interval of a few hundred microseconds, there is a partial elimination of the measuring problems if a gauge intended only for dynamic purposes is used.

A precision calibrated crystal microphone with a natural resonant frequency of about 200 kc is the Massa model M-213. This microphone has good sensitivity and directional resolution, and can withstand severe overloads. A typical pressure trace using this microphone is shown in Fig. A-6.3. A low pass filter of RC constant 20 μsec has been used to remove the initial ringing of the crystal, as shown in Fig. A-6.4.

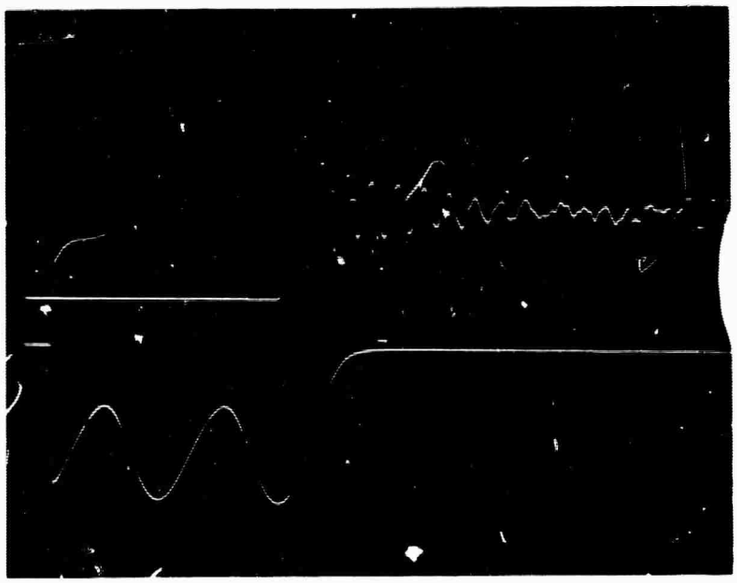

Upper Trace: Massa Microphone with no filtering - gain 15 db

5 volt/cm.

Lower Trace: Electric Field Detector - 50 mv/cm.

Sweep Time: 20 μs/cm.

Initial Pressure: 3 mm Hg - Air.

Shock Velocity: 3000 meters/sec.

Figure A-6.3

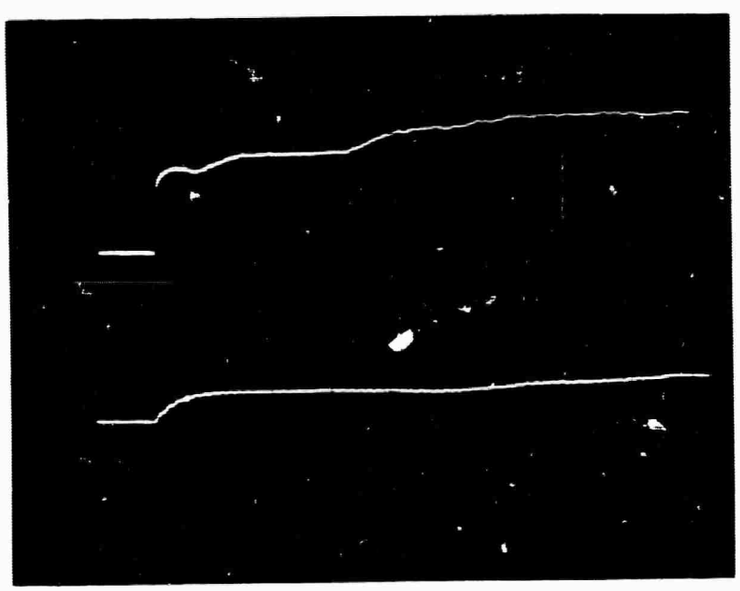

Upper Trace: Heat transfer gauge current 10 ma, 5 mv/cm.

Lower Trace: Massa Microphone with RC = 20 μs filter - gain 20 db

5 volts/cm.

Sweep Time: 50 μs/cm.

Initial Pressure: 2 mm Hg - N_2

Figure A-6.4

Shock Tube Instrumentation, Typical Traces

Since this crystal microphone is only us ul for dynamic pressure measurements, its calibration is difficult. In general the calibration supplied with the microphone is adequate. If doubtful, the microphone can be mounted in an inflated balloon, the pressure statically measured with respect to atmosphere, and the balloon punctured. The resultant step pressure change supplies a positive calibration point. Since the gauge and amplifier are relatively inexpensive, their use is strongly recommended if similar dynamic measurements are required.

A-7 MICROWAVE INSTRUMENTATION

Microwave Circuit

The circuit is as shown in Fig. A-7.1 includes a microwave signal generator (2-4 kmc, 60 mw), a coupling device delivering this signal to the shock tube, detectors of electric and magnetic fields, a recording system, consisting of oscilloscopes and photographic cameras, marker generators, wave shapers and delay generators. Sometimes a counter is used to measure the time between markers and consequently the speed of the shock.

The microwave signal generator is a reflex klystron with external tunable cavity. This klystron is powered by a power supply which has the possibility to change reflector, grid and beam voltage. The frequency stability of this generator was good enough for our purpose, but the measurements being made were particularly sensitive to changes in the amplitude of the signal. Normally the klystron is switched on and off and the maximum tolerated short term change in the power output should be below 2%. Among the various methods tested, the one using negative pulses in the grid together with a Zener-stabilized bias power supply was found to be the most convenient.

Fig. A-7.1 Microwave and recording circuit

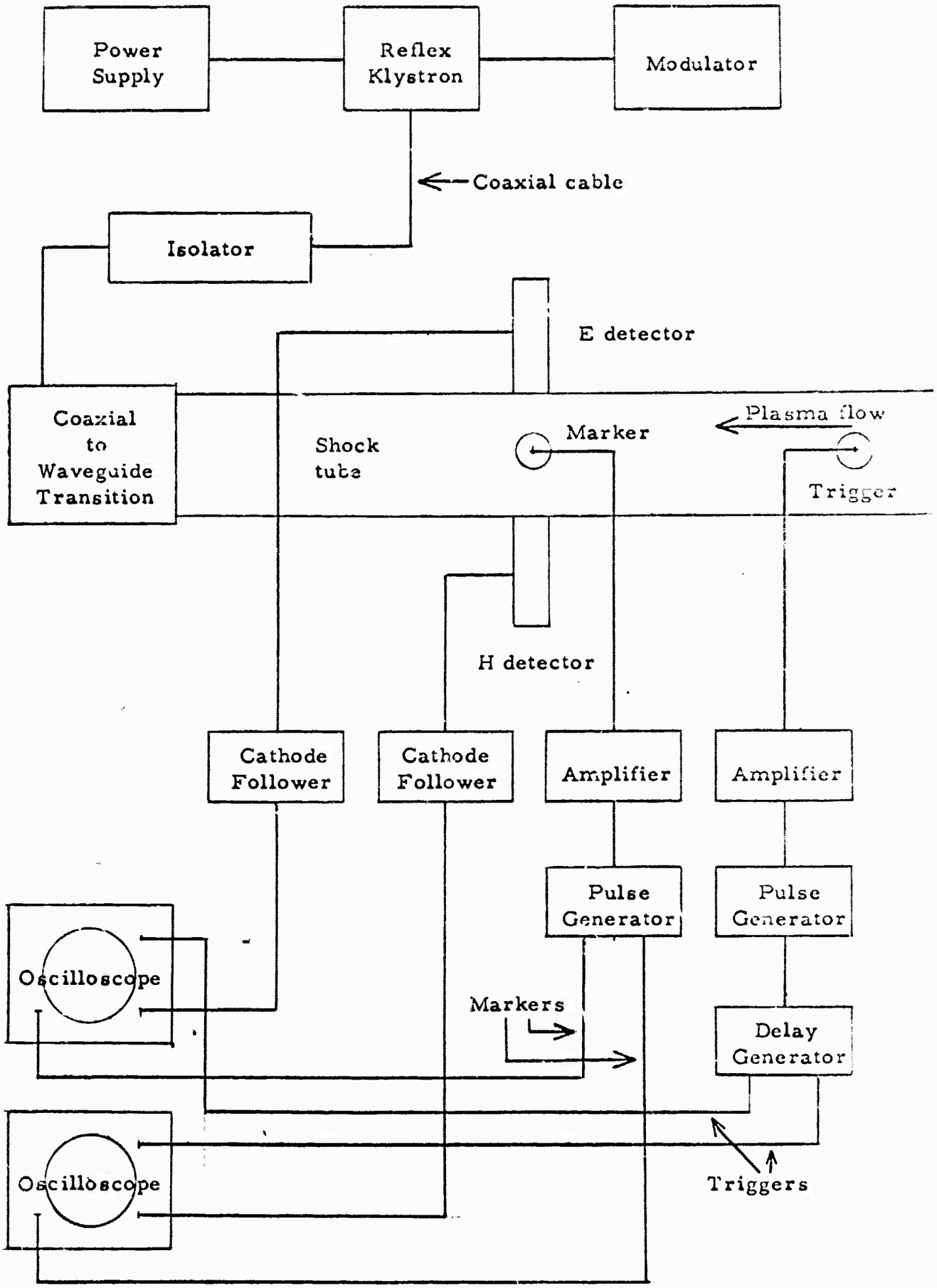

Coupling System

The output of the klystron is fed through an attenuator to a coaxial cable an isolator, and from this to the coaxial waveguide transition. The shock tube is equivalent to a circular waveguide operating in the TE_{11} mode. The coaxial to waveguide transition is shown in Fig. A-7.2. Matching is made by changing the penetration of the antenna and the position of the short circuit piston. The additional short circuit stub allows for adjustment of the bandwidth changing its length. The shock-tube must be vacuum tight, and this is achieved by using a phenolic tube around the antenna and a bellows on the piston.

Matching

The matching of the coaxial line to waveguide is very important. All the measurements are based on the fact that the amplitude of the microwave signal coupled into the shock tube is constant. This condition is difficult to obtain because the plasma produces a strong reflection; standing wave ratio of twenty is not unusual. This reflected signal must be absorbed without reflection in the isolator. If reflections take place, they superimpose on the incoming signal with a phase that changes as the plasma moves. This effect is equivalent to a fluctuation of the input signal. The standing wave pattern

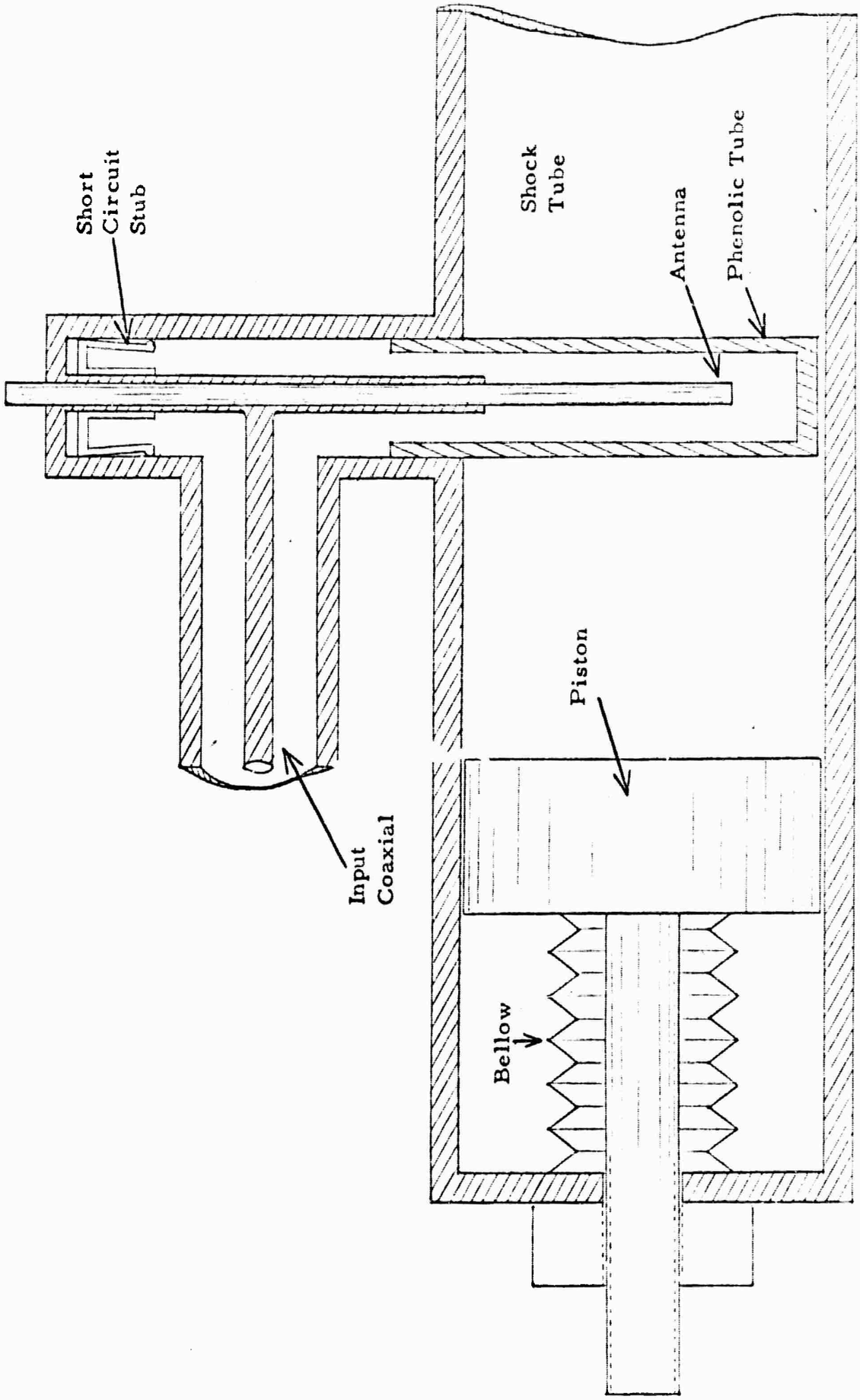

Fig. A-7.2 Coaxial to Waveguide Transition

then becomes a function of the position of the plasma or reflecting surface which is undesired.

Electromagnetic detectors mounted on the waveguide surface pick up the sum of both standing wave and fluctuation patterns both having the same periodicity. A detector moving with the reflecting surface picks up the fluctuation only. The phase between the two patterns may take any value: if it is coincident with one, for instance E, the output from this detector will give a higher standing wave ratio than the output from the other. If the phase angle between the two patterns has any value the resultant pattern is not symmetric. In the computation of the plasma properties it is assumed that the electromagnetic energy is perfectly coupled to the waveguide, hence perfect symmetry must be obtained to utilize the measurement.

Several methods have been used to get the desired matching but the only one accurate and simple enough is the following. A short circuit piston is displaced along the shock tube, simulating a strong reflecting plasma. Moving with the piston is a detector picking up the magnetic field near the wall where it is maximum. The output from this detector gives the fluctuation produced by the mismatch only. Successive adjustments of the antenna to waveguide transition are made attempting to

eliminate this fluctuation, thus giving a constant output when the piston moves.

In order to reduce the frequency sensitivity of the antenna, the signal from the generator is altered slightly. The antenna short circuit stub is then adjusted until a minimum change occurs in the output of the piston detector during this frequency change.

The limit of this system of matching comes mainly from incomplete contact between piston and wall. A typical value of the fluctuation after the matching has been performed is 2%, but this corresponds to a smaller value when the plasma is reflecting the signal because of the significantly better reflecting properties of the metallic piston.

Detectors

The electromagnetic wave propagated inside the tube has a wavelength λ_g which is a function of the frequency, mode of propagation and diameter of the tube. Some of the radiating energy is reflected from the plasma and the ratio of reflected to incident power is a function of electron density, collision frequency and profile of the plasma. The combination of incident and reflected waves combines to form a system of standing waves along the tube. This pattern has a period of $\frac{\lambda_g}{2}$. When

the plasma moves the pattern also moves with the same speed, provided the properties of the plasma remain constant.

A device detecting the electromagnetic field and located in a fixed position detects a signal whose amplitude goes from a maximum value equal to the sum of incident and reflected fields to a minimum equal to the difference between these two. For a plasma velocity v this fluctuation has a frequency $f_m = \frac{2v}{\lambda_g}$.

Two types of detectors have been used, one for the electric and the other for the magnetic field amplitude, as shown in Fig. A-7.3. The electric field detector is located in the region where it takes its maximum value, picking up the component parallel to the antenna and using a small, flush mounted surface in order to avoid introducing anything inside the shock tube which would disturb the flow. This surface is connected to a coaxial resonant circuit that matches impedances to the crystal detector and short circuits the currents produced by the flow of charges from the plasma to the tube walls. The magnetic field detector is a slot excited by the current flowing in the wall. Because of the relation between magnetic field and current this slot is equivalent to a loop located in a plane perpendicular to the slot. The field to be checked is the transversal component of H. The slot should be oriented in a transverse section of

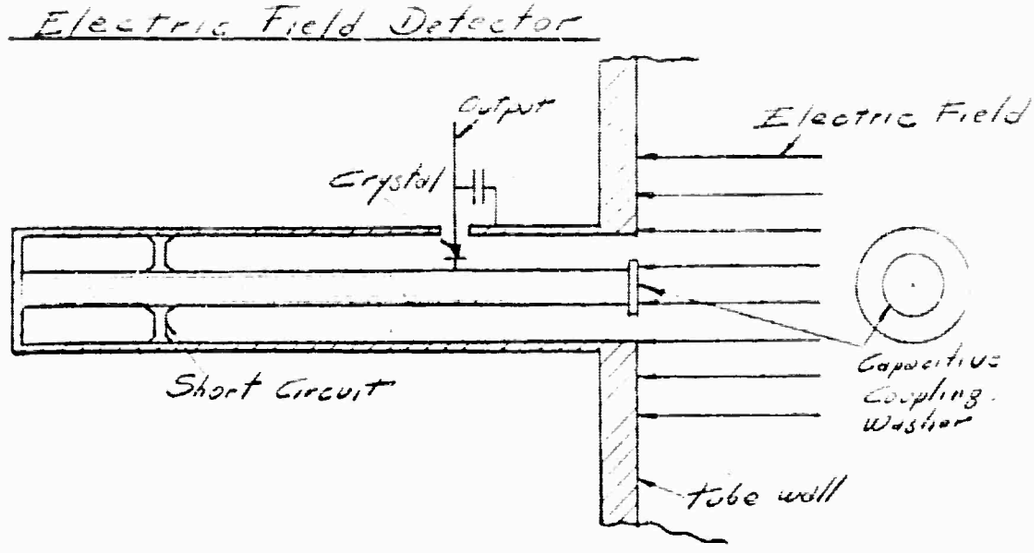

Figure A-7.3 (a)

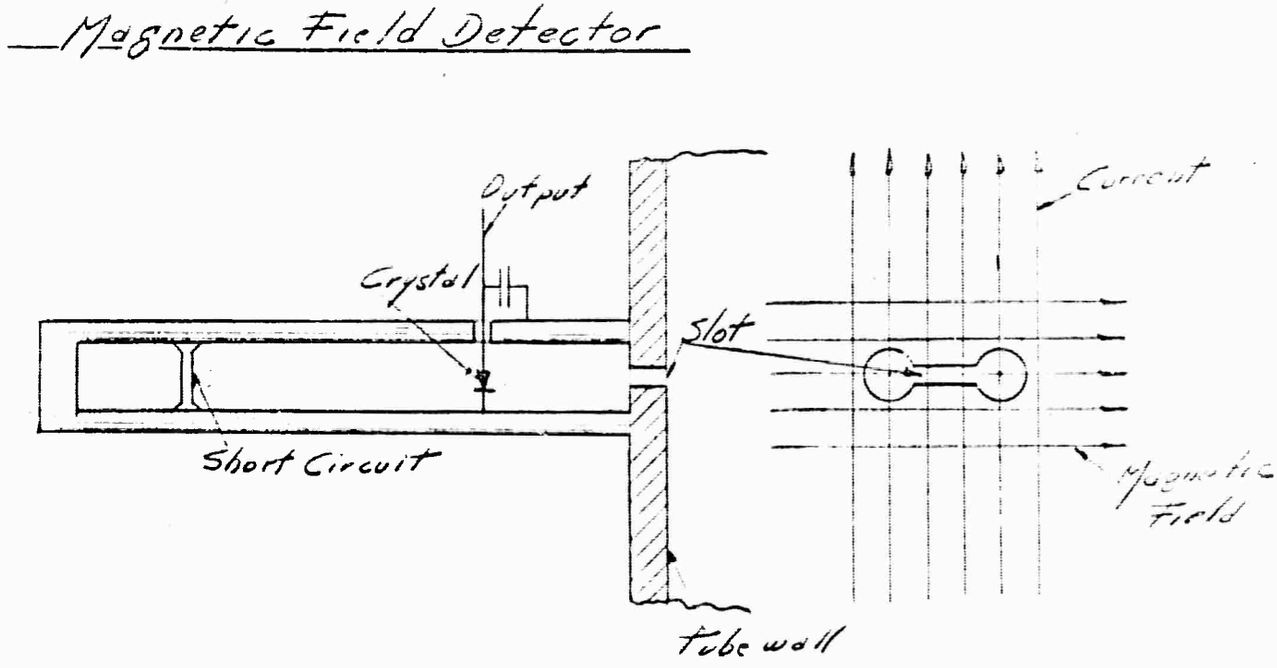

Figure A-7.3 (b)

MICROWAVE DETECTORS

the tube and at the point where the electric field is maximum. The signal induced in the slot is coupled to a two line resonant circuit and to a crystal detector.

For both E and H crystal detectors an output is obtained which is related to the amplitude of the respective field. The characteristics of the crystals cannot be considered linear nor quadratic and the required accuracy demands a calibration. The time response of the detectors is less than 10^{-7} sec if their output is directly connected to cathode followers. For simplicity's sake, ac amplifiers are used exclusively hence the dc level is not present. However switching off the klystron gives this zero level reference, permitting the absolute amplitude determination from the single trace. The markers are equally spaced at known intervals providing a timing reference and a means of compensating for nonlinearities in the sweep.

To perform the calculation of the plasma properties the electric and magnetic fields should be determined in the same transversal section of the tube. A special section has been constructed allowing the placing of the two detectors plus a shock front detector in the same transversal section. In this arrangement when the signal from one detector is maximum the other is minimum and vice versa. The oscilloscopes are triggered using various shock front detectors as discussed in A-6.

A-8 DATA RECORDING

The only economically feasible method of recording analog data consistent with shock tube time is the oscilloscope, although it is possible to record some data with video type tape recorders. However, the cost and resolution favor the oscilloscope and camera. While this basic technique is commonplace, to achieve optimum fidelity of the data consistent with the errors in the system, each step of the process must be carefully analyzed. This error analysis is in many instances a function of the recording time. The range of interest for this facility are sweep times of from 5 μsec to 500 μsec.

Two types of distortion can be delineated in the over-all process; these are amplitude and time distortion. To trace the source of these and estimate their relative and absolute magnitudes, the over-all recording process is divided into the following categories: the input amplifier up to the vertical deflection plates of the CRT, the sweep generator and horizontal amplifier up to the horizontal deflection plates, and the distortion in the CRT. Also, the photographic transfer of the CRT face, and the subsequent extraction of numerical data from the photographic traces must be considered. By far, the greatest offender in these distortion processes is that due to the

CRT itself. While the other factors are not always unimportant, each of the other parts of the process except numerical data reduction can be maintained to an order of magnitude better than the CRT distortion if care is taken. Even with the best selected tubes, in order to obtain distortion levels on the order of .5%, only the central region of the CRT screen can be utilized. Of course by so doing, this also tends to reduce all the other distortion causes listed. However, if these processes are independently investigated it becomes clear that the CRT is the arch criminal.

The specific procedure used to obtain the data for the shock electron density profile analysis discussed in Section B-3 is outlined below. The critical traces were made using selected CRT's so as to minimize distortion. The photographic transfer of the trace was made using a modified scope camera to reduce the image size. Polaroid 10,000 speed film, extremely fast, enables the use of a small lens aperture. With this arrangement no distortion of a precision grid placed on the CRT was observable. The picture obtained was converted to a transparency by using a very small aperture on the enlarging lens. The subsequent transparency was enlarged in a 3" x 4" slide projector. In this projector a 3/8" aperture was placed inside the

standard lens assembly and a green filter was added to reduce chromatic abberation. The resultant enlargement of about 12 diameters was negligibly distorted. The projection screen consisted of a layer of fine frosted glass backed by Plexiglass. The Plexiglass was precision scribed with .1" squares. The scribed lines were painted with phosphorescent paint. By using a "black lite" fluorescent behind the screen, the scribed marks were clearly visible, and direct transfer of numerical data from the picture could be taken by working from behind the screen. Such traces have also been made on large graph paper, but such paper is very often distorted, introducing significant errors. Under the best conditions, the over-all error from amplifier input to data output was estimated to be .4% for the maximum values increasing to 2% for values 1/20 of maximum. The increase in error becomes significantly large for small numerical values because the trace cannot be resolved.

CHAPTER III

ELECTRON DENSITY MEASUREMENT

B-1 ANALYTICAL FORMULATIONS FOR DETERMINING ELECTRON DENSITY

The following is a summary of the analytical expressions used to determine the electron density in the combined shock tube - waveguide. The polarized radiation is introduced in the downstream end of the tube. Probes to detect the radial electric field and the tangential magnetic field are upstream of the antenna as described in Section A-7. To determine the point-by-point variations in electron density as the plasma moves past the detector station, expressions are required relating the measured field quantities to the local electron density.

For the TE_{11} mode of propagation, the radial electric field and the tangential magnetic field at the surface of the waveguide are given by,

$$E_r = A J_1(\gamma R) \cos\theta \, u(x) \, e^{i\omega t} \tag{B-1}$$

$$H_\theta = \frac{i}{\mu\omega} \frac{u'(x)}{u(x)} E_r \tag{B-2}$$

where γ for the TE_{11} mode is 1.842/R, R being the tube radius.

The function u(x) is an undefined function which, however, contains the plasma properties. It must be a solution to,

$$u'' + u\left(\frac{\omega^2}{c^2} K - \gamma\right) = 0 \qquad \text{(B-3)}$$

where primes indicate space derivatives, and ω is the radiating frequency, with

$$K = 1 + \frac{\omega_p^2}{\omega^2\left(1 - i\frac{\nu}{\omega}\right)} \qquad \text{(B-4)}$$

ω_p and ν being the plasma frequency and collision frequency respectively. Assuming the field components are measured at right angles, with the E_r field in the direction of polarization of the radiation, then

$$E_r = A_o u(x)\ e^{i\omega t} \qquad \text{(B-5)}$$

$$H_\theta = \frac{i}{\mu\omega}\frac{u'(x)}{u(x)} E_r = \frac{i\ A_o}{\mu\omega} u'(x)\ e^{i\omega t} \qquad \text{(B-6)}$$

Since the values of the fields that are measured, assuming a square law detection, are the square of the real parts of the respective field the measured quantities are,

$$E_r E_r^* = A_o^2 u(x)\ u^*(x) \qquad \text{(B-7)}$$

$$H_\theta H_\theta^* = \frac{A_o^2}{\mu^2 \omega^2} u'(x)\, u^*(x)' \qquad \text{(B-8)}$$

where * indicates the complex conjugate. Solving for K^2 in Eq. (B-3),

$$K^2 = \frac{c^2}{\omega^2}\left[\gamma^2 - \frac{u''}{u}\right] \qquad \text{(B-9)}$$

The solution of K^2 in terms of the field values of Eqs. (B-7) and (B-8) can be shown to be,

$$\text{Re } K^2 = c^2\mu^2 \frac{H_\theta H_\theta^*}{E_r E_r^*} - \frac{c^2}{2\omega^2}\frac{(E_r E_r^*)''}{E_r E_r^*} + \frac{c^2\gamma^2}{\omega^2} \qquad \text{(B-10)}$$

and

$$\text{Im } K^2 = \frac{\left[\text{Re } K^2 - \frac{c^2}{\omega^2}\gamma^2\right]\frac{(E_r E_r^*)'}{E_r E_r^*} + c^2\mu^2 \frac{(H_\theta H_\theta^*)'}{E_r E_r^*}}{\sqrt{4\omega^2\mu^2 \frac{H_\theta H_\theta^*}{E_r E_r^*} - \left[\frac{(E_r E_r^*)'}{E_r E_r^*}\right]^2}} \qquad \text{(B-11)}$$

The plasma properties in terms of Re K^2 and Im K^2 are given as,

$$\frac{\omega_p^2}{\omega^2} = (1 - \text{Re } K^2)\left[1 + \left(\frac{\nu}{\omega}\right)^2\right] \qquad \text{(B-12)}$$

and,

$$\frac{\nu}{\omega} = \frac{\text{Im } K^2}{\text{Re } K^2 - 1} \qquad \text{(B-13)}$$

The values of the field in the above equations are in MKS units. However, it may be noted that each field quantity

appears in a ratio. All that is required for solution in terms of the nondimensional measured quantities are the appropriate scaling ratios.

If the measured values of the field are designated as E^2 and H^2, then the distance axis scaling needed for the ratios $\frac{(E^2)'}{E^2}$ and $\frac{(E^2)''}{E^2}$ can be determined from the ratio of the measured wavelength $\bar{\lambda}_g$ (in units of the elongated trace). That is, if the horizontal (distance axis) coordinate is measured in units of Z and the real coordinate in X units, then,

$$\frac{\bar{\lambda}_g}{\lambda_g} \equiv S$$

where λ_g is the actual waveguide wavelength (MKS units). Hence to scale the absolute ratios of field values to the measured quantities,

$$\frac{(E_r E_r^*)'}{E_r E_r^*} = S \frac{(E^2)'}{E^2}$$

and,

$$\frac{(E_r E_r^*)''}{E_r E_r^*} = S^2 \frac{(E^2)''}{E^2}$$

To scale the combined ratios of electric and magnetic fields, it may be noted that in the free space region, the

ratios of the maximum field values (occurring 180° apart) is given by,

$$\frac{(H_\theta H_\theta^*)_{max}}{(E_\theta E_\theta^*)_{max}} = \frac{4\pi^2}{\mu^2 \omega^2 \lambda_g^2}$$

If the ratio of the same measured quantities is designated by (a), i.e.,

$$\frac{H^2_{max}}{E^2_{max}} = a \ ,$$

then,

$$\frac{H_\theta H_\theta^*}{E_r E_r^*} = \frac{4\pi^2}{\mu^2 \omega^2 \lambda_g^2 a} \frac{H^2}{E^2} \ .$$

Then Eqs. (B-10) and (B-11) can be put in terms of measured quantities to give,

$$\text{Re } K^2 = \frac{c^2}{\omega^2} \frac{4\pi^2}{\lambda_g^2 a} \frac{H^2}{E^2} - \frac{S^2 c^2}{2\omega^2} \frac{(E^2)''}{E^2} + \frac{c^2}{\omega^2} \qquad \text{(B-14)}$$

$$\text{Im } K^2 = \frac{\left[\text{Re } K^2 - \frac{c^2}{\omega^2} \gamma^2\right] S \frac{(E^2)'}{E^2} + \frac{c^2 S}{\omega^2} \frac{4\pi^2}{\lambda_g^2 a} \frac{(H^2)'}{E^2}}{\sqrt{\frac{16\pi^2}{\lambda_g^2 a} \frac{H^2}{E^2} - S^2 \left[\frac{(E^2)'}{E^2}\right]^2}}$$

Hence, the plasma properties can be obtained through the use of Eqs. (B-12) and (B-13).

In summary, to calculate the plasma properties at any point behind the shock the following parameters are required.

λ_g	waveguide wavelength
$a = \frac{H^2_{max}}{E^2_{max}}$	taken in the free space region
$S = \frac{\bar{\lambda}_g}{\lambda_g}$	distance scaling ratios ($\bar{\lambda}_g$ measured wavelength on enlarged trace)
$\lambda = \frac{1.842}{R}$	R is tube radius
$\omega = 2\pi f$	f radiating frequency

and E^2, $(E^2)'$, $(E^2)''$, H^2, $(H^2)'$, the field values and derivatives at the wall of the waveguide.

B-2 DATA PROCESSING PROGRAM

In the preceding section describing the analytical formulation necessary for the electron density measurement, the basic quantities required for solution are the real value of electric field squared (EE*), its first and second derivatives, the real value of magnetic field squared (HH*), and its first derivative. It was shown that no absolute measurement of these quantities was required, if the ratio $\frac{EE^*_{max}}{HH^*_{max}}$ could be obtained in the free space region in front of the shock. The precision of the final calculation is extremely sensitive to these measured quantities. While it has been indicated in Section A-8 that the relative accuracy for part of the recorded data is about .4%, it is important to note that this accuracy is related to the data taken at that instant of time. Because all of the components of the measuring system are constantly varying, it is essential that all of the critical information be obtained from one set of traces taken at one time.

The greatest variables in this system are the crystal detectors, although sweep rates and amplifier gains may also change. If the desired signal to be detected is for instance EE*, the crystal detector must have a square law behavior. Since this requirement is never precisely true a correction

must be made on the output signal. It will be shown how this correction can be made directly from the numerical data derived from the single trace, thus avoiding the need for corroborating data taken at a different time.

The calculation of electron density is divided into three operations. First, the raw numerical data taken from the scope trace is corrected for the non-square law behavior of the crystal. Second, from this corrected data, first and second derivatives are computed. Third, the corrected data and derivatives are combined point-by-point as prescribed by the analytic equations of the preceding section.

Processing of the Raw Data

The basic input for the calculation is approximately 150 data points from each of the raw electric and magnetic field detector output traces. These traces include one full period of the sinusoidal-like function preceding the plasma.

Because careless errors may be introduced in the transcription or punching of the raw data, the program first checks if successive points are monotonically increasing or decreasing. The object of this procedure is to identify data that is clearly impossible, and allow corrections or changes.

Once the data passes this initial test the points are smoothed by a least square fitting procedure. In this computation eight points are used to obtain the constants of a second power equation by least squares fit. Having computed the equation constants, the values of the function for the center two points are calculated and stored as smooth data. The program then jumps two points and recomputes the least square fit for the next eight points which of course includes six from the previous calculation. After this procedure has been performed for all data points the initial raw data is destroyed and the smoothed values inserted in its respective place. The need for smoothing the data is comparable to the use of a "French" curve in graph plotting. The basic assumption is that the data is originally smooth and that conversion to digits has introduced a random error in the least significant place. By reducing these errors an improvement can be obtained in the subsequent derivatives that must be taken.

The next step is to modify the data for the incorrect response of the detector. This correction procedure is based on the fact that the data function outside the plasma must be a sinusoid if the detectors are measuring EE^*. The basic problem is to find a multiplicative function $[g,x)]$ such that when multiplied by the data function $[f'x,]$ the resulting function will be a sinusoid elevated above zero.

i.e., $$g(x)\ f(x) = A \sin \theta + A + \alpha$$

The difficulty in determining the g(x) function is that since α, which is related to the standing wave ratio, is unknown, then there are an infinite set of g(x) functions which will satisfy the above criteria. The solution to this dilemna is found in the fact that the crystal nonlinearity (to the square law) must be a smooth and slowly varying function, a fact clear from the physics of the semiconductor. If α is on the order of A/3 or smaller, the latter condition becomes a very stringent limit on possible g(x) functions. The first step to determine the g(x) function is to determine the period of the sinusoidal-like function f(x) in the free space region. This is accomplished by computing a function like a derivative over the entire curve. This derivative procedure consists of computing multiple differences at each point and averaging the result. The reason for this technique is to establish the zero slope points with the least error being introduced from the random data scatter.

After locating the first two zeros, forty points are generated by interpolation between zeros, which of course correspond to the first maximum and minimum or the reverse of the original curve. The forty points are chosen such that if the

function were a true sine, then the increment of the function between points would be equal. This is done so that the g(x) function will not be unduly weighted by a preponderance of points at each end. The first trial g(x) function is generated by assuming the perfect sine curve has the same magnitude as the data function. Hence the g(x) function at maximum and minimum (A and B in Fig. B-2.1) is identically one. This then produces a g(x) typically like that in Fig. B-2.2. On the g(x) curve, the region from A to D, where D is arbitrarily 1/2 f(x), is least square-fitted by a second order polynomial. Point C, the value of g(x) for f(x) min is computed from the curve fit constants and this value is used to compute the value of α.

Distorted Sine Function

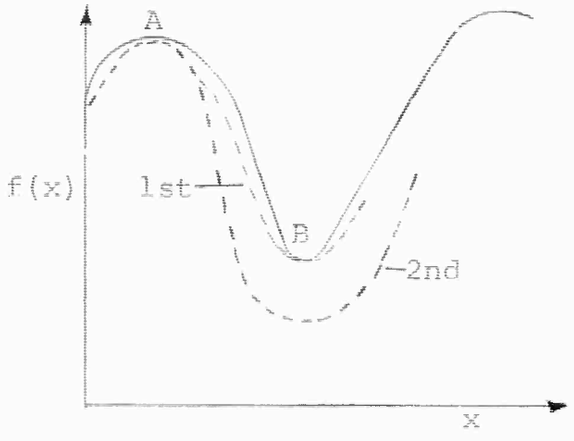

Fig. B-2.1

g(x) Determination

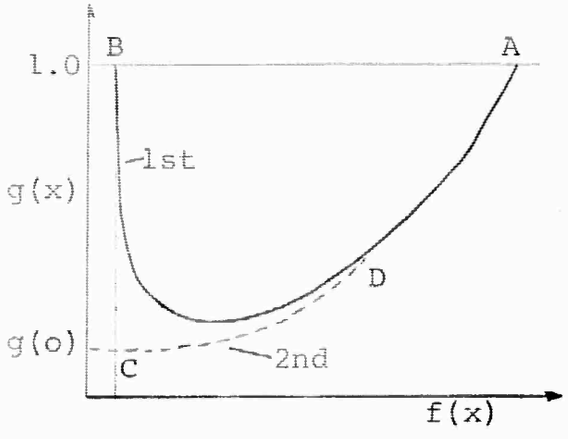

Fig. B-2.2

Using this value, a new magnitude A is computed and the entire g(x) function for each point of f(x) is generated. This second trial g(x) function is again curve-fit to a second order polynomial by method of least squares. From the constants of the polynomial, the value of g(o) and the standing wave ratio are calculated and the difference between the curve fit g(x) and the trial computed g(x) points is printed. At this time in the proceeding, the computer is tired and returns control to the operator. The operator, making a human type judgment on the basis of the differences in the last points, may choose a different value by a few percent of g(o) and the above process will be repeated.

It is desirable that the companion curve, HH*, to the EE* curve be processed up to the determination of the g(x) correction function as indicated above. If the g(x) functions have been properly chosen for each curve, the standing wave ratio will be identical. With a little practice the standing wave ratios can be made to agree to better than 2%.

Once the g(x) functions are satisfactorily determined, all the data is corrected thus yielding the "true" values of EE* and HH* along the curves. By a method of multiple differences, the derivative of these functions are taken yielding (EE*)', (EE*)" and (HH*)'.

The computer program thus far described is intended to take data derived from a single trace, apply corrections and produce derivatives at fixed intervals. The functions generated must not only be self-consistent, but also should be consistent with the data derived from the companion curve. (EE* and HH* form a set.) It has been shown how the program "forces" an over-all amplitude correction by assuming the detected function in the free space region is sinusoidal. This type of correction will compensate for most amplitude distortions due to any cause that is not a function of the time coordinate (horizontal position on the CRT).

Additional information which can be obtained from the data is the relative wavelength of the sinusoidal function in the free space region. It may be recalled that the wavelength determination was necessary to establish the period of the "forcing" sinus function. Since the waveguide wavelength of the microwave radiation can be accurately measured prior to testing, it is used as the only additional piece of information that is not directly obtained from the picture. If the measured wavelength and the relative wavelength are combined, an over-all scaling is achieved. In addition, if the scaling factors for the EE* and HH* are compared, an accurate contraction

or expansion factor can be obtained and used to provide exact time correlation between points on either curve. If one additional marker (such as the location of the shock front) is common to both curves an exact relation between the curves can be made. If the trace also contains time markers, the shock velocity can be obtained. It may be noted that the time markers also provide the location of the zero amplitude axis at the instant the trace was made, a procedure which removes the uncertainty due to drift in all systems.

An additional piece of information required for the calculation of electron density is the ratio of the maximum on the electric field trace in the free space region to the maximum on the magnetic detector trace $\frac{EE^*_{max}}{HH^*_{max}}$. This ratio provides all the scaling information needed to use the nondimensional curve data in an absolute determination of electron density. It may be recalled that the maximum values required were obtained to provide amplitude information for the "forcing" sinusoidal correction function.

Hence, it has been demonstrated that the complete set of information required to compute the electron density, with the exception of the waveguide wavelength is directly obtainable from the two detector curves. The advantage of this procedure

is that no absolute measurements are required, with the exception of the waveguide wavelength and interval between time markers. (The latter is used only for the velocity determination.) This clearly implies that no absolute calibration and maintenance of that calibration is needed for the instruments used in recording. Except for the requirement of a linear time scale (assuming shock velocity constant), an over-all correction of most of the distortions occurring in all phases of the data collection process is obtainable from the data.

All of the information obtained in the "data processing" phase of the program is subsequently used in the point-by-point determination of electron density as per the formulations of the preceding section. Since this computation is entirely straightforward no discussion will be given here.

B-3 EXPERIMENTAL DETERMINATION OF THE ELECTRON DENSITY BEHIND A NORMAL AIR SHOCK

The following is a brief description of the experimental conditions for which the longitudinal electron density profile has been determined. A series of six independent sets of data have been processed corresponding to nearly identical shock conditions. The purpose of the nearly redundant data was to check the over-all repeatability and the effect of small variations in shock condition about the mean.

The specific shock conditions are tabulated below.

Case	Shock Velocity (meter/sec)	Initial Pressure (mm Hg)	Note
1	3100	2.5	Upper curve
2	2900	1.5	Lower curve
3	3030	2.0	
4	3015	2.05	Mean values plotted
5	3035	1.95	
6	3020	2.0	

The velocities quoted above were calculated directly from the electric and magnetic field detector traces as previously described in Section B-2. The microwave instrumentation used is described in Section A-7. The specific waveguide wavelength for all of the runs was 20.2 cm.

One typical set of traces is shown in Fig. B-3.1. Note the periodic time markers which also give the zero level of the signals. The location of the shock front was determined from a third trace.

The numerical data from these curves was obtained in the manner described in Section A-8. Subsequent numerical analysis was carried out using the computer program described in Section B-2. The results for the six cases are summarized in Fig. B-3.2. Here the mean curve represents the results for cases 3 through 6 which correspond to the same velocity conditions ±.3%. Cases 1 and 2 correspond to higher and lower velocities respectively. It may be noted that the behavior of the electron density is in correspondence with these conditions. The values of equilibrium electron density were calculated for these shock conditions using the procedure outlined in B-4 and Fig. B-4.2.

Because the shock front marker detector used in these runs was derived from a pressure detector as described in Section A-6, a small displacement uncertainty existed in the results consistent with the "jitter" of the relatively slow rise of the detector. The "mean" curve in Fig. B-3.2 represents a repositioning of the separate results, where the maximum shift corresponded to .75 cm.

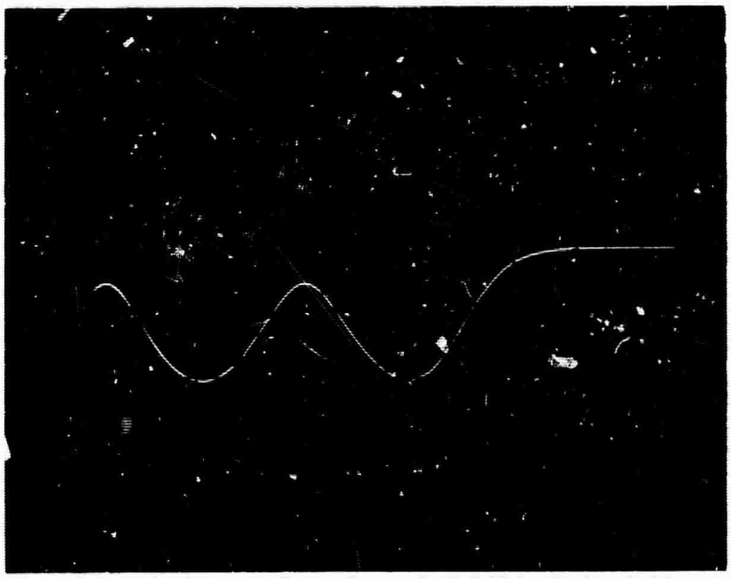

Electric Field Trace

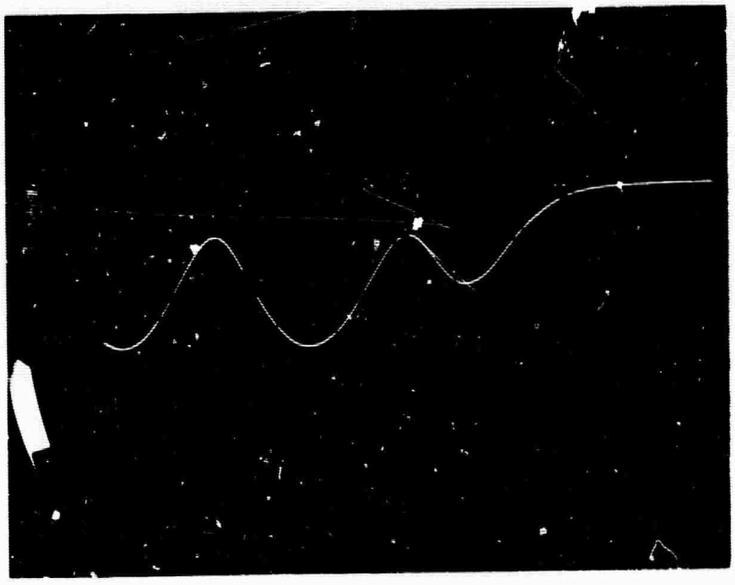

Magnetic Field Trace

Set of Electric and Magnetic Field traces used as starting data in the calculation of the electron density profile behind the shock. (Case 4 in table).

Figure B-3.1

THIS PAGE INTENTIONALLY LEFT BLANK

The test gas for all of these cases was commercial compressed breathing air. The basic result has not been significantly modified by any of the following procedures.

(1) Addition of a liquid nitrogen "freezeout" trap on the test gas. Such a trap would of course remove all water and oil present.

(2) Liquid nitrogen trap in the vacuum system to remove any trace of pump oil from the tube.

(3) Mixing of high purity oxygen and nitrogen in proportion to "normal" air and slight variation about the standard mixture. These gases were also liquid nitrogen trapped to remove water or oil.

(4) The design of the mechanical valve discussed in Section A-3 was motivated by the desire to remove the possibility of cor . mination due to the use of plastic diaphragms. However, no significant change of the electron density profile was observed after the conversion to the mechanical valve.

B-4 SUPPORTING EXPERIMENTAL AND ANALYTICAL INFORMATION

Radial Uniformity of the Plasma

One assumption made in the analysis of Section B-1 for the electron density was that of radial uniformity of the plasma density. Such uniformity can be altered by two factors. First is the presence of a boundary layer along the walls in the region behind the shock. However, for the penetration distances indicated by the results, this should have an insignificant effect on the assumption of uniformity.

The second effect is that of ambipolar diffusion. A calculation of this effect for two operating conditions has been performed as summarized in the following subsection. The result indicates the assumption of radial uniformity is basically correct.

The ambipolar diffusion equation for electrons in cylindrical coordinates is:

$$\frac{1}{r}\frac{\partial}{\partial r}\left(r\frac{\partial n_e}{\partial r}\right) + \frac{\partial^2 n_e}{\partial z^2} - \frac{u_n}{D}\frac{\partial n_e}{\partial z} + \frac{\dot{n}_e}{D} = 0 \qquad \text{(B-15)}$$

where $D = \frac{uk\,T}{M_i \nu_i}$ is the ambipolar coefficient. No Φ dependence of the electron distribution is included.

Only diffusion normal to the wall will be studied and for that particular case Eq. (B-15) becomes:

$$\frac{1}{r}\frac{d}{dr}\left(r\frac{\partial n_e}{\partial r}\right) + \frac{\dot{n}_e}{D} = 0 \qquad \text{(B-16)}$$

The term, $\dot{n}_e$ which is related to the creation of electrons due to chemical reactions inside the ionized gas, as yet must be defined.

The mechanism for the creation of the electron is given by the motion of a shock wave along a tube. From the several reactions which can generate electrons in air due to the effect of the shock wave, the most important is:

$$N + O \rightarrow NO^+ + e \qquad \text{(B-17)}$$

Therefore,

$$\dot{n}_e = k_r(K_c n_N n_O - n_e^2) \qquad \text{(B-18)}$$

Replacing (B-18) into (B-16) we have:

$$\frac{1}{r}\frac{\partial}{\partial r}\left(r\frac{\partial n_e}{\partial r}\right) + \frac{k_r}{D}(K_c n_N n_O - n_e^2) = 0 \qquad \text{(B-19)}$$

Eq. (B-19) can be written in the form:

$$\frac{1}{r}\frac{\partial}{\partial r}\left(r\frac{\partial y}{\partial r}\right) + \frac{k_r n_{eo}}{D}\left(\frac{K_c n_N n_O}{n_{eo}^2} - y^2\right) \qquad \text{(B-20)}$$

where n_{eo} is the equilibrium electron number density.

It is known from chemistry considerations (see Penner, Chemistry Problems in Jet Propulsion), that,

$$\frac{K_c n_N n_O}{n_{eo}^2} = 1 \tag{B-21}$$

Then Eq. (B-20) becomes:

$$\frac{1}{r}\frac{\partial}{\partial r}\left(r\frac{\partial y}{\partial r}\right) + \frac{k_r n_{eo}}{D}(1-y^2) = 0 \tag{B-22}$$

This equation has a boundary condition given by the following relation (see Section D-3).

$$\frac{D}{n_e}\frac{dn_e}{dr} = \sqrt{\frac{kT}{m_i}} \tag{B-23}$$

which can be written,

$$\frac{D}{y}\frac{dy}{dr} = \sqrt{\frac{kT}{m_i}} \tag{B-24}$$

The Eq. (B-22) with the condition (B-24) must be solved numerically and it has been done for 5 shock wave configurations. The data, corresponding to these configurations appear in Table I.

TABLE I

Shock Velocity (m/sec)	T (°K)	ρ/ρ_o	n_{eo} (cm^{-3})	α (cm)
2750	2790	8.45×10^{-3}	4.4×10^{9}	1.404
3000	3000	1.00×10^{-2}	2.10×10^{10}	.639
3250	3210	1.08×10^{-2}	7.2×10^{10}	.348
3500	3390	1.22×10^{-2}	2×10^{11}	.204
3750	3660	1.30×10^{-2}	6.2×10^{11}	.120

Of primary interest is the effect of the coefficient,

$$\frac{1}{\alpha^2} = \frac{k_r n_{eo}}{D} \qquad \text{(B-25)}$$

upon the electron distribution.

The coefficient α has the dimension of a length and can be considered to be a characteristic diffusion length. Table I shows that α changes greatly; it implying that for the cases where α is small, the diffusion will be very slow at the beginning but will fall off sharply near the wall of the cylinder. This does not happen for much higher values of α (see Fig. B-4.1). The experimental investigation made at GASL for a case where the shock wave velocity was 3100 m/sec corresponds to large values of α. For this velocity case, the transverse gradients are small over most of the tube radius, becoming large only in the thin outer sheath.

Fig. B-4.1 Radial Electron Distribution for Two Shock Configurations

Microwave Interferometer

A conventional phase detection interferometer was adapted to a special test section of the shock tube. This test section was made of thin glass with the identical inside diameter of the shock tube. A supporting housing provided the necessary structural capacity and housed the microwave horns. The nominal wavelength of the radiation was about 1 cm. The nominal beamwidth resolution was on the order of 2.5 cm.

With this instrument, the shock tube was operated using air. For the range of pressures and velocities indicated in Fig. B-4.2, the electron density was within 20% of the equilibrium values. Further, the change across the shock front with the probable 2.5 cm resolution appeared essentially as a step.

Sensitive Check on the Equilibrium Electron Density

By assuming a simple model for the plasma behind the shock to be a sharp transition from free space to equilibrium electron density levels, a formulation for the standing wave ratio due to the addition of the transmitted and reflected signals from such a plasma can be easily made.

By combining the formulation of the SWR with the properties of the gas behind an air shock as a function of shock velocity and initial pressure, a comparison with experimental results can be made. This procedure is summarized below.

First, the standing wave ratio will be calculated in terms of the electron density and collision frequency which are assumed uniform in the plasma region.

The generalized propagation constant as defined by

$$\frac{d^2E}{dx^2} + K^2 E = 0$$

is given by,

$$K = \sqrt{\frac{\omega^2}{c^2}\left[1 - \frac{\omega_p^2}{\omega^2\left(1-i\frac{\nu}{\omega}\right)}\right] - \gamma^2}$$

where

ω = the propagating frequency

ω_p = the plasma frequency

ν = the collision frequency

γ = the root of the Bessel function for the TE_{11} circulator waveguide mode divided by the tube radius.

The propagation constant can be formed as follows. Define

$$K = k_o K_g$$

where

$$k_o = \sqrt{\frac{\omega^2}{c^2} - \gamma^2}$$

$$K_g = \sqrt{1 - \frac{\omega_p^2}{c^2 k_o^2\left(1-i\frac{\nu}{\omega}\right)}}$$

Now let the radial electric field and the tangential magnetic field in the free space region be given by

$$E_r = A\, e^{-ik_o x} + B\, e^{-ik_o x}$$

$$H_\theta = k_o \sqrt{\frac{\epsilon_o}{\mu_o}} \left[A\, e^{-k_o x} - B\, e^{ik_o x} \right]$$

and in the uniform plasma region,

$$E_r = C\, e^{ik_1 x}$$

$$H_\theta = k_1 \sqrt{\frac{\epsilon_o}{\mu_o}} \left[C\, e^{-ik_1 x} \right]$$

Normalizing $A \equiv 1$, the boundary conditions are matched yielding,

$$E_r = e^{-ik_o x} + \theta\, e^{ik_o x}$$

with

$$\theta = \frac{1 - K_g}{1 + K_g}$$

Thus, the real component of the field produced is,

$$E_r E_r^* = 1 + \theta\theta^* + \theta\theta^*\, e^{-ik_o x}\, e^{ik_o x}$$

This is reduced to,

$$E_r E_r^* = \left[1 \pm \sqrt{(R_e\theta)^2 + (I_m\theta)^2}\right]^2$$

The two solutions give the maximum and minimum values. Thus the standing wave ratio is,

$$SWR = \left[\frac{1 + \sqrt{(R_e\theta)^2 + (I_m\theta)^2}}{1 - \sqrt{(R_e\theta)^2 + (I_m\theta)^2}}\right]^2$$

where θ is a function of ω_p and ν.

By solving the normal set of aerodynamic equations and using a programmed Mollier diagram, the conditions behind the shock can be given as a function of shock velocity and initial pressure.

To simplify the calculation of equilibrium electron density from temperature and density, standard tables were programmed for the computer. Thus as a function of shock velocity, the equilibrium electron density is computed with the initial pressure as a parameter. Figure B-4.2 shows this plot. The collision frequency is computed from the approximation

$$\nu = \frac{5 \times 10^{12} p}{\sqrt{T}}$$

with p the pressure in atmospheres, T in $^{\circ}K$.

Figure: B-4.2

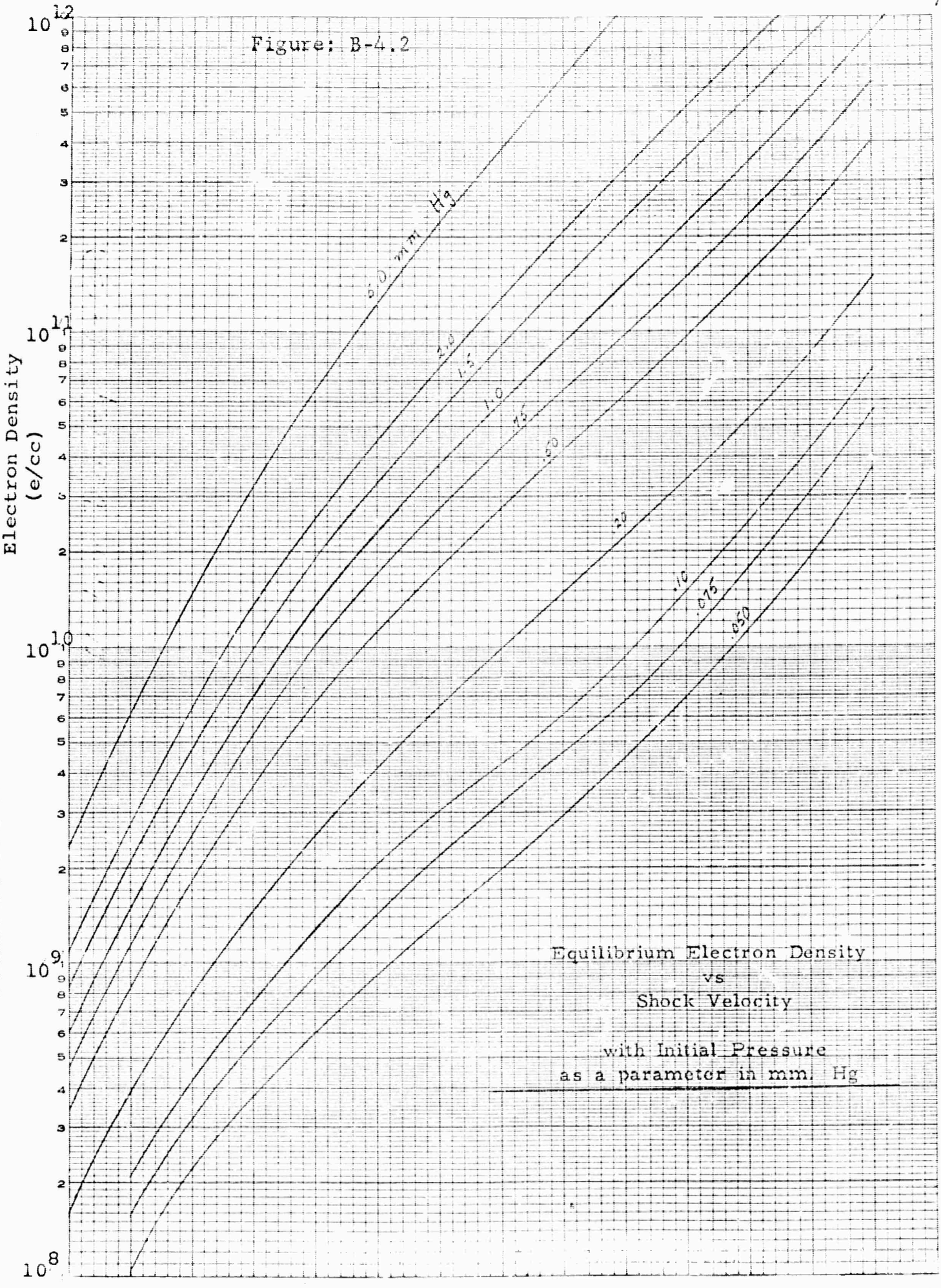
Electron Density (e/cc)
10^{12}
10^{11}
10^{10}
10^{9}
10^{8}
2600
2800
3000
3200
3400
3600
3800
4000
.50 mm Hg
2.0
1.5
1.0
.75
.50
.25
.10
.075
.050
Equilibrium Electron Density
vs
Shock Velocity
with Initial Pressure
as a parameter in mm. Hg

If now these plasma properties are used to compute K_g, the standing wave ratio can be calculated using the previous formulation as a function of shock velocity with the initial pressure as a parameter (Fig. B-4.3). Hence as a function of accurately determinable quantities, the electromagnetic characteristics of the entire system can be computed and subsequently compared with the experimental quantities.

It should be appreciated that such a comparison is a very sensitive check on the assumptions made. First, the aerodynamic properties behind the shock must precisely follow the gas dynamic theory. Second, the electron density and collision frequency must, on the average, be identical with the equilibrium values. Third, the assumed geometric uniformity of the plasma region must be nearly correct. Fourth, the calculation of the SWR based on the simple step model should be right. When comparing with experimentals, the variables measured must be identically the same as those used in the formulation. For instance, the electric field detector after correction should indeed be measuring only EE*.

In this light, the correspondence between the analytically determined and the measured SWR as presented in Fig. B-4.4 is remarkable. Note here that since the driver pressure is constant

for all these tests, in order to change the shock velocity there is a corresponding change in initial pressure. Hence, Fig. B-4.4 corresponds to a cross plot of Fig. B-4.3 using the operating characteristic curve in Fig. B-4.5. This agreement provides probable verification of the simple analytical model used in the computation. The basic assumptions of that model are uniform plasma densities both radially and transversely and that the density levels are as computed from the equilibrium thermodynamic state of the shocked gas.

Figure: B-4.3

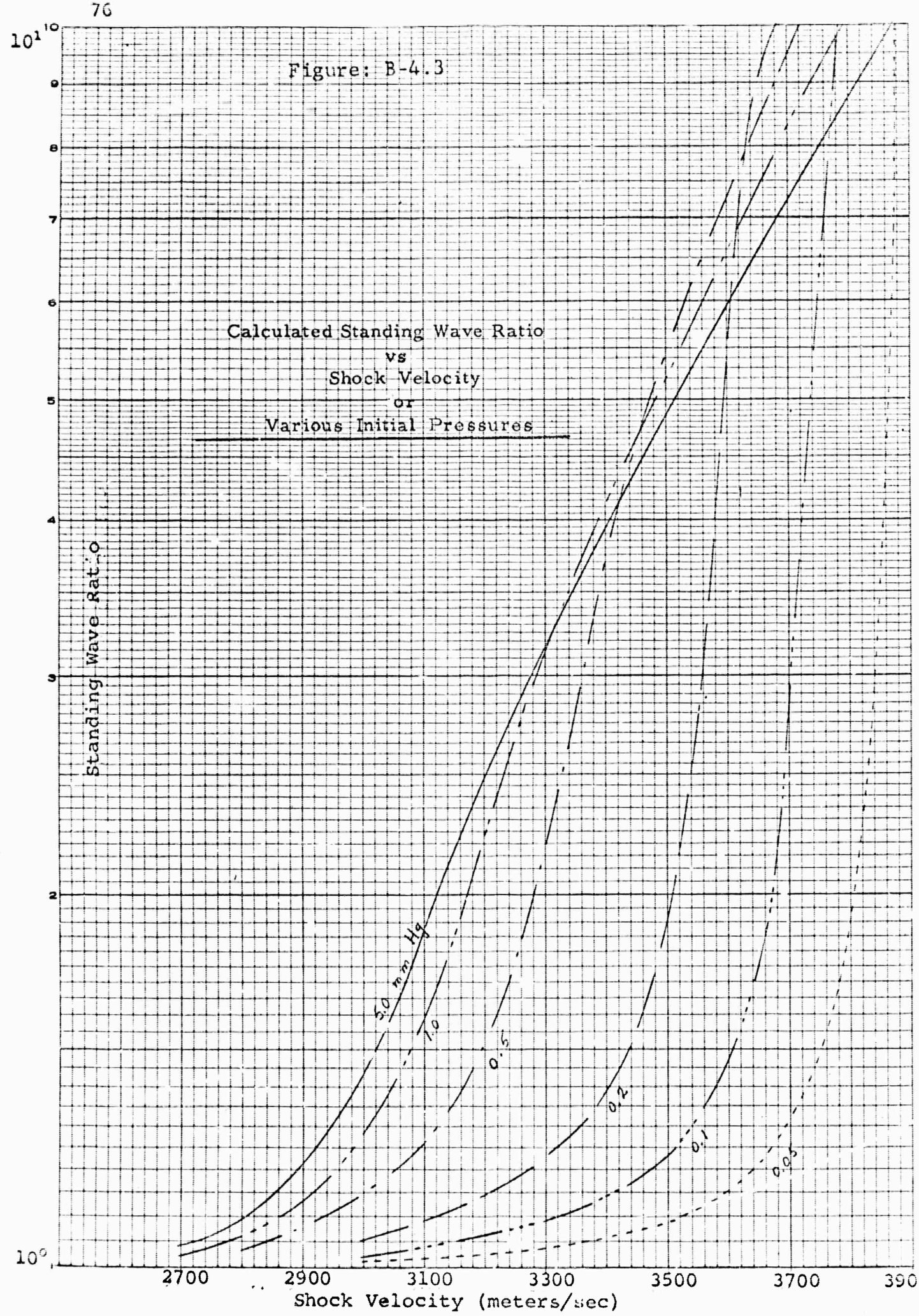
Calculated Standing Wave Ratio
vs
Shock Velocity
or
Various Initial Pressures
Standing Wave Ratio
10^{10}
9
8
7
6
5
4
3
2
10^{0}
5.0 mm Hg
1.0
0.5
0.2
0.1
0.05
2700
2900
3100
3300
3500
3700
Shock Velocity (meters/sec)

Figure: B-4.4

Standing Wave Ratio
vs
Shock Velocity

(following actual operating conditions of shock tube. (See Fig. B-4.5))

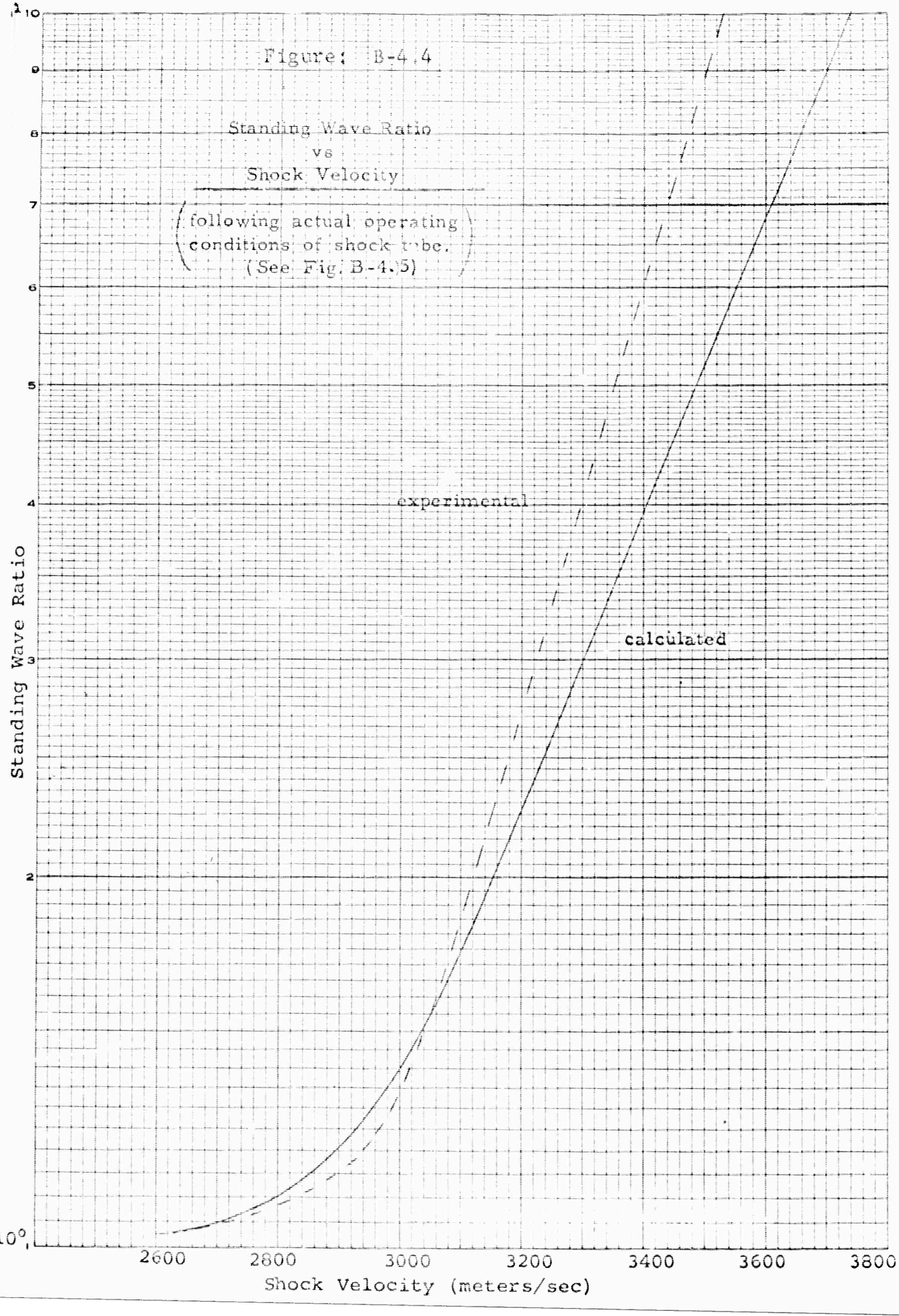

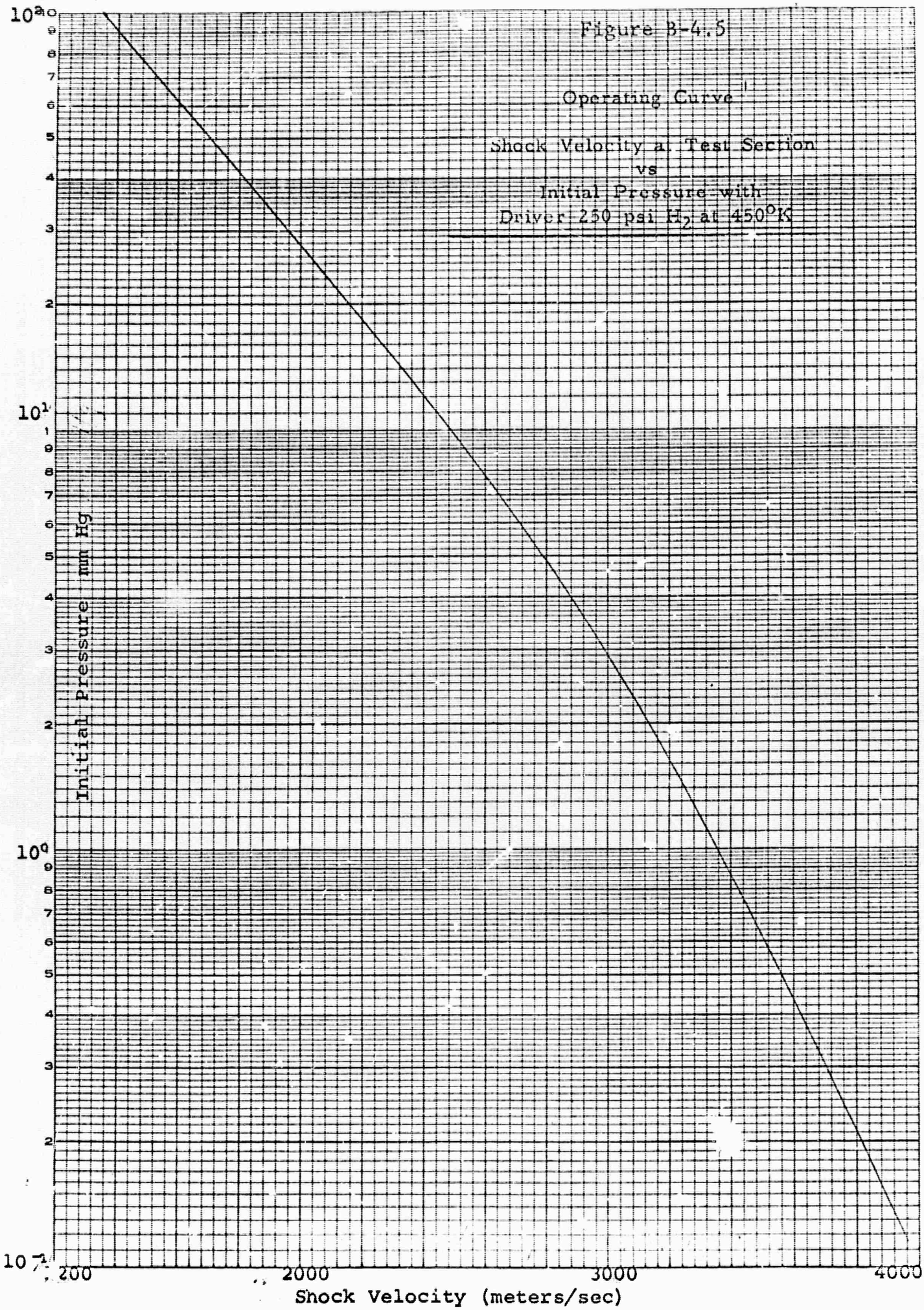
Figure B-4.5
Operating Curve
Shock Velocity at Test Section
vs
Initial Pressure with
Driver 250 psi H_2 at 450°K
Initial Pressure mm Hg
10^2
10^1
10^0
10^{-1}
200
2000
3000
4000
Shock Velocity (meters/sec)

CHAPTER IV

COMPARISON BETWEEN EXPERIMENTAL AND ANALYTICALLY DETERMINED ELECTRON DENSITY PROFILE

C-1 INTRODUCTION

Historically the shock tube has been one of the primary tools used to investigate the non-equilibrium air chemistry. Like most scientific endeavors, the purpose of such research is to provide a model consistent with all the data which may be used to predict the behavior of the system under a variety of conditions. The obvious complexity of the air system and the difficult experimental techniques used for investigation have severely limited the extent and reliability of the input data.

One of the important tests of the air chemistry model is the prediction of the non-equilibrium electron density. On the basis of this test disagreement has been found between the experiments conducted herein and the "state of the art model" that has been devised.

The following sections detail the digital computer program used to operate on the air chemistry model. Secondly, the air chemistry model is considered with the addition of impurities to ascertain their effects. Thirdly, the experimental

spectroscopic investigation of the shock produced plasma is discussed. And in section four, the results of the experimental and analytical programs are compared. Because of the complexity of the problem and the inclusive data obtained from all sources, it would be reckless to draw firm conclusions from the material presented here. However it is probable that the observed discrepancy may be fully acounted for - in terms of impurities.

C-2 ONE-DIMENSIONAL NON-EQUILIBRIUM AIR CHEMISTRY PROGRAM (REF. 2)

As an integral part of the work performed in this investigation, a digital computer program has been developed to study one-dimensional chemically reacting flows. The characteristic features of this program, as well as the philosophy behind it, will now be described.

To one familiar with the problem, it is evident that the program should be so structured that the number and kinds of species and chemical reactions can be easily changed. The chemical rate constants should also be amenable to a quick alteration if desired. The reason for this stems from the complexity of the chemistry and also the uncertainty of the related data. Much of the empirical data is obtained from extrapolations of data into ranges of temperature and into situations which differ appreciably from the conditions under which the original measurements were made. Such limitations suggest that provision be made for varying or correcting the data in a routine manner.

Accordingly, the present study has as its purpose the complete formulation of the problem of generalized one-dimensional chemically reacting flows with molecular vibrational relaxation, and includes the lowing features:

Optional Relaxation of Vibrational Energy of Diatomic Species

The diatomic molecules of a given species are assumed to be distributed over the vibrational energy spectrum with a Boltzmann distribution characterized by a vibrational temperature T_{v_i}. The relaxation of the vibrational energy is computed from a relation of the form

$$\frac{d\bar{U}_{v_i}}{dt} = \frac{\bar{U}_{v_i}(T) - \bar{U}_{v_i}(T_{v_i})}{\tau_i}$$

where τ_i is an empirical relaxation time. If desired, any diatomic species may, instead, be considered to be in vibrational equilibrium at the translational temperature T.

Coupling of Vibrational Energy to Rate of Dissociation

With the assumption that dissociation occurs from every vibrational level at a rate proportional to the population at that level and to the number of particles having a translational kinetic energy of sufficient magnitude to cause dissociation, the rate coefficient for the dissociation process is computed from the rate coefficient at vibrational equilibrium (at the same temperature) modified by a factor depending upon T, T_{v_i}, and the characteristic vibrational temperature of the species. This is the so-called CVD model.

Provision for More Elaborate Vibrational Relaxation Models

The contribution of each chemical reaction to the production rate and removal rate of the related species is individually computed, and the net production is determined only after all reactions have been treated. In this way not only are possible losses of significant figures concentrated at one point, but the net molar production and removal rates are individually available for more elaborate vibrational relaxation models, the CVDV model for example.

Choice of Chemical Reactions

A large number of chemical reactions (up to fifty) may be provided with the structure easily adaptable to more if desired. The computations may be carried out with any combination of reactions as well as with none at all. Not only may air chemistry be treated, but also hydrogen combustion, etc.

Choice of Species

The program is so structured that any combination of species (initially up to twenty) may be considered. Single species may be studied as well as a full complement. New species may be added without program modification by simply adding a standard format of the applicable physical data for the species.

Choice of Process

Both duct flow (prescribed area process) and the prescribed pressure process are available, and the computations may proceed from one to the other in a single problem.

Provision for Wall Friction and Heat Transfer

The effects of friction and heat transfer are accounted for by means of a conventional wall friction factor and a heat flux parameter. The heat flux may be treated as a function of stream temperature, if desired, and may thus accommodate thermal radiation as well as other modes of heat transfer.

Modification of Analysis to Avoid Iteration

Usually, the only differential equation needed for the thermodynamic properties is the momentum equation, which for frictionless flows is simply the Euler equation, $dp = -\rho V dV$. When pressure is prescribed, the velocity derivative immediately follows, and the enthalpy may be computed. The temperature is then computed from the caloric equation of state by a time-consuming trial-and-error procedure. Here, however, the equations are reformulated to yield a differential equation for the temperature so that the enthalpy may now be determined directly from the caloric equation of state without iteration. The velocity is then found from an algebraic relationship.

Statistical Calculation of Species Data

The internal energy of each species as well as the equilibrium constants for all reactions are calculated from partition functions obtained through the application of statistical mechanics to tabulated spectroscopic data.

Flexibility in Treatment of Electronic Energy

The electronic energy is included in the computation of the internal energy of the species; however, the number of levels of excitation may be separately chosen for the individual species. The electronic energy may also be omitted entirely, if desired. Furthermore, a separate electronic temperature is included, common to all species as a first approximation, so that the electronic energy may be relaxed if a suitable relaxation differential equation is provided.

Provision for Oblique Shocks

An oblique shock may be introduced at any point in the calculation. Either the shock angle or the turning angle may be specified, and the vibrational energy may be treated as frozen or in equilibrium as desired. The composition, however, is frozen.

Comprehensive Output

The output of data as the calculations proceed is designed to provide a comprehensive survey of not only the gas mixture, but the individual species and the chemical reactions.

In its current operational form, the program incorporates a 39 reaction scheme for 13 pure air species (O_2, O, N_2, N, NO, e^-, NO^+, O_2^+, O^+, N_2^+, N^+, O_2^-, O^-) coupled with a 12 reaction scheme for the species Na, Cl, NaCl, NaO, Na^+, and Cl^-. The reactions considered and their associated rate constants are given in Appendix I.

C-3 AIR CHEMISTRY MODEL WITH THE INCLUSION OF IMPURITIES

The one-dimensional chemically reacting flow program discussed in Section C-1 has been used to simulate the experimental shock tube conditions described in this report. The calculation for pure air under typical shock conditions (U_s = 3 mm/μsec; p_1 = 2 mm Hg; T_1 = 273°K), utilizing a seven species, seven reaction model (O_2, O, N_2, N, NO, e^-, NO^+, reactions 1-7, Appendix I), yields the electron density profile shown in Fig. C-3.1A. A nine species, nine reaction model (add to above: O_2^-, O^-; reactions 36, 37) yields essentially identical results.

In order to investigate the effects of some naturally-occurring contaminants on the electron density profile in otherwise pure air, calculations were carried out with trace amounts of NaCℓ and Na. The initial mass fraction of contaminants was varied from 10^{-9} to 10^{-6}, and the resultant electron density profiles are shown in Figs. C-3.1B,C and C-3.2. Note that in all cases except for the 10^{-6} contaminant mass fraction, where the difference is slight, the equilibrium electron density level is equal to that for pure air.

From Fig. C-3.1 it can be seen that for pure air, or for air contaminated with NaCℓ, the seven species, seven reaction and the nine species, nine reaction air models yield identical

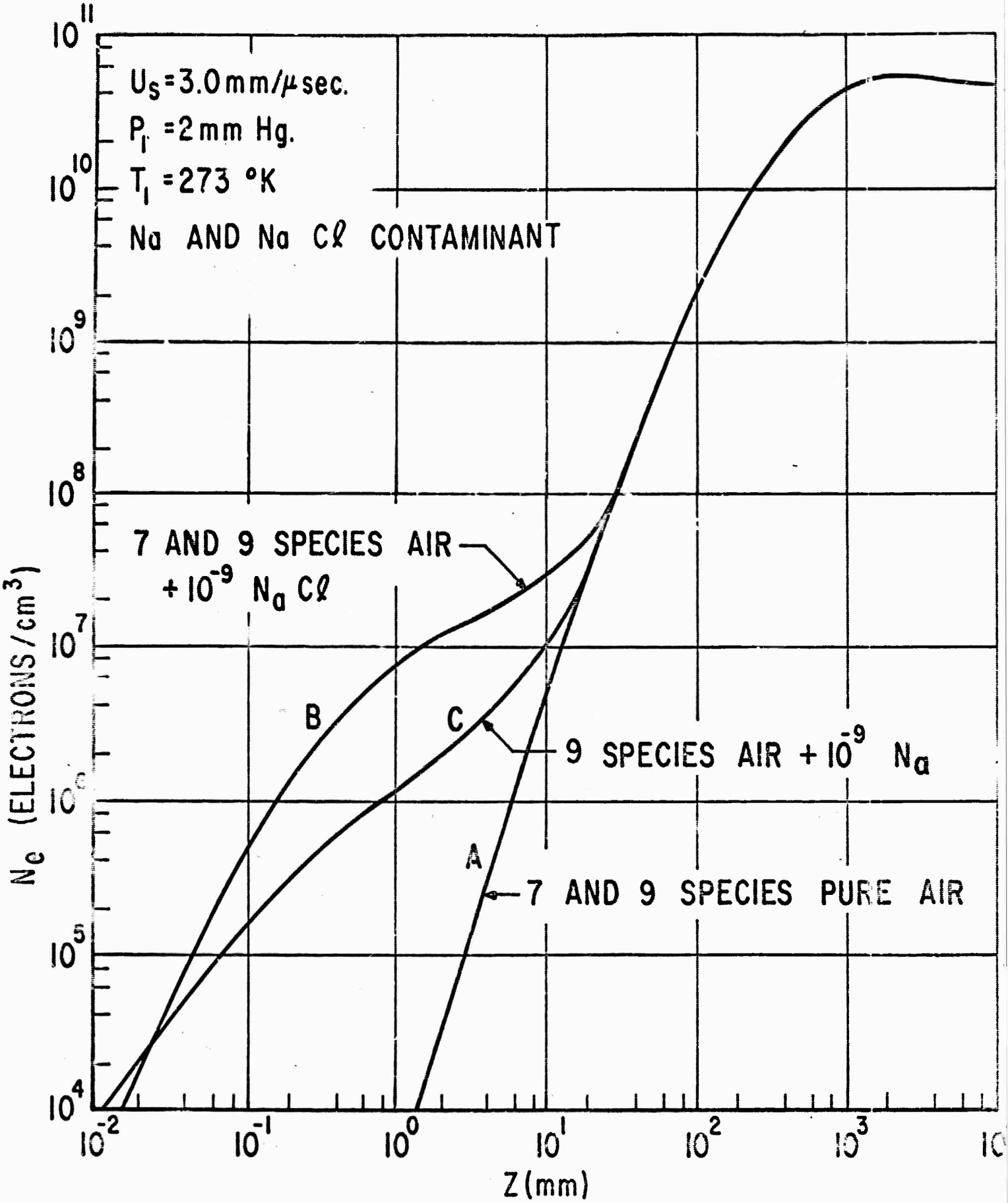

FIG. C-3.1 ELECTRON DENSITY BEHIND NORMAL SHOCK IN CONTAMINATED AIR

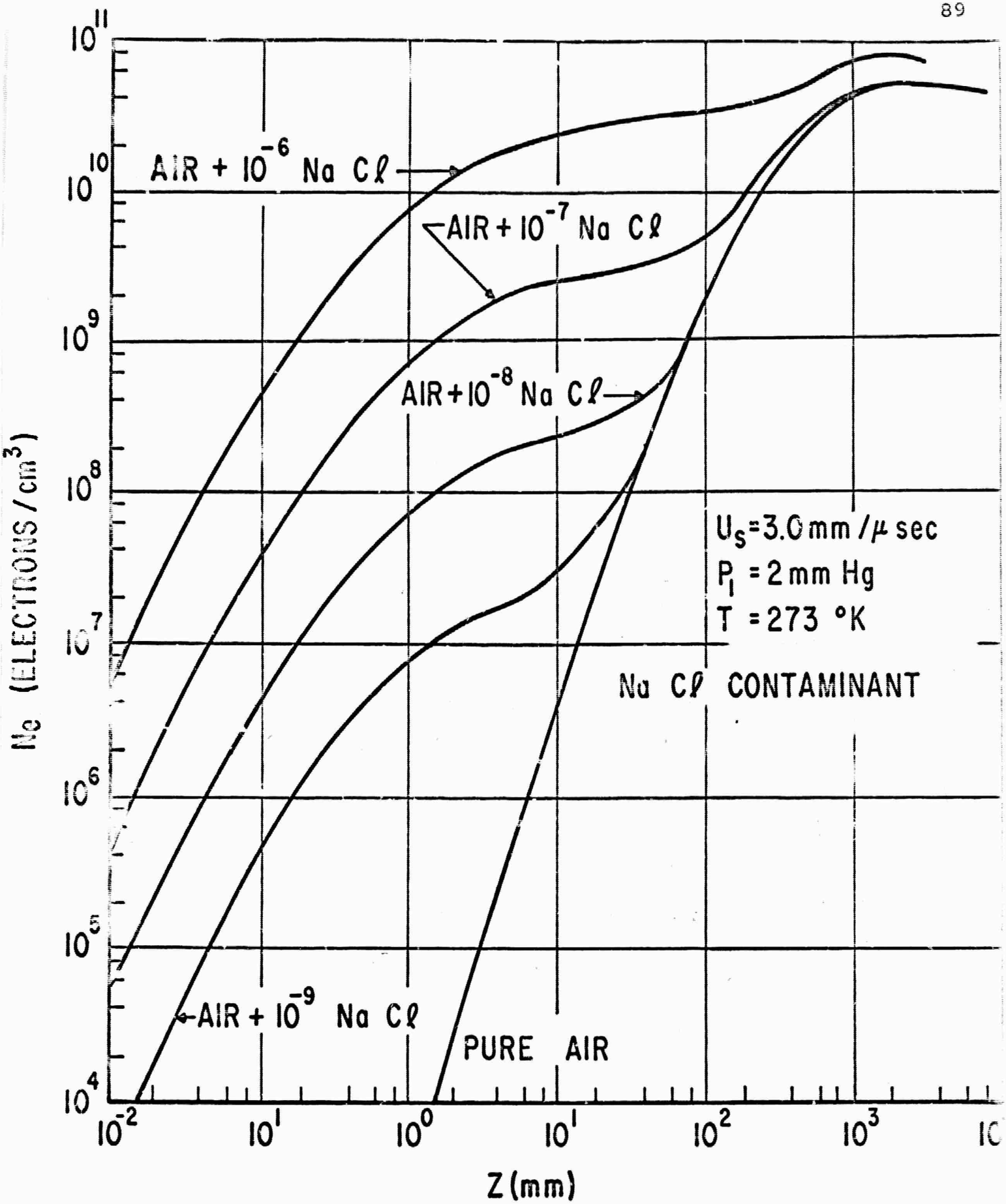

FIG. C-3.2 ELECTRON DENSITY BEHIND NORMAL SHOCK IN CONTAMINATED AIR

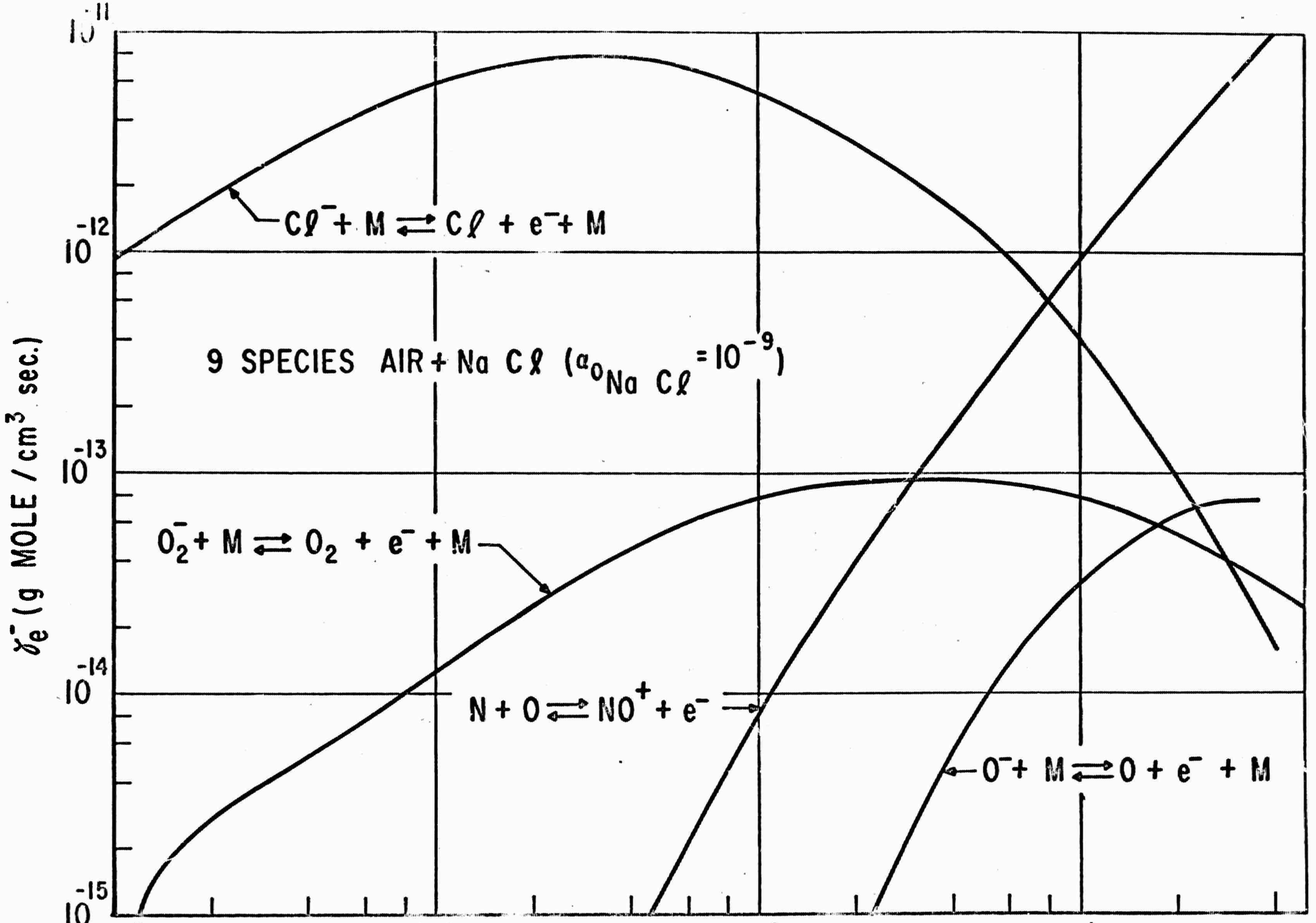

FIG. C-3.3 NET RATE OF ELECTRON PRODUCTION PER REACTION

FIG. C-3.3 NET RATE OF ELECTRON PRODUCTION PER REACTION

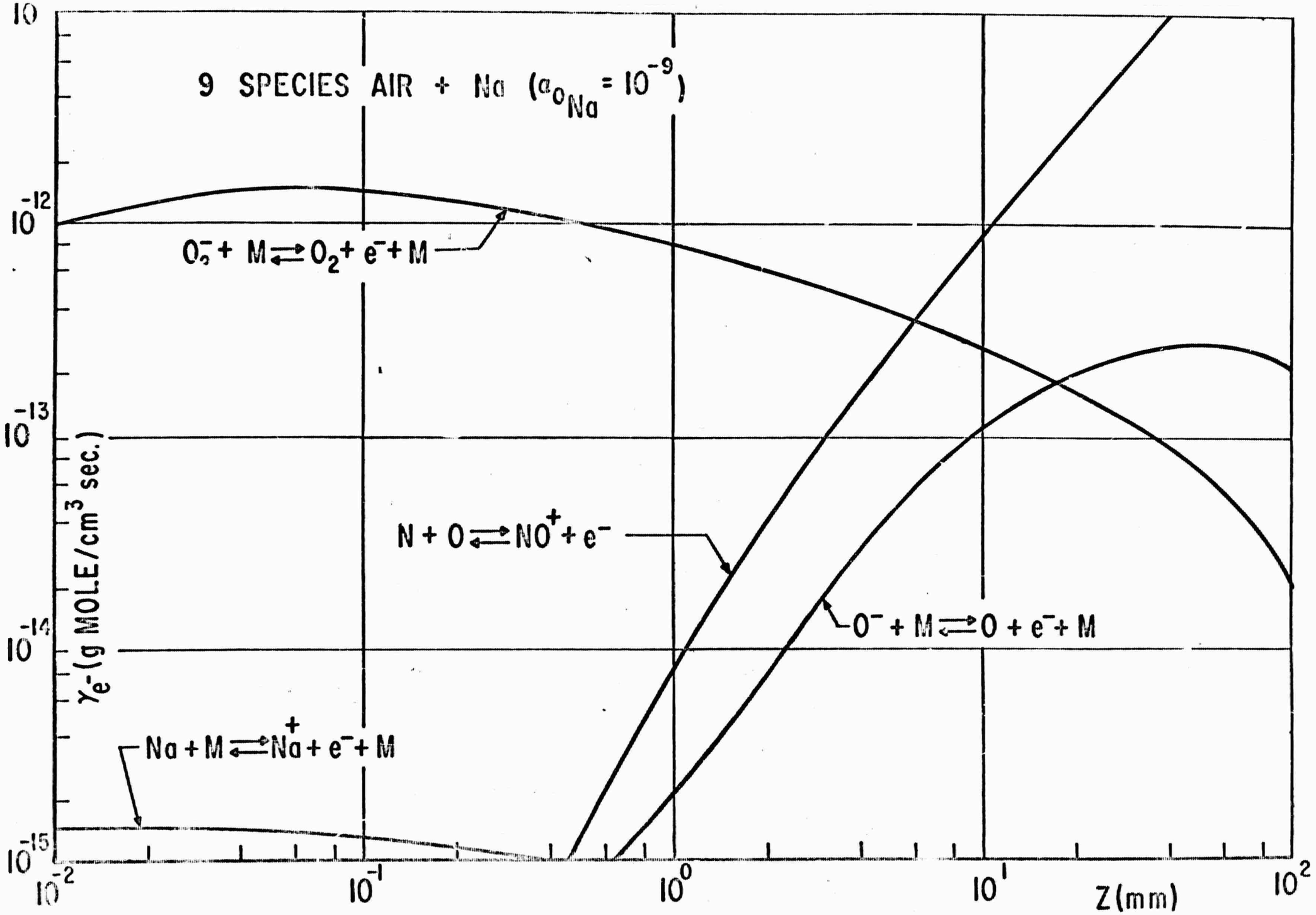

FIG. C-3.4 NET RATE OF ELECTRON PRODUCTION PER REACTION

results, but that for air contaminated with Na the "nine air" model must be used. This is a consequence of the varying importance of different electron-producing reactions. Figures C-3.3 and C-3.4 depict the electron production rates of various reactions used in the "nine air" plus NaCℓ and "nine specie air" plus Na calculations. It can be seen that when NaCℓ is present, the initial production of electrons behind the shock is due to $Cℓ^-$ detachment, and reactions involving O_2^- and O^- are nowhere of importance. On the other hand, when Na is the only contaminant, O_2^- detachment accounts for the initial electron production mechanism. In both situations, far downstream of the shock, the only important electron producing reaction is that of N +O collisional ionization.

C-4 SPECTROSCOPIC SEARCH FOR IMPURITIES

The validity of an analytical model used to represent a physical system is premised on the fact that the components of the physical system are substantially included in the model. When the data obtained from air shock is compared with the model, obviously both the test conditions and the model should represent the same physical system. It is clear from the recent work described in Section C-3 that small amounts of impurities may totally mask the behavior of the "pure" system.

To investigate what impurities do exist in the shock tube system, an extensive spectroscopic study was undertaken. The fundamental tool used was a Jerrell Ash model 75,000 grating spectrograph. This instrument has an extremely large effective aperture ($f \sim 4$). The grating used provided approximately 20 Å/mm dispersion over an exit width of about 15 cm.

Extensive calibration of the instrument has been made using an rf-excited discharge tube. This discharge tube was designed so that any given gas or impurity could be introduced and tested at known pressures. While the conditions of this source are not the same as the shock tube, the basic energy levels of the species are, of course, unaltered, even if the relative intensities are dissimilar. Hence, if a specific

impurity is suspected, extensive tests can be made to establish its detailed spectra which can then be used to verify or eliminate the existence of such an impurity in the shocked gas spectra.

A subordinate piece of equipment to the spectrograph is a recording densitometer. A somewhat unique and inexpensive densitometer has been built using the basic parts of the precision enlarging facility used to obtain numerical data from the scope trace.

The spectrographic plate (5 x 7) is loaded in a modified plate holder for the 3 x 4 projector. One-half of the seven-inch plate is enlarged about 15 diameters. This enlargement reduces the requirement for high precision stages and slits usually required in such an instrument. At the normal image focal plane, a set of silicon photo cells, one with a slit, is mounted on a precision platform driven by a synchronous motor. At the lens of the projector, a light chopper is used to achieve about 200 cps fluctuation. The use of the fluctuating light source allows the use of narrow band ac amplifiers to increase the output from the photo cells, thus simplifying the design of the amplifiers and minimizing the effects of changes in ambient lighting conditions.

Two photo cells are used, one with a narrow slit (.010") to sample the trace, and the other with no slit (¼" sq. in area) to sample the unexposed part of the plate. The outputs from the amplifiers for these two photo cells are put in bucking series in a diode detecting circuit. The purpose of the two photo cells is to compensate for changes in "fogging" conditions and remove zero drift due to changes in light intensity. In actual use no discernable drift has been observed even for intensity changes of a factor of two. The detected compensated output is recorded on a 10" synchronous driven strip recorder.

The overall system from spectrograph to output chart is repeatable to better than .1% enabling an absolute line location to better than 3.0 Å out of 3000 Å, which is twice the minimum resolution of the spectrograph.

Three specific observations of the emission spectra produced by the shocked gas were made. First, an "end on" measurement was obtained by placing a window at the end of the shock tube. Second, a side view was attempted using a window upstream of end. Third, a photoelectric measurement was made which provided the time history of the emission behind the incident shock.

"End on"Observation

The most easily obtained integrated spectra is provided by terminating the shock tube with a window and collecting the light emitted from the incident and reflected shock. The intensity of the light thus produced is sufficient so that

the event may be easily recorded on Tri X film with adequate resolution. Unfortunately, approximately 99% of the recorded intensity is due to the reflected shock. The unfortunate aspect is presented by the fact that the emission spectra contains species that may have been introduced from the walls and window by mixing. In addition the interface and driven gas may also be mixed and heated so that emission may occur from the gases and impurities carried down the tube.

With all these unsatisfactory conditions, the overriding problem of adequate light is satisfactorily solved and the information obtained represents the total aggregate of species in the system. While this provides broad limits on the total impurities, no correlation can be obtained as to if the species are located directly behind the incident shock, the region important to the electron density profile measurement.

The basic experimental arrangement was performed to minimize some of the emission problem discussed above. The entrance lens for the spectrograph was placed so that its focal point was at the inside surface of the end window. Secondly, a system of restricting tubes was used so that the spectrograph admitted light principally from the central part of the shock tube.

The impurities observed using this technique include Na, C, Fe, Ni, Co, Mn. The strong presence of the metallic elements was further investigated by the following technique. The spectra from an arc using stainless steel electrodes was recorded. A negative of this spectra with a sodium line for location was printed. This "mask" was placed in the exit plane of the spectrograph and a photo cell placed behind the mask. A second photo cell was placed to record the incident light to the spectrograph. An electrical difference between the photo cells was formed. After suitable gain adjustments, the results clearly indicate that primarily all of the stainless steel "emission" was associated with the arrival of the shock interface.

To avoid the mixing problems encountered in the stagnation region, several attempts were made to record with film the spectra emitted by the plasma directly behind the incident shock by using a window on the side of the tube. The major and defeating problem encountered was the extremely low levels of light intensity. Even by using a glass tube section so that light could be gathered from the largest possible area, and by processing Tri X film to an estimated ASA speed of 2000, no usable image could be obtained. By making a multiple exposure of thirty shot with the best conditions, only faint Na lines were visible.

As a final solution to the light problem the spectrograph was instrumented with 5 sensitive photomultipliers (1P28). The photomultipliers were positioned behind a series of slits located in the exit plane of the spectrograph. The slits were made adjustable to cover the equivalent of from 1 to 10 Å. The housing and sockets for the photomultipliers were provided with circulation passages and insulation so that the entire ensemble could be cooled toward liquid nitrogen temperatures to reduce noise.

Because of the extreme sensitivity problems anticipated, a special stabilized power supply and 3 decade logarithmic amplifiers were constructed. The somewhat unique duty cycle requirements of this particular experiment, permitted the design of relatively simple logarithmic amplifiers. However, the rise time requirement of better than 3 μsec severely limited the maximum value of the photomultipliers' load resistors. A parametric study was made to maximize the signal (gain-bandwidth product) to the noise. The amplifier circuits are shown in Fig. C-4.1.

This wavelength amplitude calibration was accomplished by using a standard quartz envelope tungsten ribbon lamp and a light chopper. After computing the emissivity connected black

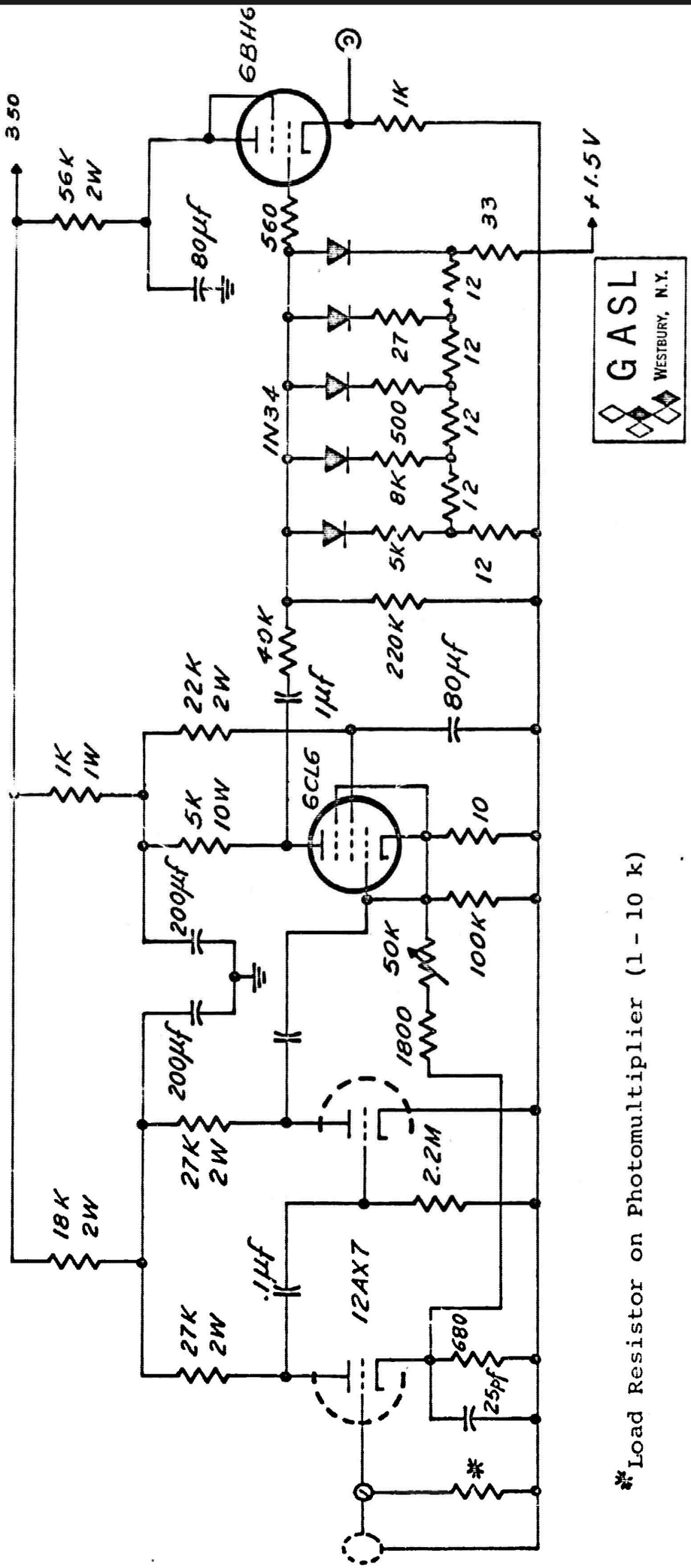

*Load Resistor on Photomultiplier (1 - 10 k)

Fig. C-4.1. Short Duty Cycle Negative Pulse 375 Decade Logarithmic Amplifier Used with Photomultipliers

body radiation curve, the individual photomultipliers were checked over the spectral range. By interchanging individual tubes to compensate for their particular sensitivities, an arrangement was found that closely matched the expected black body curve except for the red region as shown in Fig. C-4.2. Because of the inherent deficiency of the 1P28 photomultipliers in the red region (about 5900 Å), the factor of ten compromise was made.

For simplicity and interchangeability of amplifiers, the gain adjustment was ultimately made by small variations in the photomultipliers load resistors.

The wavelength vs. grating position for each slit was achieved using a low pressure Hg discharge tube. This light from the tube was chopped (synchronously with the power line) and the output from the photomultipliers recorded by a strip recorder (one channel at a time). The grating was slowly rotated with a gear-reduced synchronous motor. This procedure minimized backlash and jitter in the grating rotation system. The location of 13 principal lines was noted. These locations were least square-fit to a third order equation (nine fold redundancy) and an accurate set of grating angle vs. wavelength tables for each slit computed.

The shock tube measurement using the photoelectrically instrumented spectrometer was made from the side wall upstream

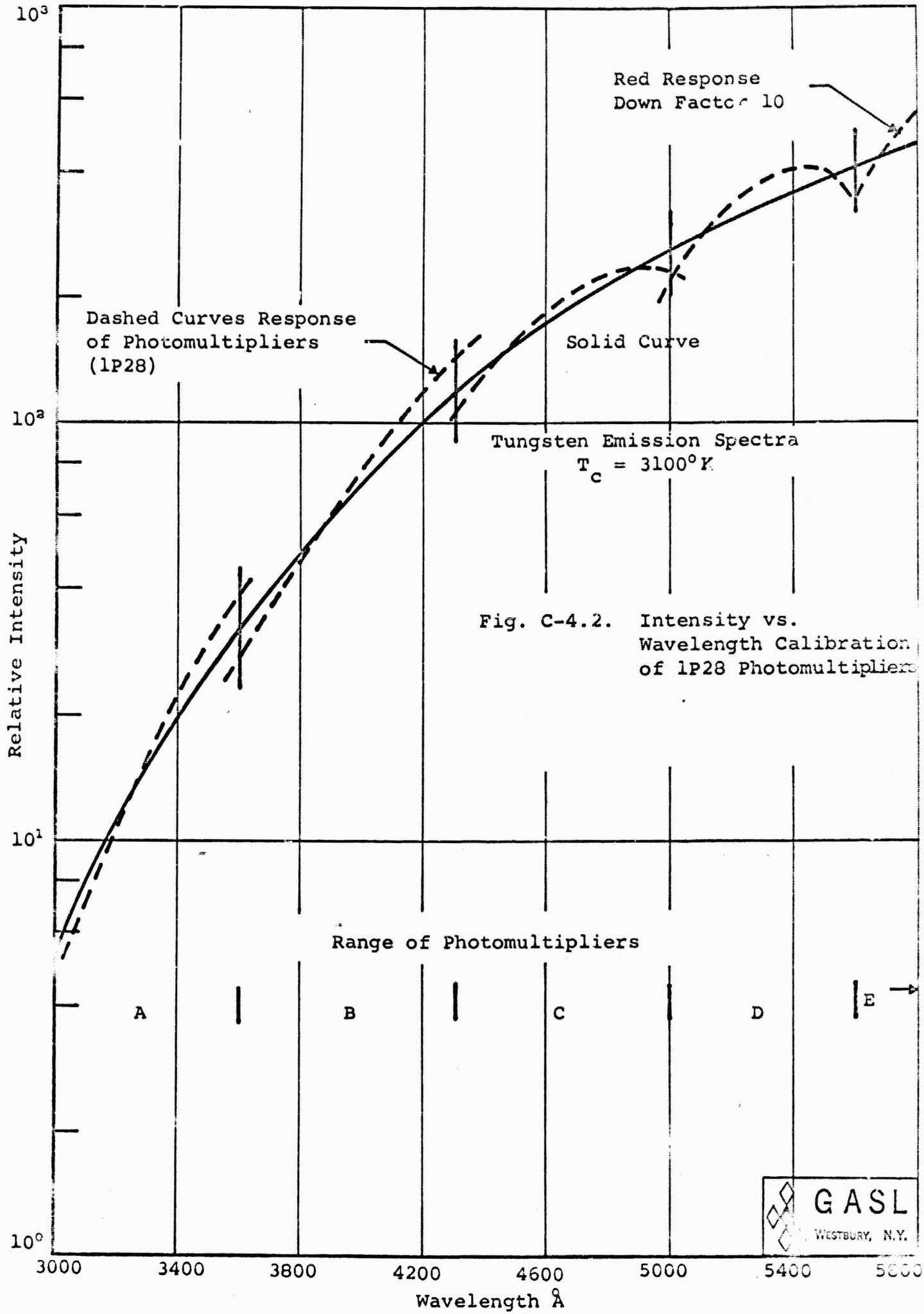

Fig. C-4.2. Intensity vs. Wavelength Calibration of 1P28 Photomultipliers

of the end. The window was contoured quartz about 2 cm diameter. It was found necessary to liquid nitrogen cool the photomultipliers to reduce the noise as anticipated. The shock conditions were maintained M ~9, 1 mm Hg initial pressure. The repeatability of the test conditions were within 1% in shock velocity by using the mechanical valve as driver. An auxiliary photo-sensitive cell was used to monitor the total light output. The integrated power recorded ranged typically within 5% of the average.

Because of the multiplicity of lines, it was necessary to reduce the effective exit slit width to 2 Å. On this basis, to cover the complete spectra about 250 shots would have been required. Unfortunately time would not permit the complete data recording process with the accompanying enormous data reduction that would be required (analysis of 1250 pictures). Instead, selective regions of the spectra were chosen for detailed analysis. Some of these selected lines (2 Å wide) are shown in Fig. C-4.3.

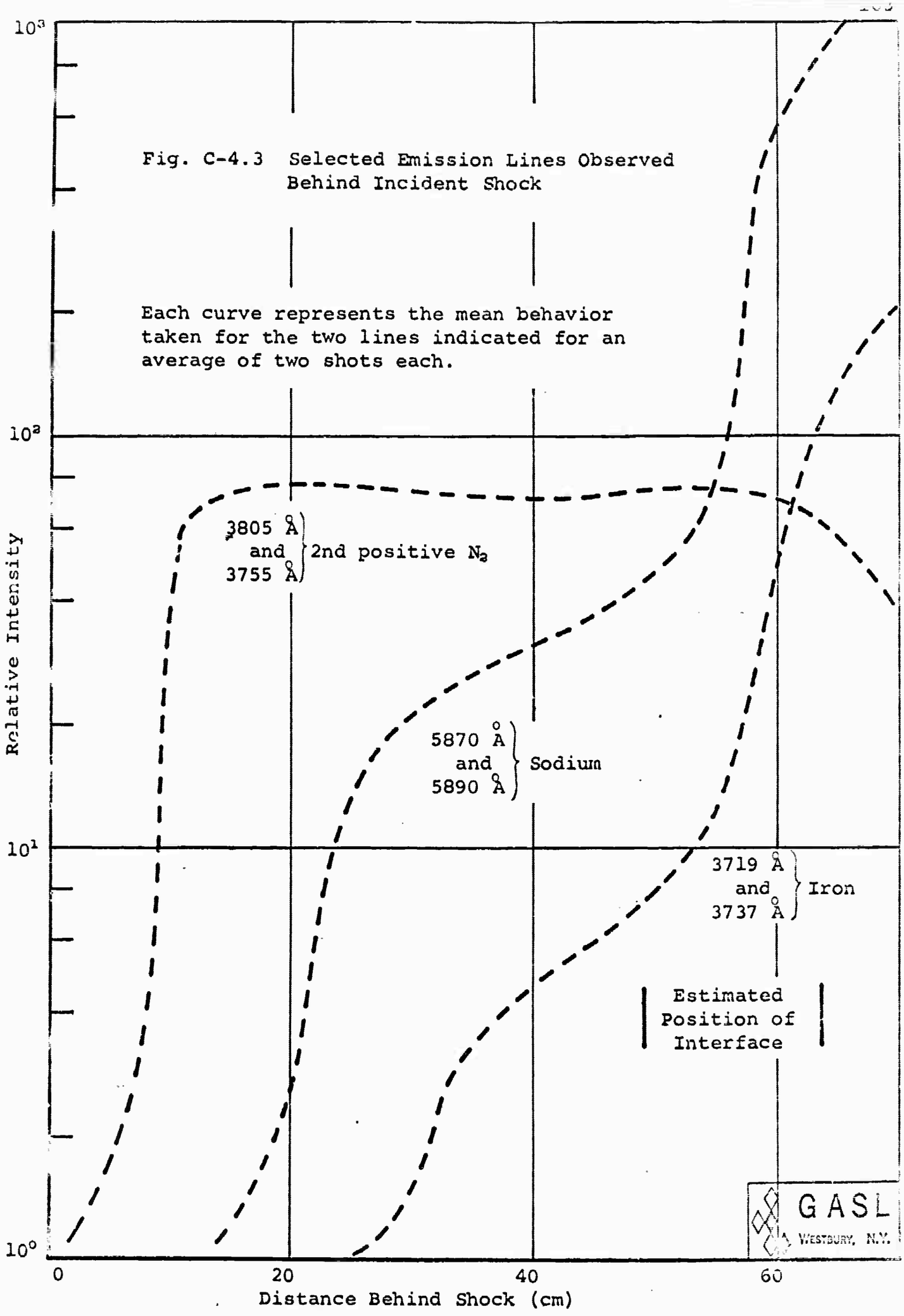
Fig. C-4.3 Selected Emission Lines Observed Behind Incident Shock
Each curve represents the mean behavior taken for the two lines indicated for an average of two shots each.
Relative Intensity
10^3
10^2
10^1
10^0
3805 Å and 3755 Å } 2nd positive N_2
5870 Å and 5890 Å } Sodium
3719 Å and 3737 Å } Iron
Estimated Position of Interface
0
20
40
60
Distance Behind Shock (cm)
GASL
Westbury, N.Y.

C-5 COMMENTS ON THE EXPERIMENTAL AND COMPUTED ELECTRON DENSITY PROFILE

The basic shock conditions for which this comparison has been made were detailed in Section B-3. The specific velocity and initial pressure correspond to Mach 8.9 shock (3025 m/s) at initial pressure of 134,000 feet altitude (2.0 mm Hg). The experimental curve in Fig. C-5.1 was taken from the "mean" determination discussed in Section B-3.3.

The analytically determined curve in Fig. C-5.1 was calculated by the program discussed in Section C-1. The obvious order of magnitude difference in Fig. C-5.1 warrants serious consideration.

The error indicated either lies with the analytical model used for the computed curve or with the experimental technique used to measure the electron density profile, or of course, some combination of each.

The experimental technique is discussed in detail in Section B and in particular, Section B-4 provides such supporting evidence as to validate the result within the broad context of the following discussion.

The analytical model may be incorrect because (1) the constituents of the model and that of the experiment differ,

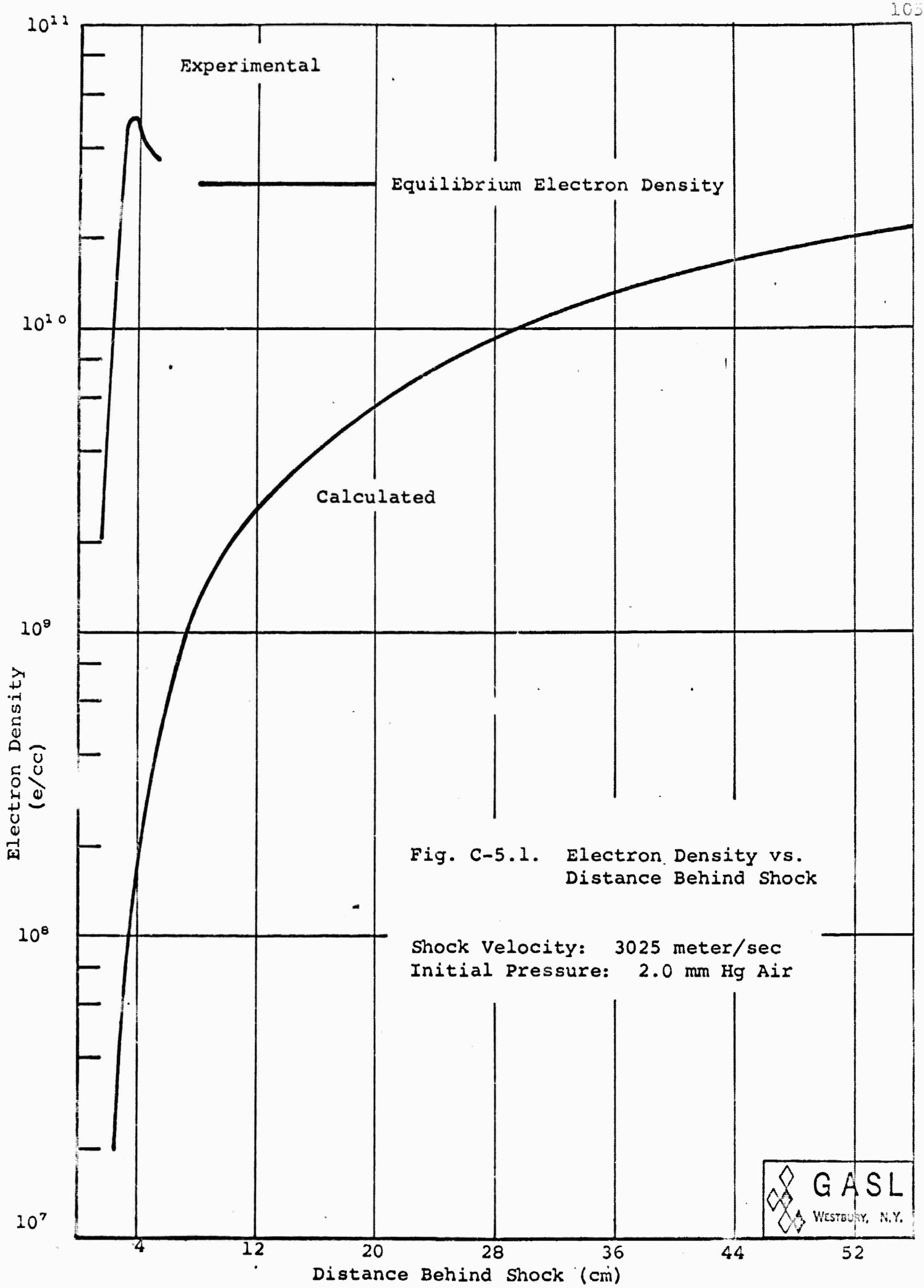

Fig. C-5.1. Electron Density vs. Distance Behind Shock

Shock Velocity: 3025 meter/sec
Initial Pressure: 2.0 mm Hg Air

GASL
Westbury, N.Y.

(2) some rate or energy data is incorrect or (3) the computational procedure is invalid. It is probable that the error is attributable to (1) even though (2) or (3) cannot be totally eliminated. In reference to item (2) several parametric studies have been made to ascertain the sensitivities of the various reactions and reacting systems. These studies showed that no reasonable alteration of constants could be made to satisfy the results of both the local test conditions of this experiment and other data for higher temperature conditions where the numerical analysis is in much better agreement with experiment.

On the other hand in reference to item (1) above, the exclusion of an impurities reacting system could reconcile the apparent difference. In Section C-2, the influence of sodium on the electron rate production is shown. It is clear from the curves in Fig. C-3.2 that for concentrations of salt similar to that approximating natural occurrence near sea water (1 part per 10^6), the electron profile should be extremely steep and yet it may be noted that the equilibrium levels are essentially unaltered. Since the experimental results easily fall between the "pure" air case and the slightly contaminated cases, it is likely that sodium or a similar agent could account for the difference observed.

It is worthy to note that the results presented in Section C-2 assume that the sodium occurs uniformly in the gas prior to the shock arrival. From the time resolved spectroscopic data in Fig. C-4.3A the initial threshold observance of the sodium emission occurs 15 cm behind the shock front and then increases rapidly. In addition it may be noted that the iron emission follows roughly the same behavior at a later time, but before the shock interface. The suggestion of this data is that the sodium, like the iron, is coming from the walls and is mixed and diffused into the shocked region. With this mechanism working, the initial reacting region behind the shock could be behaving as the "pure air" model suggests while the region slightly upstream of the shock front may be influenced by the sodium diffusing and mixing from the walls. One piece of evidence missing from this analysis is the threshold sensitivity of the spectrographic system to sodium. Unfortunately the experiment evaluation of this threshold is complicated and could not be attempted.

CHAPTER V

THEORETICAL STUDIES ON NON-UNIFORM PLASMAS

D-1 INTRODUCTION

The following chapter contains a summary and review of some of the analytical work generated as an adjunct to the experimental work. The first section considers the general analysis of the electromagnetic properties of non-uniform plasmas from microscopic and macroscopic considerations. Section two presents a detailed analysis of diffusion effects in a non-uniform plasma. Section three considers the electromagnetic propagation characteristics of a shock tube produced plasma with a radially non-uniform plasma density.

It is well known that in a first order approximation, the propagation of an electromagnetic wave may be analyzed with a simplified scheme in which the local properties of the ionized gas are given by the plasma frequency and the constant collision frequency. Even in this case the solution of two- or three-dimensional propagation problems may present tremendous mathematical difficulties. On the other hand, in a general case for a non-uniform gas, the effort required to solve these problems is not justified due to the oversimplified scheme of

the electrical properties of the gas. When the change of the macroscopic thermodynamic properties of the gas becomes important in a length of the same order of magnitude of a wavelength of the electromagnetic field, it becomes necessary to analyze the possible effects of additional phenomena such as the transport process, the anisotropic behavior of the electrical properties, the electrical polarization of the medium, etc. Furthermore, the coupling between transverse oscillations and coherent longitudinal electron oscillations may become a significant factor leading to a substantial increase of the dissipation of electromagnetic energy in thermal energy in the ionized gas. If the relative importance of these phenomena could be properly evaluated from the theoretical standpoint, then it would be possible to define the set of parameters which govern the behavior of an ionized gas for each particular case. The major difficulty of a theoretical approach is due to the fact that it requires detailed information about the microscopic processes, which at the present time is rather incomplete, particularly for the case of weakly ionized air as encountered in flight conditions.

D-2 ELECTROMAGNETIC PROPERTIES OF NONUNIFORM PLASMAS

(1) Microscopic Considerations (Ref. 4)

The effect of microscopic inhomogeneities on the electromagnetic characteristics of a plasma are of interest. In order to estimate such effects it is necessary to calculate certain distribution functions, directly deducible from Boltzmann's equations. If inhomogeneities are present (due to gradients of concentration, of temperature, etc.) as far as we know, no actually developed method of calculation exists.

For this reason we decided to examine various models beginning with the simplest ones:

(a) Plasma assumed to be a weakly ionized Lorentzian gas, considering electrons and neutral molecules and neglecting Coulomb interactions.

(b) Three-component plasma (electrons, ions, neutral molecules) taking Coulomb interactions into account.

Since the analysis of model 2 has appeared particularly difficult from a general point of view (for the reason it implies the solution of a system of Boltzmann's equations), first of all we decided to carry out in a detailed way, a

method of actual calculation, in order to face the simplest model 1 even if it is not very realistic. In addition, for the scheme 1 we have decided to examine separately the various inhomogeneity effects and also, to keep near to the model studied from the macroscopic viewpoint, we have selected the detailed examination of the influence of temperature gradient in a slab containing the plasma, whose walls are absorbing and emitting with a Maxwellian distribution.

The complete physico-mathematical characteristics (in our opinion not so wholly developed in the literature) of model 1 are described up to the deduction of final equations.

In addition, a known analytical method used for solving the equations of Section 1 (series expansion of eigen functions of the collision operator) is described.

(2) Macroscopic Properties (Refs. 3 and 4)

The electromagnetic properties of a macroscopically neutral non-uniform plasma are considered by an approach based on the thermodynamics of irreversible processes. A three-fluid model of the plasma is assumed and, in this first stage, the plasma is considered to be at rest in a suitable reference frame, the components are in mutual thermal equilibrium and imposed magnetic fields are absent. The non-uniformities are

those connected with the presence of gradients of state parameters such as temperature, pressure and concentrations.

The presence of these gradients induces a polarization in the medium even in the absence of external electric fields. It will be shown that, in the stationary state, the induced polarization depends on only two independent gradients, which, for convenience, are taken to be those of the temperature and the pressure. An expression for the induced polarization is derived, which is valid for a most general case which is later simplified to the case of the imperfect Lorentz gas (i.e., weakly ionized plasma for which the mass ratio ξ between the negative charge carriers and neutral molecules is much smaller than one) and the perfect Lorentz gas (i.e. weakly ionized plasma with $\xi = 0$).

The phenomenological coefficients relating the induced polarization to the temperature and pressure gradients are first expressed in terms of thermodynamic properties of the plasma. It is then shown how these coefficients can be expressed only in terms of simple binary diffusion coefficients and thermal diffusion coefficients pertinent to the plasma constituents. This last step furnishes the linking element between the present macroscopic approach and the more refined,

but usually less general, statistical approach. Indeed it indicates how the subject phenomenological coefficients can be rigorously evaluated, in terms of the "microscopic" characteristics of the plasma constituents, once the statistical approach has gone far enough to provide workable results. In the meantime, however, the fact that one needs to know only the binary transport coefficients provides a possibility of readily performing order of magnitude analysis by utilizing the available experimental data on electron-ions, electron-molecules and ion-molecules collisions.

The results of the present stage of the analysis already open up two possible ways of utilization, both of noticeable interest.

In the first place, as mentioned before, several order-of-magnitude comparative analyses can be carried out. For instance, one can evaluate the relative importance of the different inhomogeneities with respect to the polarizations they are able to induce (e.g., is a temperature or a pressure gradient more important to this effect?). Also, one can compare the polarization induced by the inhomogeneities with that induced by an external electric field and thus determine the ranges within which the former one can be neglected and the medium treated as homogeneous.

The second application of equal practical interest follows from the consideration of the electromagnetic field which is created by the induced polarization (which, in principle, can be computed by evaluating the Hertz potential whose source is the induced polarization). When we induce into the plasma a polarization by means of controlled suitable inhomogeneities, part of the energy furnished to maintain the gradients is spent to "create" the induced electromagnetic field. This is nothing but the underlying idea of energy conversion systems and the present results can be used to investigate both the feasibility and efficiency of a number of such systems.

The steps of the analysis reported are as follows:

The irreversible thermodynamic description of the system is performed. The extensive and intensive state parameters and the pertinent mass and energy fluxes for a mixture of three fluids, of which two have negative and positive charges, are defined. The "kinetic" relations between fluxes and generalized forces are established and, through suitable use of the basic theorems of the thermodynamics of irreversible processes, the general expression for the mass fluxes in terms of pressure, temperature, the electric potential (Φ) gradients and thermodynamic properties of the plasma is arrived at.

The general expression for the polarization is obtained, for a macroscopically neutral plasma, in the form:

$$\text{grad } \Phi = \alpha_1 \text{ grad } T + \alpha_2 \text{ grad } p$$

where the α_i are phenomenological coefficients. Their expression in terms of the thermodynamic properties of the plasma is also derived in this section, both for the general case and for the simplified case of the Lorentz gas.

The problem of relating the coefficients α_i to binary transport coefficient is considered. By suitable transformation of fluxes and affinities it is shown how they can be expressed in terms of three binary diffusion coefficients D_{12}, D_{23}, D_{13} and two thermal diffusion coefficients, D_1^T, D_2^T, which refer to the plasma constituents. General expressions are presented but no attempt is yet made to either simplify them or evaluate their comparative order of magnitude.

(3) Electromagnetic Properties of Non-uniform Plasmas in Thermal Equilibrium, Isotropic Case (Ref. 3)

Using the three fluid models and an approach based on the thermodynamics of irreversible processes, the effect of non-uniformities due to gradients of state parameters (temperature and density) on the electromagnetic properties are considered. The presence of these gradients induces an electric field

(i.e.f.) in the medium, even in the absence of external electric fields. It will be shown that, in the stationary state and in conditions of macroscopic neutrality, the induced e.f. depends only on one independent gradient which, for convenience, is taken to be that of temperature. An expression for the i.e.f. is derived, which is valid for a most general medium and which is later simplified to the case of an imperfect Lorentz gas (i.e., weakly ionized plasma for which the mass ratio between the negative charge and neutral molecules is much smaller than one).

The electrical conductivity σ defined as the ratio between the electric current I and the electric potential gradient in a first-order stationary state in which a given non-uniform distribution of $\nabla \Phi$ is maintained on the boundaries of a system is also determined.

The phenomenological coefficients are first expressed in terms of thermodynamic properties of the plasma. It is shown how these coefficients can be expressed in terms of only simple binary molecular diffusion coefficients and thermal diffusion coefficients pertinent to the plasma constituents.

This last step makes it possible, by utilizing the available experimental and/or theoretical data on electron-ion,

electron-molecule, and ion-molecule collisions, to express the phenomenological coefficients in terms of the local thermodynamic state of the medium. It was possible to observe that the i.e.f. increased with the temperature difference and the degree of ionization. These results qualitatively agree with the theoretical conclusions which are arrived at in the present report.

The steps of the analysis are as follows: Part 1, the irreversible thermodynamic description of the system is performed. The extensive and intensive state parameters and the pertinent mass and energy fluxes for a mixture of three fluids, one with negative and one with positive charges, are defined. The dynamic relations between fluxes and generalized forces are established and, through suitable use of the basic theorems of the thermodynamics of irreversible processes, the general expression for the mass fluxes in terms of electron concentration, temperature, and electric potential gradients is arrived at. Parts 2 and 4, the general expressions for the i.e.f. and the electrical conductivity are obtained. Part 3, the problem of relating these phenomenological coefficients to binary transport coefficients is considered. By suitable transformation of fluxes and affinities it is shown how they can be expressed

in terms of three binary diffusion coefficients D_{12}, D_{23}, D_{13} and two thermal diffusion coefficients D_1^T, D_2^T, which refer to the plasma constituents.

In addition, the evaluation of the molecular and thermal diffusion coefficients for a plasma is carried out and in Part 2 an analysis of the order of magnitude for the transport coefficients is performed for the case of a weakly ionized imperfect Lorentz's gas.

D-3 DIFFUSION EFFECTS IN A NON-UNIFORM PLASMA

(1) Basic Equations

In the experimental conditions encountered in the shock tube measurement the gas is still weakly ionized. Therefore, in a theory describing the electric properties of the gas, the collisions between charged particles may be neglected and only electron-neutral collisions and ion-neutral collisions will be taken into account. Furthermore, one neglects the perturbation of the neutral component of the gas due to the ionization and recombination processes and to the motion of the charged particles. Thus the electron and ion momentum equations are written in the form:

$$\left.\begin{aligned} n_e m_e \left[\frac{\partial}{\partial t} + \vec{u}_e \cdot \nabla\right] \vec{u}_e &= - n_e q \vec{E} - \nabla p_e - \frac{m_e m_n}{m_e + m_n} n_e \nu_e (\vec{u}_e - \vec{u}_n) \\ n_i m_i \left[\frac{\partial}{\partial t} + \vec{u}_i \cdot \nabla\right] \vec{u}_i &= n_i q \vec{E} - \nabla p_i - \frac{m_i m_n}{m_e + m_n} n_i \nu_i (\vec{u}_i - \vec{u}_n) \end{aligned}\right\} \quad \text{(D-1)}$$

In Eq. (D-1) no external electromagnetic field is applied to the plasma and $\vec{E}$ is the intensity of electric field induced by a small space charge distribution; $\vec{u}_i$, $\vec{u}_e$, $\vec{u}_n$, are the ion, electron and neutral particles average velocities; n_i, n_e, are the ion and electron densities and q is the value of the elementary electric charge, m_i, m_e, m_n, are the ion, electron and neutral particle masses and

$$\frac{m_e m_n}{m_e+m_n} \approx m_e \ , \quad \frac{m_i m_n}{m_i+m_n} \approx \frac{1}{2} m_i \tag{D-2}$$

ν_e is the collision frequency of an electron with the neutral particles and ν_i is the collision frequency of an ion with the neutral particles. One assumes that electrons and ions are in thermal equilibrium with the neutral gas. Thus if the temperature T is assumed constant throughout the plasma, one has:

$$\nabla p_e = k T \nabla n_e \ , \quad \nabla p_i = k T \nabla n_i \tag{D-3}$$

where k is the Boltzmann constant. The left side of Eq. (D-1) corresponds to the electron and ion accelerations. Let us confine the analysis to a steady state situation where $\partial/\partial t = 0$. Outside of the plasma sheet at the wall of the container and in a region of sufficiently small gradients of electron and ion densities, the acceleration terms are negligible compared to the last terms on the right side of Eq. (D-1), and the momentum equations may be written again in the form:

$$\left.\begin{aligned} n_e \vec{u}_e &\simeq n_e \vec{u}_n - D_e \nabla n_e - n_e \mu_e \vec{E} \\ n_i \vec{u}_i &\simeq n_i \vec{u}_n - D_i \nabla n_i - n_i \mu_i \vec{E} \end{aligned}\right\} \tag{D-4}$$

where

$$\left.\begin{aligned} \mu_e &= \frac{q}{m_e \nu_e} \qquad D_e = \frac{kT}{m_e \nu_e} \\ \mu_i &= \frac{2q}{m_i \nu_i} \qquad D_i = \frac{2kT}{m_i \nu_i} \end{aligned}\right\} \tag{D-5}$$

μ_e, μ_i, are the electron and ion mobilities. D_e, D_i are the electron and ion diffusion coefficients. The intensity of electric field is related to the electron and ion densities through the Poisson's equation

$$\nabla \cdot E = \frac{q}{\epsilon_o} (n_i - n_e) \tag{D-6}$$

where ϵ_o is the dielectric permeability or permittivity of vacuum. Furthermore, in a steady state situation the electron and ion continuity equations reduce to

$$\nabla \cdot (n_e \vec{u}_e) = \nabla \cdot (n_i \vec{u}_i) = \dot{n}_e \tag{D-7}$$

where $\dot{n}_e$ indicates the rate of creation of electrons per unit volume; $\dot{n}_e$ depends upon the electrons, ions and neutral particle densities according to the particular ionization and recombination processes which occur in the ionized gas. By virtue of (D-7), from Eq. (D-4) one obtains:

$$\left.\begin{aligned} \frac{1}{\mu_e}\nabla\cdot(n_e\vec{u}_n) - \frac{D_e}{\mu_e}\nabla^2 n_e - \nabla\cdot(n_e\vec{E}) &= \frac{1}{\mu_e}\dot{n}_e \\ \frac{1}{\mu_i}\nabla\cdot(n_i\vec{u}_n) - \frac{D_i}{\mu_i}\nabla^2 n_i + \nabla\cdot(n_i\vec{E}) &= \frac{1}{\mu_i}\dot{n}_e \end{aligned}\right\} \qquad \text{(D-8)}$$

Outside of the plasma sheet and in a region of sufficiently small density gradient, one can assume

$$|n_e - n_i| \ll n_e \qquad \text{(D-9)}$$

Thus the sum of Eq. (D-8) leads to

$$D\,\nabla^2 n_e - \nabla\cdot(n_e\vec{u}_n) + \dot{n}_e = 0 \qquad \text{(D-10)}$$

where

$$D = \frac{\mu_e D_i + \mu_i D_e}{\mu_e + \mu_i} \qquad \text{(D-11)}$$

D is the ambipolar diffusion coefficient.

The local electric current density is given by

$$\begin{aligned} j &= q\,(n_i\vec{u}_i - n_e\vec{u}_e) \qquad \text{(D-12)} \\ &\approx n_e\,q\,(\vec{u}_i - \vec{u}_e) \end{aligned}$$

By virtue of Eqs. (D-4) and (D-9), Eq. (D-12) becomes:

$$\vec{j} \approx q\,(D_e - D_i)\,\nabla n_e + q\,n_e\,(\mu_e + \mu_i)\,\vec{E} \qquad \text{(D-13)}$$

$\vec{E}$ may be written in terms of the electrostatic potential Φ

$$\vec{E} = -\nabla\Phi \tag{D-14}$$

In particular if no electric current is flowing in the plasma, and no external electric field is applied to the gas, Eq. (D-13) reduces to

$$\Phi = \frac{D_e - D_i}{\mu_e + \mu_i} \ell n\, n_e + \Phi_o \tag{D-15}$$

where Φ_o is an arbitrary constant.

From Eq. (D-13) one obtains

$$\nabla\cdot\vec{E} \cong \frac{1}{q(\mu_e+\mu_i)} \vec{j}\cdot\nabla \frac{1}{n_e} - \frac{D_e-D_i}{\mu_e+\mu_i}\left[\frac{1}{n_e}\nabla^2 n_e - \frac{1}{n_e^2}(\nabla n_e)^2\right] \tag{D-16}$$

Hence the difference between electron and ion densities is:

$$n_e - n_i \cong \frac{\epsilon_o}{q^2(\mu_e+\mu_i)} \frac{1}{n_e^2} \vec{j}\cdot\nabla n_e + \frac{\epsilon_o}{q}\frac{D_e-D_i}{\mu_e+\mu_i}\left[\frac{1}{n_e}\nabla^2 n_e - \frac{1}{n_e^2}(\nabla n_e)^2\right] \tag{D-17}$$

It is of interest to observe that Eq. (D-15) implies that in the absence of an electric current, the electrons are trapped in the distribution of electric field due to the space charge in the plasma.

(2) Boundary Conditions

Inside the plasma we assume that the electrostatic potential is zero where the electron density becomes equal to

the equilibrium density n_{e_o}. n_{e_o} is the electron equilibrium density which corresponds to the uniform temperature and density of the neutral particles of the gas. Eq. (D-15) becomes

$$\Phi = \frac{D_e - D_i}{\mu_e + \mu_i} \ln \frac{n_e}{n_{e_o}} \tag{D-18}$$

By virtue of Eqs. (D-5), $D_e >> D_i$, $\mu_e >> \mu_i$. Thus (D-18) reduces to

$$n_e \approx n_{e_o} e^{\frac{q\Phi}{kT}} \tag{D-19}$$

Let the plasma sheet be defined as the small layer adjacent to the wall, where collisions of the charged particles with the neutral particles may be neglected. On the other hand a strong negative potential of the wall with respect to the plasma must arise in order to maintain the condition of zero electric current. Let x_s be the thickness of the plasma sheet, and let us analyze the electron and ion motion in the steady state. One may analyze the motion assuming a one-dimensional problem where the axis x is perpendicular to the wall and $x = 0$ at the wall. If the electrons are almost entirely reflected back into the plasma due to the negative potential distribution in the proximity of the wall, throughout the plasma sheet solution (D-19) is valid, as far as the electron density is concerned.

On the other hand strong accelerations of the ions may be expected in the plasma sheet and the ion momentum equation leads to

$$\frac{1}{2} m_i u_{ix}^2 + q \Phi = \frac{1}{2} m_i u_{ixs}^2 + q \Phi_s \qquad \text{(D-20)}$$

where u_{ixs} and Φ_s are the ion velocity and the electrostatic potential at the edge of the plasma sheet ($x = x_s$). The continuity of ion velocity at $x = x_s$ requires that

$$u_{ixs} \approx - \frac{qD}{kT} \left(\frac{d\Phi}{dx} \right)_s \qquad \text{(D-21)}$$

where $(d\Phi/dx)_s$ is the derivative of Φ at $x = x_s$. Let Φ_o be the electrostatic potential of the wall and assume that ions and electrons recombine as they collide with the wall. The number of electrons reaching the wall per unit time and unit area is

$$n_{e_o} \left(\frac{kT}{2\pi m_e} \right)^{\frac{1}{2}} e^{\frac{q\Phi}{kT}} \qquad \text{(D-22)}$$

On the other hand the ion flow toward the wall per unit area and unit time is

$$- n_i u_{ix} = - n_{is} u_{ixs} \approx \frac{q D n_{e_o}}{kT} e^{\frac{q\Phi_s}{kT}} \left(\frac{d\Phi}{dx} \right)_s \qquad \text{(D-23)}$$

With no electric current at the wall the ion flow must be equal to the electron flow. Thus:

$$- n_i u_{ix} \approx n_{e_o} \left(\frac{kT}{2\pi m_e}\right)^{\frac{1}{2}} e^{\frac{q\Phi_o}{kT}} \tag{D-24}$$

and the ion velocity at $x = x_s$ is:

$$u_{ixs} \approx - \left(\frac{kT}{2\pi m_e}\right)^{\frac{1}{2}} e^{\frac{q}{kT}(\Phi_o - \Phi_s)} \tag{D-25}$$

Thus from Eq. (D-20) one obtains

$$\frac{1}{n_i^2} = - \frac{4\pi m_e q}{n_{e_c}^2 m_i kT} e^{- \frac{2q\Phi_o}{kT}(\Phi - \Phi_s')} \tag{D-26}$$

where

$$\Phi_s' = \Phi_s + \frac{m_i kT}{4\pi m_e q} e^{\frac{2q}{kT}(\Phi_o - \Phi_s)} \tag{D-27}$$

Inside the plasma sheet the Poisson equation reduces to

$$\frac{d^2\Phi}{dx^2} = - \frac{q}{\epsilon_o} n_{e_o} \left[\frac{1}{2} \sqrt{\frac{m_i kT}{\pi q m_e}} e^{\frac{q\Phi_o}{kT}} \frac{1}{\sqrt{\Phi_s' - \Phi}} - e^{\frac{q\Phi}{kT}} \right] \tag{D-28}$$

which may be easily integrated, leading to

$$\frac{1}{2} \left(\frac{d\Phi}{dx}\right)^2 = n_{e_o} \frac{q}{\epsilon_o} \left[\sqrt{\frac{m_i kT}{\pi q m_e}} e^{\frac{q\Phi_o}{kT}} \sqrt{\Phi_s' - \Phi} + \frac{kT}{q} e^{\frac{q\Phi}{kT}} \right] + C \tag{D-29}$$

where C is the integration constant. The constant C is computed with the aid of the boundary condition

$$\frac{d\Phi}{dx} = \left(\frac{d\Phi}{dx}\right)_s \quad \text{at } \Phi = \Phi_s \tag{D-30}$$

Without entering into the details of the solution of Eq. (D-29) one may observe that $d^2\Phi/dx^2$ has a negative or zero value if

$$\frac{1}{2}\sqrt{\frac{m_i kT}{\pi q m_e}}\, e^{\frac{q\Phi_o}{kT}} \frac{1}{\sqrt{\Phi_s - \Phi}} \geq e^{\frac{q\Phi}{kT}} \tag{D-31}$$

i.e.

$$\Phi_s - \Phi \leq \frac{m_i kT}{4\pi q m_e}\, e^{\frac{2q}{kT}(\Phi_o - \Phi_s)} \left[e^{\frac{2q}{kT}(\Phi_s - \Phi)} - 1 \right] \tag{D-32}$$

In particular, condition (D-32) is verified in the proximity of the edge of the plasma sheet ($\Phi \approx \Phi_s$) if

$$\Phi_s - \Phi \leq \frac{m_i kT}{4\pi q m_e}\, e^{\frac{2q}{kT}(\Phi_o - \Phi_s)} \frac{2q}{kT}(\Phi_s - \Phi) \tag{D-33}$$

which requires that

$$\frac{m_i}{2\pi m_e}\, e^{\frac{2q}{kT}(\Phi_o - \Phi_s)} \geq 1 \tag{D-34}$$

By virtue of (D-25), condition (D-34) becomes

$$\frac{1}{2} m_i u_{ixs}^2 \geq \frac{1}{2} kT \qquad \text{(D-35)}$$

If condition (D-35) were not satisfied, the ion density would drop faster than the electron density at the entrance of the plasma sheet and this would be inconsistent with a distribution of electrostatic potential inside the plasma sheet where Φ steadily decreases toward the wall.

(3) Steady State Distribution of a Plasma in a Cylinder

It is of interest to discuss in some detail the consequences of the previous considerations for a situation similar to the experimental conditions in the shock tube. In order to do so, assume a simple case for which the recombination rate of the electric charges is negligible and the electron creation rate may be written in the form

$$\dot{n}_e = \alpha n_e \qquad \text{(D-36)}$$

where α is a function of the neutral particle density alone for a given value of the electron temperature. Equation (D-36) would correspond to an ionization process due to electron-neutral particle collisions. Assume further a cylindrical system of reference r, Φ, z, where $r = r_o$, corresponds to the wall of the cylinder. Furthermore the neutral particle velocity u_n

is assumed to be uniform and parallel to the z-axis and α is assumed to be constant. From Eq. (D-10) one obtains

$$\frac{1}{r}\frac{\partial}{\partial r}\left(r\frac{\partial n_e}{\partial r}\right) + \frac{\partial^2 n_e}{\partial z^2} - \frac{u_n}{D}\frac{\partial n_e}{\partial z} + \frac{\alpha}{D} n_e = 0 \qquad \text{(D-37)}$$

where no Φ dependence of the electron distribution is taken into account. A particular solution of (D-37) in the plasma outside of the plasma sheet is:

$$n_e \approx J_o(\gamma r)\ Z(z) \qquad \text{(D-38)}$$

where z satisfies the equation

$$\frac{d^2 Z}{dz^2} - \frac{u_n}{D}\frac{dZ}{dz} + \frac{\alpha}{D} Z - \gamma^2 Z = 0 \qquad \text{(D-39)}$$

J_o is the Bessel function of the first kind and order zero and γ is a constant to be determined by the boundary conditions. Assume that a steady state situation is found where the electron density is independent of z. In this case the constant γ is referred to the coefficient α and the ambipolar diffusion coefficient through the equation

$$\gamma = \sqrt{\frac{\alpha}{D}} \qquad \text{(D-40)}$$

The radial ion velocity is given by:

$$u_{ir} = - \frac{D}{n_e} \frac{dn_e}{dr} = \gamma D \frac{J_1(\gamma r_s)}{J_0(\gamma r_s)} \tag{D-41}$$

Let r_s be the radius of the edge of the plasma sheet. At the edge of the plasma sheet the space charge separation is negligible. Consequently, by virtue of condition (D-35), the minimum value of u_{ir} at $r = r_s$ must be:

$$u_{ir_s} \approx \sqrt{\frac{kT}{m_i}} \tag{D-42}$$

and by virtue of (D-41) one obtains:

$$\gamma D \frac{J_1(\gamma r_s)}{J_0(\gamma r_s)} \approx \sqrt{\frac{kT}{m_i}} \tag{D-43}$$

Taking into account the definition of the ambipolar diffusion coefficient and assuming that the thickness $r_o - r_s$ of the plasma sheet is small compared to the radius of the cylinder, condition (D-43) leads to

$$\gamma r_o \frac{J_1(\gamma r_o)}{J_0(\gamma r_o)} \approx \frac{\nu_i \, r_o}{4} \sqrt{\frac{m_i}{kT}} \tag{D-44}$$

i.e.

$$\gamma r_o \frac{J_1(\gamma r_o)}{J_o(\gamma r_o)} \approx \frac{1}{2\pi} \frac{r_o}{\sqrt{\lambda_i}} \qquad \text{(D-45)}$$

where

$$\lambda_i = \frac{2}{\nu_i} \sqrt{\frac{2kT}{\pi m_i}} \qquad \text{(D-46)}$$

is the mean free path for the ions. Taking into account that λ_i must be small compared to the radius of the cylinder, Eq. (D-45) reduces to

$$J_o(\gamma r_o) \approx 2.01 \frac{\lambda_i}{r_o} \qquad \text{(D-47)}$$

n_e must be a positive density throughout the plasma. Thus $\gamma r_o < 2.405$ and with $\lambda_i \ll r_o$, Eq. (D-47) leads to the conclusion that the electron density at the edge of the plasma sheet must be small compared to the electron density at the center of the cylinder. It is worthwhile pointing out that condition (D-47) implies that the rate of creation of electrons in the plasma balances the rate at which electrons and ions diffuse toward the wall of the cylinder.

(4) Concluding Remarks

The quantitative solution of the system of equations of Section (1) and of Eq. (D-29) must be carried out in order

to determine the electron density inside the plasma and the thickness of the plasma sheet. Nevertheless, the above considerations indicate that a large effect in the transversal diffusion should be expected due to the large value of the diffusion velocity of the ions at the edge of the plasma sheet. As a relatively simple illustration of the above phenomena, the one-dimensional diffusion effects between two regions of air at different temperatures and separated by a plane boundary are presented in Appendix II.

D-4 ELECTROMAGNETIC PROPAGATION IN A WAVEGUIDE CONTAINING A RADIALLY NON-UNIFORM PLASMA

The object of this section is to study a particular problem of propagation of electromagnetic waves in a plasma contained inside a metallic cylinder. The plasma is assumed to be non-uniform in the radial direction, but its properties are independent of both the axial and angular coordinates.

Specifically, the non-uniform properties of the plasma correspond to an electron density which is a function of the radial coordinate. Furthermore, we assume that the plasma collision frequency is negligible with respect to the frequency of the electromagnetic wave. Such a radial non-uniformity of the plasma can, for example, be attributed to the ambipolar diffusion process of charges which move perpendicular to the metallic wall. An explanation of such a process of diffusion may be found in Section D-3 of this report.

It is known that an infinite number of modes of propagation are found inside a cylinder. In order to analyze the effect of non-uniformity in the most simple case, we shall treat the case where all the components of the electromagnetic field are independent of the coordinate θ, namely the TM_{01} mode. The other modes of practical interest will be studied later.

(1) Analysis of the Problem

Due to the nature of the propagation along the z-axis the solution of the Maxwell equations may be written in the form:

$$\bar{E} = \bar{E}_o \, e^{-ihz+i\omega t} \tag{D-48}$$

$$\bar{H} = \bar{H}_o \, e^{-ihz+i\omega t} \tag{D-49}$$

where $\bar{E}_o$ and $\bar{H}_o$ are functions of r. The quantity h is the eigenvalue which is to be determined from the boundary conditions which shall be stated later.

The system of equations which define the non-zero components of the electromagnetic field is:

$$-\left(hi \, E_{or} + \frac{\partial E_{oz}}{\partial r} \right) = i\omega \, \mu_o \, H_{o\theta} \tag{D-50}$$

$$ih \, H_{o\theta} = -i\omega \, \epsilon_o \, K^2 \, E_{or} \tag{D-51}$$

$$\frac{1}{r} \frac{\partial}{\partial r} (r \, H_{o\theta}) = -i\omega \, \epsilon_o \, K^2 \, E_{oz} \tag{D-52}$$

where K^2 is defined by the expression

$$K^2 = 1 - \frac{e^2 \, n_e}{m_e \, \epsilon_o \, \omega^2} \tag{D-53}$$

According to the discussion in Section D-3 concerning the diffusion inside a cylinder, the differential equation for n_e when the plasma is radially non-uniform is:

$$\frac{d^2 n_e}{dr^2} + \frac{1}{r}\frac{dn_e}{dr} + \frac{\alpha}{D} n_e = 0 \qquad \text{(D-54)}$$

This implies that the electron density which appears in the Eq. (D-53) can be defined, in agreement with Eq. (D-54), by the expressions:

$$n_e = n_{eo}\, J_o\left(\sqrt{\frac{\alpha}{D}}\, r\right) \quad \text{if} \quad \frac{\alpha}{D} > 0$$

$$n_e = n_{eo}\, I_o\left(\sqrt{\frac{\alpha}{D}}\, r\right) \quad \text{if} \quad \frac{\alpha}{D} < 0$$

where n_{eo} is the electron density at the axis of the cylinder.

The system of Eqs. (D-50), (D-51), and (D-52) can be reduced to the solution of the following equation:

$$\frac{d^2 E_{oz}}{dr^2} + \left[\frac{1}{r} - \frac{h^2}{K^2(k^2K^2 - h^2)}\frac{dK^2}{dr}\right]\frac{d\,E_{oz}}{dr} + (k^2K^2 - h^2)E_{oz} = 0 \qquad \text{(D-55)}$$

In this problem the z-component of the electric field has to be zero at the wall. This condition will be used to determine the eigenvalues of h in Eq. (D-55). Since it is not possible to

find a solution to Eq. (D-55) in closed form, the eigenvalues must be found by numerical procedures.

(2) Nondimensional Analysis

As stated previously, a numerical computation is necessary to determine the eigenvalues of h appearing in Eq. (D-55). In order to do this, it is convenient to transform Eq. (D-55) to a nondimensional form. Let us define:

$$\frac{[E_{oz}]}{[E_{oo}]} = E'_{oz}$$

$$[k]\,[r] = \bar{r}$$

$$\frac{[h]}{[k]} = \bar{h}$$

$$\left[\frac{\alpha}{D}\right] \cdot \left[\frac{1}{k^2}\right] = \frac{\alpha}{Dk^2}$$

$$\frac{[\omega^2]}{[c^2]} = [k^2]$$

Thus, we have used [k] in order to reduce the lengths to a nondimensional form and E_{oo}, the electric field at the axis of the cylinder, to reduce the E_{oz} component to a nondimensional form.

If we multiply Eq. (D-55) by $\frac{1}{[E_{oo}]\,[k^2]}$, we obtain:

$$\frac{d^2 E'_{oz}}{d\bar{r}^2} + \left[\frac{1}{\bar{r}} + g(\bar{r})\right] \frac{d\,E'_{oz}}{d\bar{r}} + [K^2 - \bar{h}^2]\,E'_{oz} = 0 \qquad \text{(D-56)}$$

where

$$g(\bar{r}) = \frac{-\bar{h}^2}{(K^2-\bar{h}^2)K^2} \cdot \frac{\partial K^2}{\partial \bar{r}} \qquad \text{(D-57)}$$

From these equations, the eigenvalues of $\bar{h}$ may be determined.

(3) Determination of the Eigenvalues of $\bar{h}$

Equation (D-53) can be written in the form:

$$K^2 = 1 - \frac{e^2 n_{eo}}{m_e \epsilon_o \omega^2} \cdot J_o\left(\sqrt{\frac{\alpha}{Dk^2}}\,\bar{r}\right), \quad \text{if} \quad \frac{\alpha}{D} > 0$$

$$K^2 = 1 - \frac{e^2 n_{eo}}{m_e \epsilon_o \omega^2} \cdot I_o\left(\sqrt{\frac{\alpha}{Dk^2}}\,\bar{r}\right), \quad \text{if} \quad \frac{\alpha}{D} < 0$$

The plasma frequency ω_p^2 at the axis is defined according to the formula:

$$\omega_p^2 \equiv \frac{e^2 n_{eo}}{m_e \epsilon_o}$$

Thus, there are two parameters: $\frac{\alpha}{Dk^2}$ and $\frac{\omega_p^2}{\omega^2}$. These parameters were used in the numerical determination of $\bar{h}$. k was used as a variable.

(4) Results

In order to present the results in a conventional form, $\sqrt{\frac{\alpha}{D}}\,R_o$ and $\frac{\omega_p}{\omega}$ are selected as parameters, where R_o is the radius of the cylinder. The index of refraction of the waveguide, defined according to the following expression:

$$\bar{h} = \frac{h}{k} = \frac{hc}{\omega} = \frac{c}{\omega/h} = \frac{c}{V_f}$$

has been plotted in Figs. 1 - 4 as a function of the signal wave length $\frac{\lambda}{R_o}$ for four values of $\frac{\omega_p}{\omega}$, where $\lambda = \frac{2\pi}{k}$. It is seen that as λ approaches zero, $\frac{c}{V_f}$ must approach 1.

In each of the figures the curve corresponding to the limit case of $\omega_p = 0$ is shown. This particular case is defined by the equation:

$$\frac{c^2}{V_f^2} + \left(\frac{2.405}{2\pi}\right)^2 \frac{\lambda^2}{R_o^2} = 1$$

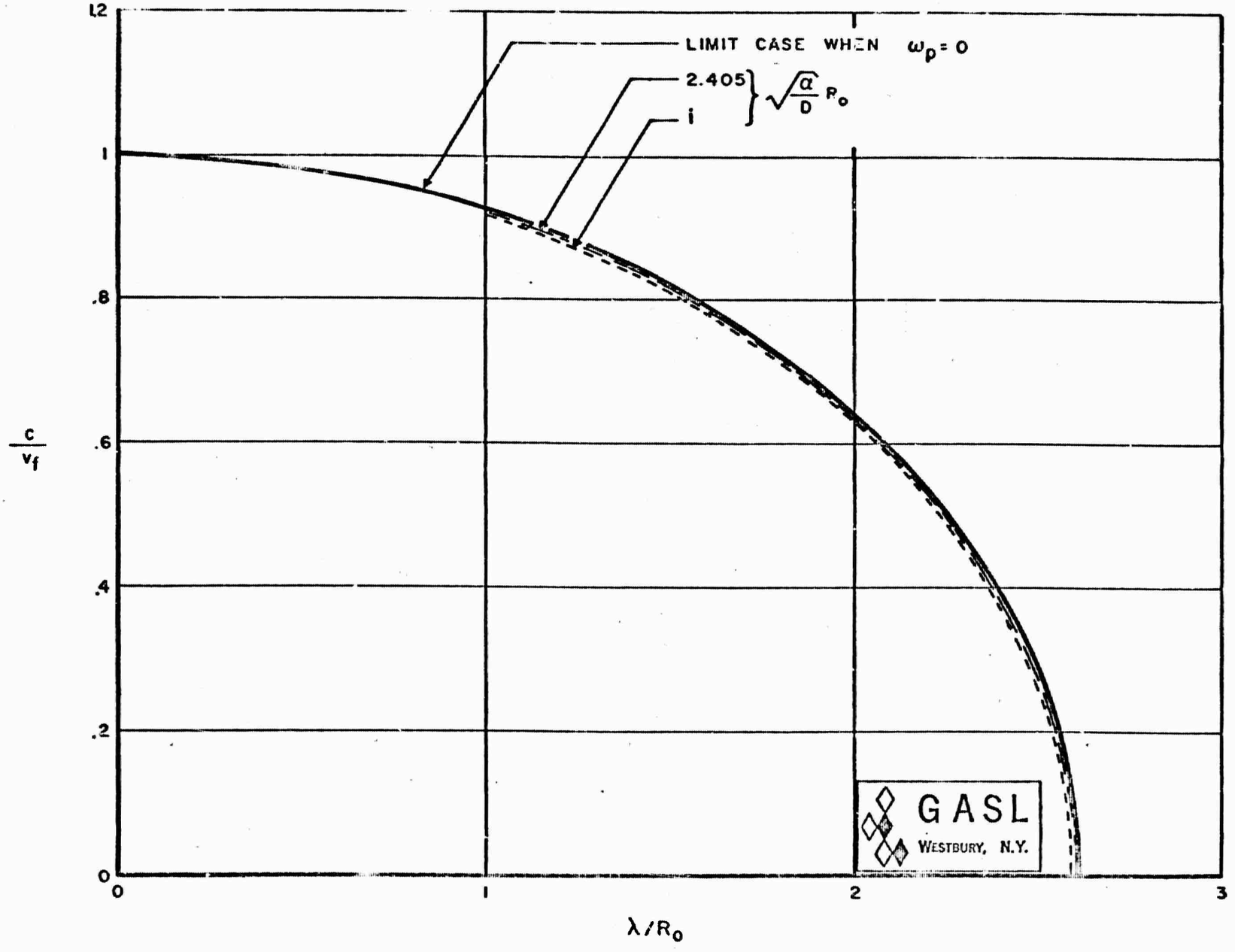

Fig. D-4.1

Wave Guide Index of Refraction as a Function of Signal Wave Length for $\frac{\omega_p}{\omega} = .0, .10$

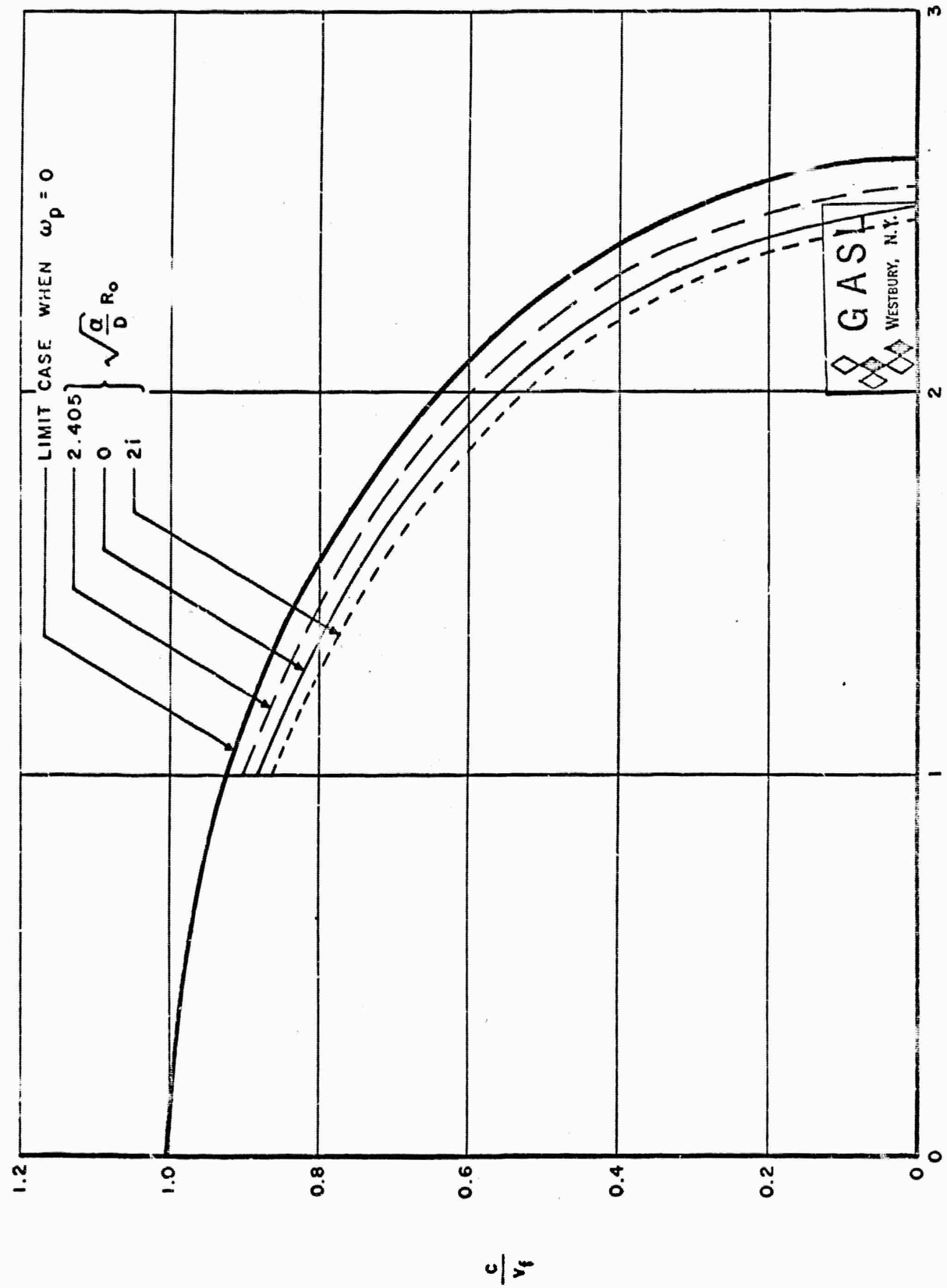

Fig. D-4.2

Wave Guide Index of Refraction as a Function of Signal Wave Length for $\frac{\omega_p}{\omega} = 0.316$

Wave Guide Index of Refraction as a Function of Signal Wave Length for $\frac{\omega_p}{\omega} = 0.316$

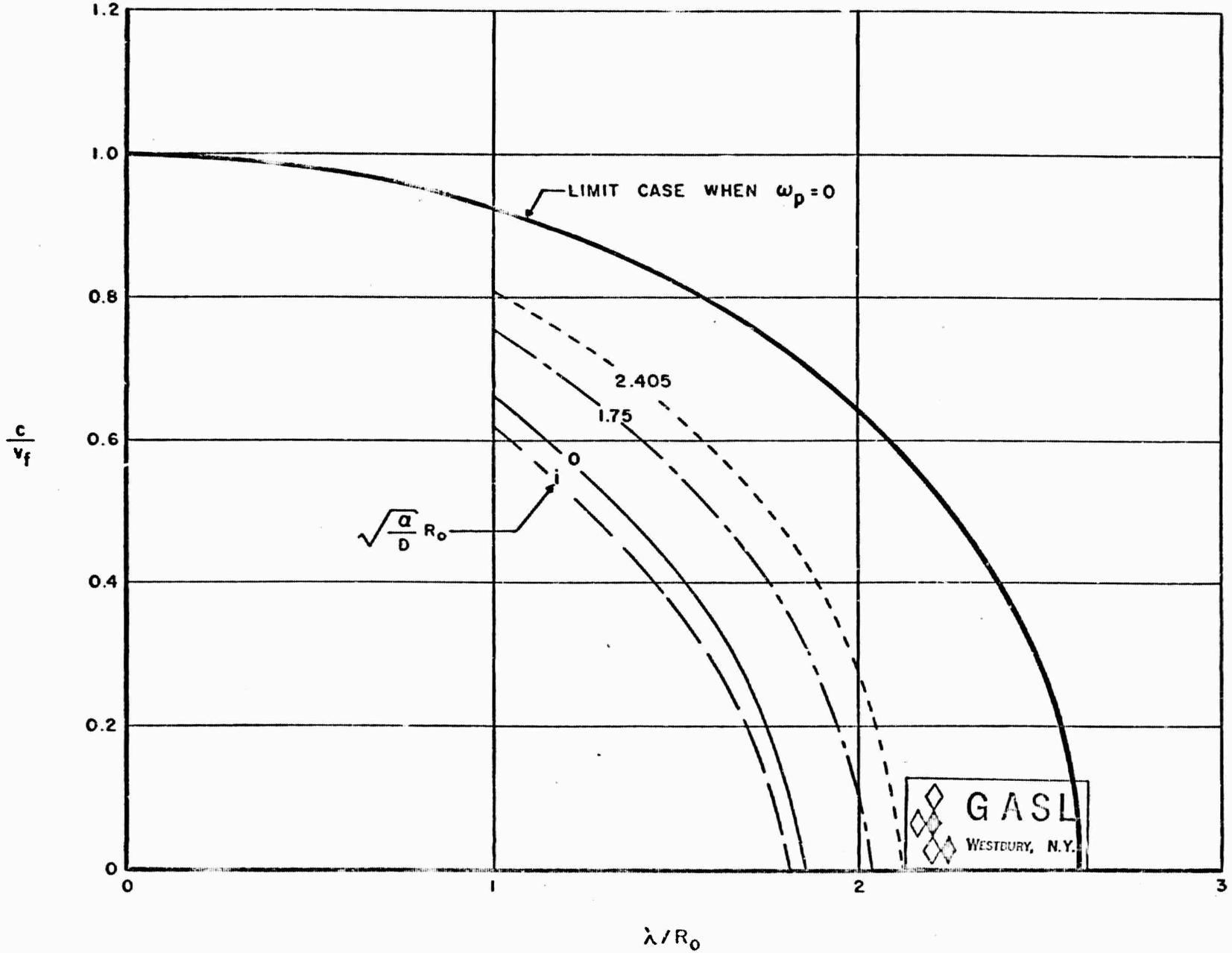

Fig. D-4.3

Wave Guide Index of Refraction as a Function of Signal Wave Length for $\frac{\omega_p}{\omega} = 0.707$

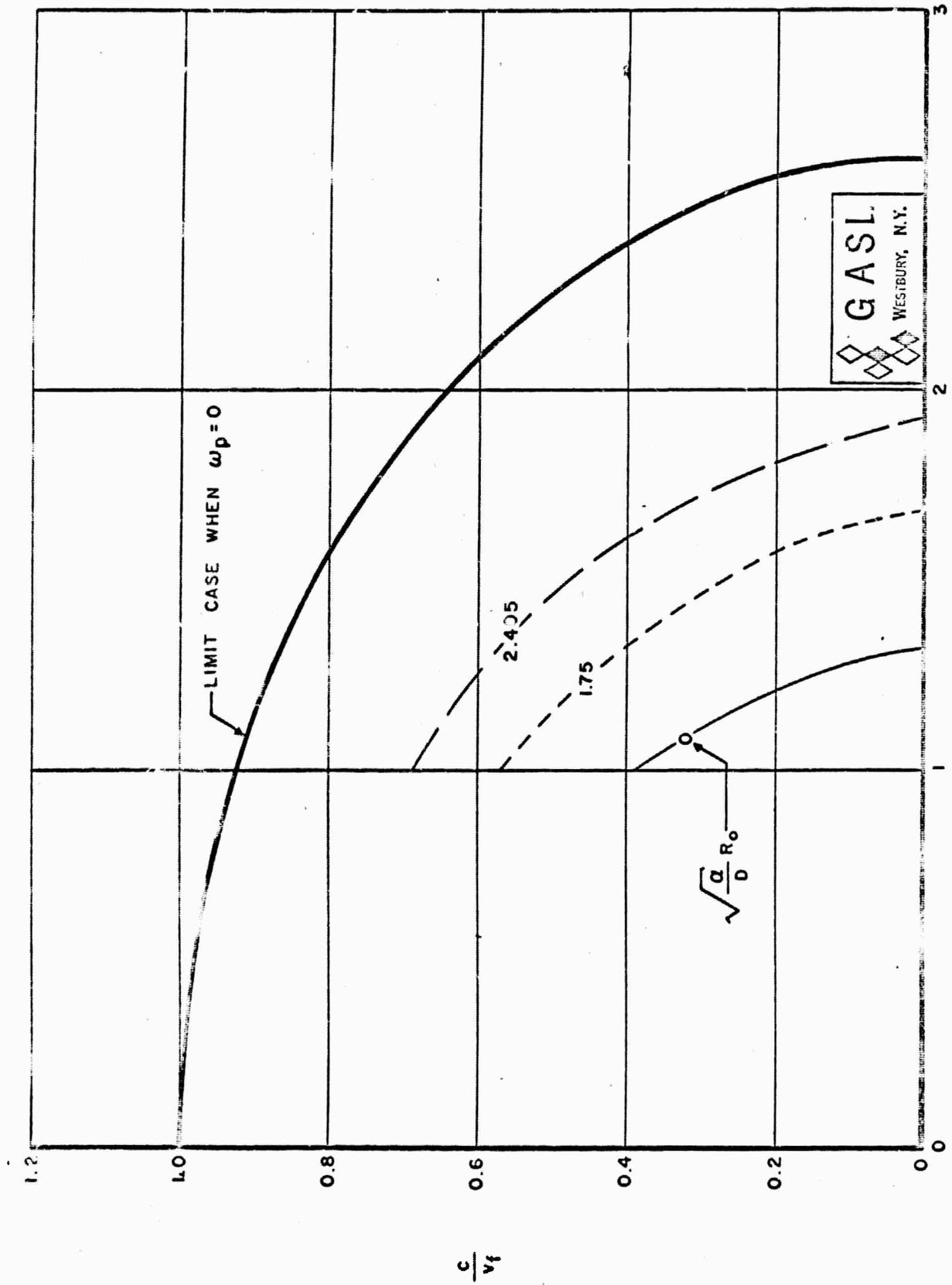

Fig. D-4.4

Wave Guide Index of Refraction as a Function of Signal Wave Length for $\frac{\omega_p}{\omega} = 0.866$

REFERENCES

1. Tomagno, J., Instruction Techniques for Heat Transfer Measurement in Hypersonic Shock Tunnel, GASL TM-102, Jan. 1964.

2. Gavril, B. D., Generalized One-Dimensional Chemically Reacting Flows with Molecular Vibrational Relaxation, GASL TR-426, April 1964.

3. Abele, M., Napolitano, L., Caldirola, P., Lane, F., Tomboulian, R., Wecker, M., and Moretti, G., Studies of the Electromagnetic Characteristics of Moving Ionized Gases, First Semiannual Technical Summary Report, GASL TR-255, November 1961.

4. Abele, M., Caldirola, P., Medecki, H., Gavril, B., Napolitano, L., Wecker, M., Tomboulian, R., Studies of the Electromagnetic Characteristics of Moving Ionized Gases, Second Semiannual Technical Summary Report, GASL TR-290, May 1962.

5. Gavril, B., Abele, M., Albertoni, S., Cercignani, C., Tomboulian, R. and Medecki, H., Studies of the Electromagnetic Properties of Nonuniform Plasmas, Third Semiannual Technical Summary Report, GASL TR-316, October 1962.

6. Abele, M., Medecki, H., Tomagno, J., and Tomboulian, R., Studies of Electromagnetic Properties of Nonuniform Plasmas, Fourth Semiannual Technical Summary Report, GASL TR-348, April 1963.

7. Abele, M., Medecki, H., and Tomboulian, R., Electromagnetic Studies in Shock Produced Plasmas, Third Annual Report, GASL TR-388, April 1964.

BLANK PAGE

APPENDIX I

SUMMARY OF CHEMICAL REACTIONS AND THEIR RATE CONSTANTS

This appendix summarizes a large number of chemical reactions which are significant at the high temperatures of reentry into the earth's atmosphere at hypersonic speeds.

The presentation here includes two classes of units, namely cm, sec, particle and meter, sec, kg mole (required for the present analysis). The tables are self-explanatory, though a word of caution is in order for the ionization reactions 10 through 15. The rate constants for these reactions are tabulated as the forward (i.e. to the right) values, which is contrary to the remainder of the appendix.

SUMMARY OF CHEMICAL REACTIONS AND RATE CONSTANTS

PURE AIR

No. j	REACTION	CATALYST X	n	REVERSE RATE CONSTANT AT EQUILIBRIUM $\left(k_j^X\right)_e$ $\frac{\text{kg moles}}{\text{m}^3\text{sec}}\left(\frac{\text{m}^3}{\text{kg mole}}\right)^n$	REVERSE RATE CONSTANT AT EQUILIBRIUM $\left(k_j^X\right)_e$ $\frac{\text{particles}}{\text{cm}^3\text{sec}}\left(\frac{\text{cm}^3}{\text{particle}}\right)^n$	Reference
1	$O_2 + X + 5.1\ ev = 2O + X$	O	3	$2.3 \times 10^{14}\ T^{-3/2}$	$6.2 \times 10^{-28}\ T^{-3/2}$	
		O_2		$8.0 \times 10^{13}\ T^{-3/2}$	$2.2 \times 10^{-28}\ T^{-3/2}$	
		N_2		$6.2 \times 10^{9}\ T^{-1/2}$	$1.7 \times 10^{-32}\ T^{-1/2}$	
		all other		$3.0 \times 10^{8}\ T^{-1/2}$	$8.3 \times 10^{-33}\ T^{-1/2}$	
2	$N_2 + X + 9.8\ ev = 2N + X$	N	3	$2.4 \times 10^{15}\ T^{-3/2}$	$6.5 \times 10^{-27}\ T^{-3/2}$	
		N_2		$2.8 \times 10^{10}\ T^{-1/2}$	$7.6 \times 10^{-32}\ T^{-1/2}$	
		all other		$1.1 \times 10^{10}\ T^{-1/2}$	$3.0 \times 10^{-32}\ T^{-1/2}$	

SUMMARY OF CHEMICAL REACTIONS AND RATE CONSTANTS

PURE AIR

No. j	REACTION	CATALYST X	n	REVERSE RATE CONSTANT AT EQUILIBRIUM $\left(k_{j-}^{x}\right)_e$		Reference
				$\frac{\text{kg moles}}{\text{m}^3\,\text{sec}}\left(\frac{\text{m}^3}{\text{kg mole}}\right)^n$	$\frac{\text{particles}}{\text{cm}^3\,\text{sec}}\left(\frac{\text{cm}^3}{\text{particle}}\right)^n$	
3	$NO + X + 6.5\ ev = N + O + X$	A	3	$1.7 \times 10^{14}\ T^{-3/2}$	$4.66 \times 10^{-38}\ T^{-3/2}$	
		NO		$2.0 \times 10^{15}\ T^{-3/2}$	$5.5 \times 10^{-37}\ T^{-3/2}$	
		all other		$1.0 \times 10^{14}\ T^{-3/2}$	$2.8 \times 10^{-38}\ T^{-3/2}$	
4	$O + N_2 + 3.3\ ev = NO + N$		2	1.6×10^{10}	2.7×10^{-11}	
5	$NO + O + 1.4\ ev = N + O_2$		2	$1.3 \times 10^{7}\ T \exp\left(-\frac{3560}{T}\right)$	$2.2 \times 10^{-14}\ T \exp\left(-\frac{3560}{T}\right)$	
6	$N_2 + O_2 + 1.9\ ev = 2NO$		2	$2.4 \times 10^{80}\ T^{-5/2} \exp\left(-\frac{43,000}{T}\right)$	$0.4 \times T^{-5/2} \exp\left(-\frac{43,000}{T}\right)$	

SUMMARY OF CHEMICAL REACTIONS AND RATE CONSTANTS

PURE AIR

No. j	REACTION	CATALYST X	n	REVERSE RATE CONSTANT AT EQUILIBRIUM $\left(k^{x}_{j-}\right)_e$		Reference
				$\frac{\text{kg moles}}{\text{m}^3\,\text{sec}}\left(\frac{\text{m}^3}{\text{kg mole}}\right)^n$	$\frac{\text{particles}}{\text{cm}^3\,\text{sec}}\left(\frac{\text{cm}^3}{\text{particle}}\right)^n$	
7	$N + O + 2.8\ ev = NO^+ + e^-$		2	$1.8 \times 10^{18}\ T^{-3/2}$	$3 \times 10^{-3}\ T^{-3/2}$	
8	$2N + 5.8\ ev + N_2^+ + e^-$		2	$3.01 \times 10^{16}\ T^{-3/4}$	$5 \times 10^{-6}\ T^{-3/4}$	
9	$2O + 6.9\ ev = O_2^+ + e^-$		2	$1.2 \times 10^{18}\ T^{-3/2}$	$2 \times 10^{-3}\ T^{-3/2}$	

SUMMARY OF CHEMICAL REACTIONS AND RATE CONSTANTS

PURE AIR

No.	REACTION	CATALYST X	n	FORWARD RATE CONSTANT AT EQUILIBRIUM $\left(k^{x}_{j+}\right)_e$ * $\frac{\text{kg moles}}{\text{m}^3\text{sec}}\left(\frac{\text{m}^3}{\text{kg mole}}\right)^n$	FORWARD RATE CONSTANT AT EQUILIBRIUM $\left(k^{x}_{j+}\right)_e$ ** $\frac{\text{particles}}{\text{cm}^3\text{sec}}\left(\frac{\text{cm}^3}{\text{particle}}\right)^n$	Reference
10	$X + NO + 9.3\ ev = X + NO^+ + e^-$	all species	2	$\left.\begin{matrix}2.7\times10^{-4}\\4.5\times10^{-25}\end{matrix}\right\} T^{5/2}(1+3\times10^{-3}T)\exp\left(-\frac{107,900}{T}\right)$		* = upper content of brace
11	$N_2 + O_2 + 11.2\ ev = NO + NO^+ + e^-$		2	$\left.\begin{matrix}2.7\times10^{-4}\\4.5\times10^{-25}\end{matrix}\right\} T^{5/2}(1+3\times10^{-3}T)\exp\left(-\frac{141,000}{T}\right)$		** = lower content of brace
12	$X + O_2 + 12.1\ ev = X + O_2^+ + e^-$	N_2	2	$\left.\begin{matrix}2.7\times10^{-4}\\4.5\times10^{-25}\end{matrix}\right\} T^{5/2}(1+3\times10^{-3}T)\exp\left(-\frac{141,000}{T}\right)$		
		O_2	2	$\left.\begin{matrix}6.6\times10^{-13}\\1.1\times10^{-33}\end{matrix}\right\} T^{9/2}(1+4\times10^{-3}T)\exp\left(-\frac{141,000}{T}\right)$		
		all other	2	use value for N_2		

SUMMARY OF CHEMICAL REACTIONS AND RATE CONSTANTS

PURE AIR

No.	REACTION	CATALYST χ	n	FORWARD RATE CONSTANT AT EQUILIBRIUM $\left(k^{x}_{j+}\right)_e$	Reference
				* $\frac{\text{kg moles}}{\text{m}^3\text{sec}}\left(\frac{\text{m}^3}{\text{kg mole}}\right)^n$; ** $\frac{\text{particles}}{\text{cm}^3\text{sec}}\left(\frac{\text{cm}^3}{\text{particle}}\right)^n$	
13	$X + O + 13.6\ ev = X + O^+ + e^-$	all species	2	$\left.\begin{matrix}2.7\times10^{-4}\\4.5\times10^{-25}\end{matrix}\right\} T^{5/2}(1+3\times10^{-5}T)\exp\left(-\frac{157{,}000}{T}\right)$	*=upper content of brace
14	$X + N + 14.6\ ev = X + N^+ + e^-$	all species	2	$\left.\begin{matrix}2.7\times10^{-4}\\4.5\times10^{-25}\end{matrix}\right\} T^{5/2}(1+3\times10^{-5}T)\exp\left(-\frac{169{,}400}{T}\right)$	**=lower content of brace
15	$X + N_2 + 15.6\ ev = X + N_2^+ + e^-$	N_2 and all other	2	$\left.\begin{matrix}1.7\times10^{-7}\\2.8\times10^{-25}\end{matrix}\right\} T^{7/2}(1+3\times10^{-5}T)\exp\left(-\frac{181{,}000}{T}\right)$	

SUMMARY OF CHEMICAL REACTIONS AND RATE CONSTANTS

PURE AIR

No. j	REACTION	CATALYST X	n	REVERSE RATE CONSTANT AT EQUILIBRIUM $\left(k^{x}_{j-}\right)_e$		Reference
				$\frac{\text{kg moles}}{\text{m}^3\ \text{sec}}\left(\frac{\text{m}^3}{\text{kg mole}}\right)^n$	$\frac{\text{particles}}{\text{cm}^3\ \text{sec}}\left(\frac{\text{cm}^3}{\text{particle}}\right)^n$	
16	$N + O_2^+ + 0.2\ ev = O^+ + NO$		2	$7.8 \times 10^8\ T^{\frac{1}{2}}$	$1.3 \times 10^{-12}\ T^{\frac{1}{2}}$	
17	$NO + NO^+ + 0.9\ ev = N_2 + O_2^+$			for all reactions on this page		
18	$N + O^+ + 0.9\ ev = N^+ + O$					
19	$N_2 + N^+ + 1.0\ ev = N_2^+ + N$					
20	$NO^+ + N + 1.1\ ev = N_2 + O^+$					
21	$O + O_2^+ + 1.6\ ev = O^+ + O_2$					
22	$N_2 + O^+ + 2.0\ ev = N_2^+ + O$					
23	$O + N_2^+ + 2.2\ ev = N^+ + NO$					
24	$NO + O^+ + 2.3\ ev = O_2 + N^+$					
25	$N + O_2^+ + 2.5\ ev = N^+ + O_2$					

SUMMARY OF CHEMICAL REACTIONS AND RATE CONSTANTS

PURE AIR

No. j	REACTION	CATALY X	n	REVERSE RATE CONSTANT AT EQUILIBRIUM $\left(k^x_{j-}\right)_e$		Reference
				$\frac{\text{kg moles}}{\text{m}^3\ \text{sec}}\left(\frac{\text{m}^3}{\text{kg mole}}\right)^n$	$\frac{\text{particles}}{\text{cm}^3\ \text{sec}}\left(\frac{\text{cm}^3}{\text{particle}}\right)^n$	
26	$O_2 + NO^+ + 2.8\ ev = O_2^+ + NO$		2	$7.8 \times 10^8\ T^{\frac{1}{2}}$	$1.3 \times 10^{-12}\ T^{\frac{1}{2}}$	
27	$NO^+ + N + 3.1\ ev = N_2^+ + O$			for all reactions on this page		
28	$N_2 + O_2^+ + 3.5\ ev = N_2^+ + O_2$					
29	$NO^+ + C + 4.2\ ev = O_2^+ + N$					
30	$N_2 + O^+ + 4.2\ ev = NO + N^+$					
31	$O + NO^+ + 4.4\ ev = O^+ + NO$					
32	$NO + NO^+ + 4.5\ ev = N_2^+ + O_2$					
33	$N + NO^+ + 5.3\ ev = N^+ + NO$					
34	$N_2 + NO^+ + 6.3\ ev = N_2^+ + NO$					
35	$NO^+ + O + 6.7\ ev = O_2 + N^+$					

SUMMARY OF CHEMICAL REACTIONS AND RATE CONSTANTS

PURE AIR

No. j	REACTION	CATALYST X	n	REVERSE RATE CONSTANT AT EQUILIBRIUM $\left(k^{x}_{j-}\right)_{e}$		Reference
				$\frac{\text{kg moles}}{\text{m}^3\ \text{sec}}\left(\frac{\text{m}^3}{\text{kg mole}}\right)^n$	$\frac{\text{particles}}{\text{cm}^3\ \text{sec}}\left(\frac{\text{cm}^3}{\text{particle}}\right)^n$	
36	$X + O^- + 1.465\ ev = X+O+e^-$	all species	3	$1.1 \times 10^{13}\ T^{-1}$	$3.03 \times 10^{-29}\ T^{-1}$	
37	$X + O_2^- + 0.46\ ev = X+O_2+e^-$	O_2	3	10^{12}	2.8×10^{-30}	
38	$NO + O + 7.835\ ev = O^- + NO^+$		2	$1.0 \times 10^{15}\ T^{-\frac{1}{2}}$	$1.7 \times 10^{-6}\ T^{-\frac{1}{2}}$	
39	$NO + O_2 + 8.84\ ev = O_2^- + NO^+$		2	$1.0 \times 10^{15}\ T^{-\frac{1}{2}}$	$1.7 \times 10^{-6}\ T^{-\frac{1}{2}}$	

SUMMARY OF CHEMICAL REACTIONS AND RATE CONSTANTS

AIR PLUS NaCℓ

No. j	REACTION	CATALYST X	n	FORWARD RATE CONSTANT AT EQUILIBRIUM $\left(k^{x}_{j+}\right)_{e}$		Reference
				$\frac{\text{kg moles}}{\text{m}^3\ \text{sec}}\left(\frac{\text{m}^3}{\text{kg mole}}\right)^n$	$\frac{\text{particles}}{\text{cm}^3\ \text{sec}}\left(\frac{\text{cm}^3}{\text{particle}}\right)^n$	
40	$Na + X + 5.14\ ev \rightleftarrows Na^+ + e^- + X$	e^-	2	$3.92 \times 10^{11} T^{\frac{1}{2}} \exp\left(-\frac{59700}{T}\right)$	$6.5 \times 10^{-9} T^{\frac{1}{2}} \exp\left(-\frac{59700}{T}\right)$	
		all other	2	$3.92 \times 10^{3} T^{3/2} \exp\left(-\frac{59700}{T}\right)$	$6.5 \times 10^{-18} T^{3/2} \exp\left(-\frac{59700}{T}\right)$	
41	$Na + O + 3.68\ ev \rightleftarrows Na^+ + O^-$		2	$1.99 \times 10^{12} \exp\left(-\frac{43000}{T}\right)$	$3.3 \times 10^{-9} \exp\left(-\frac{43000}{T}\right)$	
42	$Na + O_2 + 4.70\ ev \rightleftarrows Na^+ + O_2^-$		2	$1.81 \times 10^{12} \exp\left(-\frac{54500}{T}\right)$	$3 \times 10^{-9} \exp\left(-\frac{54500}{T}\right)$	
43	$Na + NO^+ - 4.11\ ev \rightleftarrows Na^+ + NO$		2	$3.01 \times 10^{10} T^{-\frac{1}{2}}$	$5 \times 10^{-11} T^{-\frac{1}{2}}$	

SUMMARY OF CHEMICAL REACTIONS AND RATE CONSTANTS

AIR PLUS NaCℓ

No. j	REACTION	CATALYST X	n	REVERSE RATE CONSTANT AT EQUILIBRIUM $\left(k^{x}_{j-}\right)_e$		Reference
				$\frac{\text{kg moles}}{\text{m}^3\ \text{sec}}\left(\frac{\text{m}^3}{\text{kg mole}}\right)^n$	$\frac{\text{particles}}{\text{cm}^3\ \text{sec}}\left(\frac{\text{cm}^3}{\text{particle}}\right)^n$	
44	$NaO + X + 3.6$ ev $\rightleftarrows Na + O + X$	all	3	3.63×10^9	10^{-32}	
45	$Na + O_2 + 1.5$ ev $\rightleftarrows NaO + O$		2	$6.025 \times 10^9 \exp\left(-\frac{2000}{T}\right)$	$10^{-11} \exp\left(-\frac{2000}{T}\right)$	
46	$Na + NO + 2.9$ ev $\rightleftarrows NaO + N$		2	$6.025 \times 10^9 \exp\left(-\frac{2000}{T}\right)$	$10^{-11} \exp\left(-\frac{2000}{T}\right)$	

SUMMARY OF CHEMICAL REACTIONS AND RATE CONSTANTS

AIR PLUS NaCℓ

No. j	REACTION	CATALYST X	n	REVERSE RATE CONSTANT AT EQUILIBRIUM $\left(k^{x}_{j-}\right)_{e}$		Reference
				$\frac{\text{kg moles}}{\text{m}^3\ \text{sec}}\left(\frac{\text{m}^3}{\text{kg mole}}\right)^n$	$\frac{\text{particles}}{\text{cm}^3\ \text{sec}}\left(\frac{\text{cm}^3}{\text{particle}}\right)^n$	
47	$NaC\ell + X + 3.6\ ev \rightleftharpoons Na + C\ell + X$	all	3	3.63×10^{10}	10^{-31}	
48	$Na + C\ell + 1.3\ ev \rightleftharpoons Na^+ + C\ell^-$		2	$6.025 \times 10^{13} T^{-\frac{1}{2}}$	$10^{-7}\ T^{-\frac{1}{2}}$	
49	$NaC\ell + X + 4.9\ ev \rightleftharpoons Na^+ + C\ell^- + X$	all	3	3.63×10^{12}	10^{-29}	
50	$C\ell^- + X + 3.613\ ev \rightleftharpoons C\ell + e^- + X$	all		$3.63 \times 10^{14} T^{-\frac{1}{2}}$	$10^{-27}\ T^{-\frac{1}{2}}$	
51	$Na + O + O + 0.02\ ev \rightleftharpoons Na^+ + e^- + O_2$		3	3.63×10^{11}	10^{-30}	

APPENDIX II

ONE-DIMENSIONAL STEADY STATE DIFFUSION ACROSS A DISCONTINUITY IN THE THERMODYNAMIC PROPERTIES IN AN IONIZED GAS*

For the special case of a one-dimensional steady-state problem with the x-coordinate (with respect to which the non-uniformity occurs) normal to a planar discontinuity in thermodynamic properties, the reduced electron and ion momentum equations simplify to the forms:

$$n_e u_e = n_e \mu_e \frac{d\Phi}{dx} - D_e \frac{dn_e}{dx} \qquad \text{(II-1)}$$

$$n_i u_i = -n_i \mu_i \frac{d\Phi}{dx} - D_i \frac{dn_i}{dx} \qquad \text{(II-2)}$$

where

$\mu_e = \frac{q}{m_e \nu_e}$ = electron mobility

$\mu_i = \frac{2q}{m_i \nu_i}$ = ion mobility

$D_e = \frac{kT}{m_e \nu_e}$ = electron diffusion coefficient

$D_i = \frac{2kT}{m_i \nu_i}$ = ion diffusion coefficient

---

*This Appendix was prepared by Dr. Frank Lane

Next, Eqs. (II-1) and (II-2) are divided by μ_e and μ_i respectively, differentiated with respect to x, and added. This gives

$$\frac{1}{\mu_e}\frac{d}{dx}(n_e u_e) + \frac{1}{\mu_i}\frac{d}{dx}(n_i u_i) = \frac{d}{dx}\left(n_e \frac{d\Phi}{dx}\right) - \frac{d}{dx}\left(n_i \frac{d\Phi}{dx}\right) - \frac{D_e}{\mu_e}\frac{d^2 n_i}{dx^2} - \frac{D_i}{\mu_i}\frac{d^2 n_i}{dx^2} \qquad \text{(II-3)}$$

Next, the assumption that n_i is nearly equal to n_e is invoked (i.e. their difference is a quantity small of first order). Furthermore the relation between $\Delta\Phi$ and $(n_i - u_e)$ shows that the electric field $\left(\frac{\partial\Phi}{\partial x}\right)$ should also be small of first order. Then the potential $\left(\frac{d\Phi}{dx}\right)$ terms, whose difference occurs in (II-3), may be dropped. Using the equivalence of the electron and ion production rates and setting $\frac{d^2 n_e}{dx^2} \sim \frac{d^2 n_i}{dx^2}$, there results the following relation:

$$\dot{n}_e\left(\frac{1}{\mu_e} + \frac{1}{\mu_i}\right) = -\frac{d^2 n_e}{dx^2}\left(\frac{D_e}{\mu_e} + \frac{D_i}{\mu_i}\right) \qquad \text{(II-4)}$$

or

$$\dot{n}_e = -\frac{d^2 n_e}{dx^2}\frac{D_e\mu_i + D_i\mu_e}{\mu_e + \mu_i} = -D\frac{d^2 n_e}{dx^2} \qquad \text{(II-5)}$$

where

$$D = \frac{D_e\mu_i + D_i\mu_e}{\mu_e + \mu_i} = \text{ambipolar diffusion coefficient.}$$

If we now approximate the electron or ion production rate $\dot{n}_e$ by the expression

$$\dot{n}_e = \alpha \left(1 - \frac{n_e^2}{n_{e_o}^2} \right) \tag{II-6}$$

where n_{e_o} is equilibrium electron number density and α is the electron creation rate per unit volume, then Eq. (II-5) takes the form

$$D \frac{d^2 n_e}{dx^2} + \alpha \left(1 - \frac{n_e^2}{n_{e_o}^2} \right) = 0 \tag{II-7}$$

This is the equation which must be solved subject to boundary conditions appropriate to the physical situation of interest.

In order to get an idea of the distances over which electron density is "smeared out" in making the transition between two asymptotic values (such as might be expected across a shock) the following idealized one-dimensional situation is proposed.

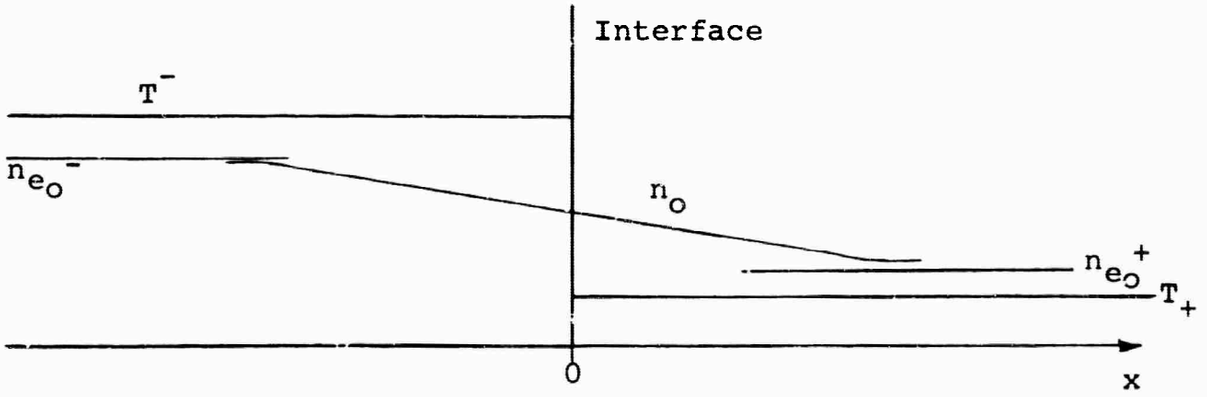

A plane interface is conceived across which temperature jumps discontinuously. The temperature is assumed constant in each half space. The electron density assumes its equilibrium value $n_{e_o}^{+}$ as $x \to +\infty$, and a different higher equilibrium value $n_{e_o}^{-}$ as $x \to -\infty$. The system is to be analyzed for electron density distribution using Eq. (II-7) in each half space amd matching up properly the two solutions at the interface ($x = 0$). The matching conditions are continuity of electron density

$$n_e(0^+) = n_e(0^-) \tag{II-8}$$

and continuity of electron current

$$n_e u_e \Big|_{0^+} = n_e u_e \Big|_{0^-} \tag{II-9}$$

Now, from the equivalence of electron and ion production rates, we find that

$$\frac{d}{dx}(n_i u_i - n_e u_e) = 0 \tag{II-10}$$

This is equivalent to saying that Div(current) = 0 and since current vanishes at $x \to \pm\infty$ therefore current $\equiv 0$.

$$\text{or} \qquad n_e u_e = n_i u_i \tag{II-11}$$

Therefore, utilizing (II-1) and (II-2) we find that

$$n_e u_e = + n_e \mu_e \frac{d\Phi}{dx} - D_e \frac{dn_e}{dx} \qquad \text{(II-12)}$$

$$n_i u_i = - n_i \mu_i \frac{d\Phi}{dx} - D_i \frac{dn_i}{dx} \qquad \text{(II-13)}$$

Dividing (II-12) by μ_e and (II-13) by μ_i, utilizing the equivalence (II-11) and adding, we find

$$n_e u_e \left(\frac{1}{\mu_e} + \frac{1}{\mu_i} \right) = (n_e - n_i) \frac{d\Phi}{dx} - \left(\frac{D_e}{\mu_e} + \frac{D_i}{\mu_i} \right) \frac{dn_e}{dx} \qquad \text{(II-14)}$$

where again $n_e \sim n_i$ has been invoked in the last term. Since $(n_e - n_i) \frac{d\Phi}{dx}$ is small of second order, (II-14) leads to the result:

$$n_e u_e \sim - D \frac{dn_e}{dx} \qquad \text{(II-15)}$$

Therefore the second interface condition (II-9) reduces to

$$D \frac{dn_e}{dx} \Bigg|_{0^+} = D \frac{dn_e}{dx} \Bigg|_{0^-} \qquad \text{(II-16)}$$

Now the general solution to the Eq. (II-7) may be written in the form

$$\left| \frac{\sqrt{\frac{n_e}{n_{e_o}} + 2} - \sqrt{3}}{\sqrt{\frac{n_e}{n_{e_o}} + 2} + \sqrt{3}} \right| = K\, e^{\pm x\sqrt{\frac{2\alpha}{n_{e_o} D}}} \qquad \text{(II-17)}$$

where K is an undetermined constant.

The coefficients α and D and the equilibrium electron density n_o (as well as the temperature) differ in each half plane. Hence (II-17) must be applied individually to each half plane. In the right-hand half plane the (-) sign applies in the exponent whereas in the left-hand half plane the (+) sign applies. Also the constant K differs in the two half planes. Moreover, in the process of finding this solution the following expression for $\frac{dn}{dx}$ is found:

$$\frac{dn_e}{dx} = \pm\sqrt{\frac{2\alpha\, n_{e_o}}{3D}}\sqrt{\frac{n_e}{n_{e_o}} + 2}\left(\frac{n_e}{n_{e_o}} - 1\right) \qquad \text{(II-18)}$$

where the (-) sign applies in the right-hand half plane and the (+) sign applies in the left-hand half plane. This now constitutes sufficient information to solve for the values of K appropriate to the right-hand and left-hand half planes. The actual numerical work requires solution of a cubic, and this was performed graphically.

Following is a table of results, Table I. In the numerical work $n_{e_o}^{+}$ was assumed to be 10^6 and $n_{e_o}^{-}$ was given the values 10^7, 10^8, $\cdots$ 10^{12}. The values in the table were computed using a constant density $\rho = \rho$ atmospheric x 10^{-4} and temperatures corresponding to this density and the equilibrium electron number densities tabulated. This, of course, departs from jump conditions across a shock but, nevertheless the results should be indicative of the way in which electron densities vary between asymptotic values.

The representative lengths $\sqrt{\frac{n_{e_o} D}{2\alpha}}$ were computed by computing α and the ambipolar diffusion coefficient D corresponding to the appropriate density and temperature.

$$D \cong \frac{4\,k\,T}{m_i \nu_i} \qquad \text{since } m_i >> m_e \tag{II-19}$$

and

$$\nu_i \cong \frac{2\sqrt{2}}{\sqrt{\pi}}\, S_d\, n_n \left(\frac{m_i + m_n}{m_i\, m_n}\, kT \right)^{\frac{1}{2}} \tag{II-20}$$

where

S_d = collision cross section for ions and neutral particles

n_n = neutral particle number density

TABLE I

$n_{e_o}^{+}$ 1/cc	$n_{e_o}^{-}$ 1/cc	$\left\|\frac{C_m}{\sqrt{\frac{n_{e_o}D}{2\alpha}}}\right\|_+$	$\left\|\frac{C_m}{\sqrt{\frac{n_{e_o}D}{2\alpha}}}\right\|_-$	K_+	K_-	T_+ (°K)	T_- (°K)	n_{n+}	n_{n-}
10^6	10^7	330	312	.2272	.0395	2175	2380	2.48×10^{15}	2.57×10^{15}
10^6	10^8	330	260	.5407	.0638	2175	2625	2.48×10^{15}	2.68×10^{15}
10^6	10^9	330	100	.8041	.0712	2175	2990	2.48×10^{15}	2.83×10^{15}
10^6	10^{10}	330	32.5	.9315	.0724	2175	3480	2.48×10^{15}	3.00×10^{15}
10^6	10^{11}	330	12	.9774	.0738	2175	4180	2.48×10^{15}	3.28×10^{15}
10^6	10^{12}	330	6	.9918	.0793	2175	5270	2.48×10^{15}	3.83×10^{15}

$$\frac{\rho}{\rho_{atmos}} = 10^{-4}$$

n_n = neutral particle number density

m_n = neutral particle mass

and the radicand simplifies since

$$m_i \approx m_n$$

Expression (II-20) is derived from consideration of the momentum transfer in a collision between an ion and a neutral particle. The collision cross section S_d is given approximately by

$$S_d = \pi \left(\frac{r_i + r_n}{2}\right)^2 \qquad \text{(II-21)}$$

where a smooth sphere model is assumed and r_i, r_n are the ion and neutral particle radii which are assumed to be equal and of the order of 10^{-8} cm. The electron creation rate per unit volume α is computed as follows:

The dominant reaction is assumed to be

$$N + O \rightleftharpoons NO^+ + e \tag{II-22}$$

The rate of electron production is given by

$$\frac{dn_e}{dt} = k_d\, n_n\, n_O - k_r\, n_i\, n_e \tag{II-23}$$

but

$$n_i = n_e$$

so that

$$\left.\begin{aligned} \dot{n}_e &= k_d\, n_n\, n_O - k_r\, n_e^2 \\ &= k_d\, n_n\, n_O \left(1 - \frac{k_r}{k_d\, n_n\, n_O}\, n_e^2\right) \end{aligned}\right\} \tag{II-24}$$

$$= k_d\, n_n\, n_O \left(1 - \frac{n_e^2}{n_{e_O}^2}\right) \tag{II-25}$$

where

$$n_{e_O}^2 = \frac{k_d\, n_n\, n_O}{k_r} = \left(\begin{array}{c}\text{equilibrium electron} \\ \text{number density}\end{array}\right)^2$$

and where we now see that

$$\alpha = k_d \, n_n \, n_O \qquad \text{(II-26)}$$

Now $n_n \; n_O$ are computed from tables (for air) at the appropriate temperature and density, and k_d is computed using methods of classical chemical kinetics.

Figure E-2.1 gives the actual computed electron density distribution corresponding to each of the six asymptotic conditions listed in Table I. The transition becomes sharper as the hot-side electron density becomes higher.

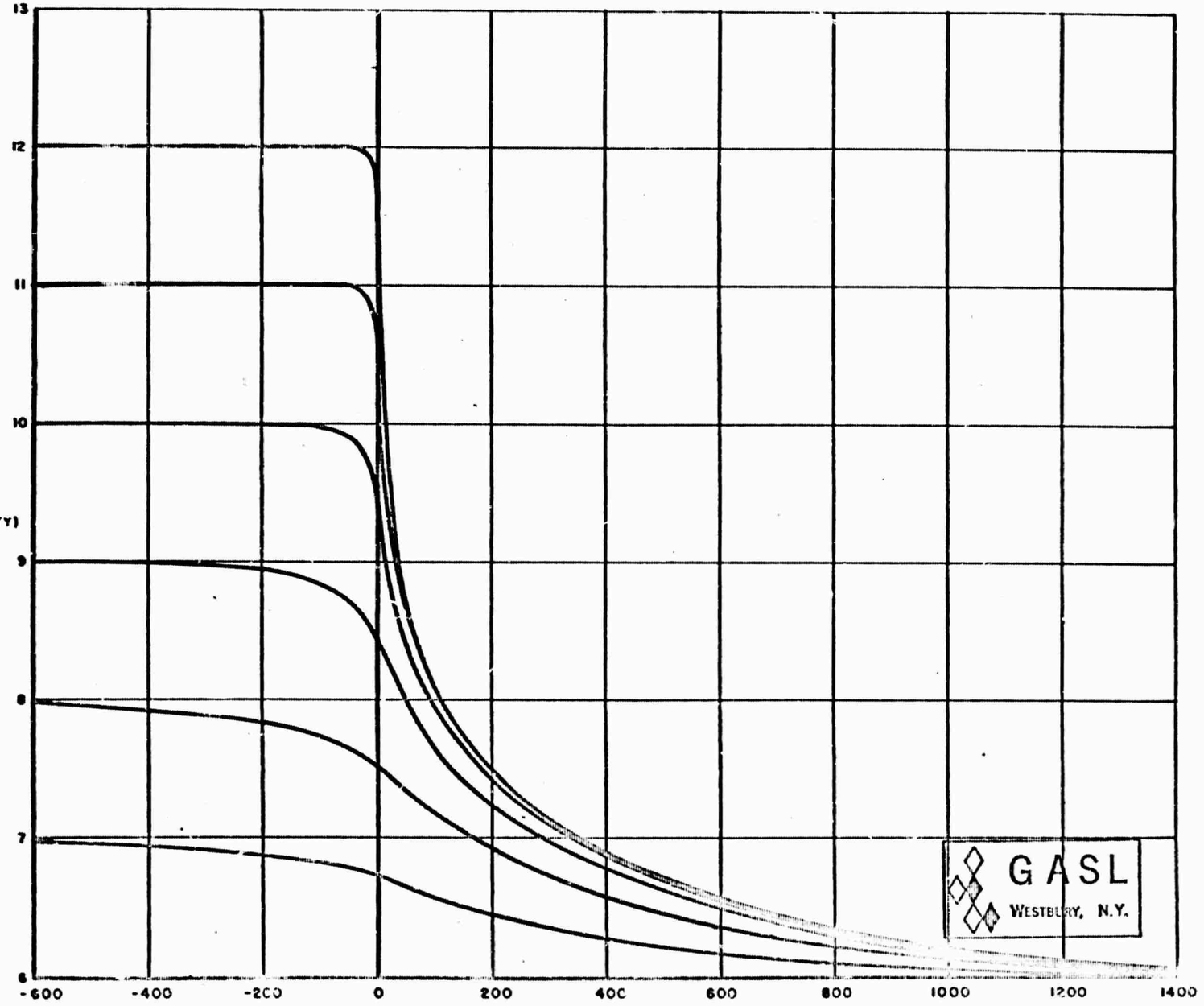

ELECTRON DENSITY DISTRIBUTION CORRESPONDING TO ONE-DIMENSIONAL DIFFUSION ACROSS DISCONTINUITY IN THERMODYNAMIC PROPERTIES IN AN IONIZED GAS

Figure E-2.1

APPENDIX III

PERIODICALLY DISTURBED PLASMA

INTRODUCTION

The simple criterion used to determine radar cross section of an ionized wake is to assume that for electron density regions where $\frac{\omega_p^2}{\omega^2} < 1$, no reflection occurs, and if $\frac{\omega_p^2}{\omega^2} > 1$ total reflection occurs. This simple criteria is useful if the collision frequency is low and the density gradients are large through the above critical conditions.

The problem of interest here is the electromagnetic characteristics of a plasma region where $\frac{\omega_p^2}{\omega^2} << 1$, but where stationary or time varying regions of higher density ($\frac{\omega_p^2}{\omega^2}$ still less than 1) occur with spacing comparable to the half wavelength or multiple of the incident radiation. This situation is comparable with a multilayered dielectric filter, except that in general the locations of the maximum electron density regions are randomly changing.

It must be noted that while it is possible to obtain a strong reflection from such a periodic dielectric structure, it is equally probable that total absorption will occur, by the same process. However, if the structure is randomly varying, the process of interest is that of reflection, which ultimately is

detected. The totally absorbed energy is equivalent to a transparent region as far as the reflected characteristics are concerned.

EXPERIMENTAL OBSTACLE

In order to properly formulate the analytical model required to generalize the problem, some basic experimental information must be supplied. Of course such information must be sufficiently quantitative that a true model can be formulated. Therein lies the experimental problem, for since the basic plasma required is strongly underdense, $\left(\frac{\omega_p}{\omega}\right)^2 << 1$, measurement of the plasma properties becomes extremely difficult.

One approach to this measurement problem is to induce the required perturbation in such a manner that the plasma properties can be accurately deduced from other parameters.

One such experimental arrangement considered was to propagate a strong sound wave into the shocked gas. With such an arrangement the amplitude and spacing of the periodic structure could easily be changed within limits. Since the maximum expected variations in pressure would be small compared to the base pressure, the electron density variation might be assumed to be directly proportional to the pressure variation. That is

$$\frac{\Delta_p}{p} = \frac{\Delta_{ne}}{n_e}$$

While all parts of this scheme are correct in concept, severe problems arise in coupling the required sound energy to the shock tube. Although several different coupling systems have been tried, the attempt to use sound waves to induce plasma variations was abandoned because of the extensive facility that would be required.

To obtain an order of magnitude estimate of the effect of a turbulent wake on the reflected radiation, an experiment was performed in the shock tube. A cylindrical bar was mounted across the tube parallel to the direction of polarization of the radiation. Several diameters were tried up to ½", which was the maximum diameter consistent with an unchoked flow. Underdense plasma conditions were run and observations were made of the reflected signal with the use of the electric field detector, in the polarized and antipolarized directions.

Even though the scale of the turbulence expected was an order of magnitude smaller than the wavelength, if very strong effects were to be associated with this type of wake, a noise signal would be imposed on the reflected power signal. Since no such signals were observed, it may be concluded that small scale effects are unimportant in this process.

RESULTS

An attempt was made to see if strong effects could be obtained under conditions where the scale of the disturbance was comparable to the wavelength, even if no precise description of this disturbance could be given.

The basic scheme used was the addition of a "Tee" section to the shock tube, where the area of the arm of the "Tee" is about half the area of the tube. As the flow passes the "Tee" section, under certain conditions, a "whistle" type effect can occur. If this is the case, periodic pressure fluctuations should be induced in the flow. Such pressure variations should, in turn, create regions of higher electron density.

In Fig. E-3.1 a trace is presented showing the pressure fluctuations occurring in the arm of the "Tee" near the main flow. Although such variations could only be obtained for a very restricted set of operating conditions, Fig. E-3.1 clearly shows that some type of periodic pressure producing mechanism is occurring.

To check the validity of the result, a simple step model for the plasma behind the shock can be used to compute the reflected signal. Assuming the pressure defect is carried with the flow, the simple model for the plasma postulates a

reflection from the front of the shock and a second reflection from the pressure disturbed region which exists behind the shock a distance (z) where $z = v_o t$ with v_o the particle velocity with respect to the shock and time t starting from the creation of the disturbance.

For the moment, if it is assumed that the waveguide wavelength is not appreciably altered in the first plasma region directly behind the shock, then it is clear that when the distance $z \frac{\lambda_g}{4}$, the reflected signal from the disturbed region will be 180° out of phase from the reflection occurring at the front of the shock, thus producing a minimum in the standing wave ratio. On the other hand, for $z = \lambda_g/2$ the two reflected signals are in phase and a maximum should occur in the SWR.

In Fig. E-3.2 a trace of the electric field is shown for the critical whistle conditions described. While this result must be considered tentative, it is clear that before the shock enters the "Tee" section, the SWR is small indicating an "underdense" plasma. After the transition of the "Tee" where the effects cannot be clearly described at the present time, the amplitude modulation of the SWR is seen to decrease and then subsequently to increase. The end transition occurs as first the plasma passes the detector and then reaches the antenna, where the

signal drops to zero. Since this type of modulating behavior is consistent with the simple model and inconsistent with other possible mechanisms, it is felt that this trace represents the type of strong reflections that can be obtained.

Top Trace: Heat transfer gauge located at entrance to "Tee" section.

Lower Trace: Pressure in arm of "Tee".

Sweep Time: 100 μs/cm.

Figure E-3.1

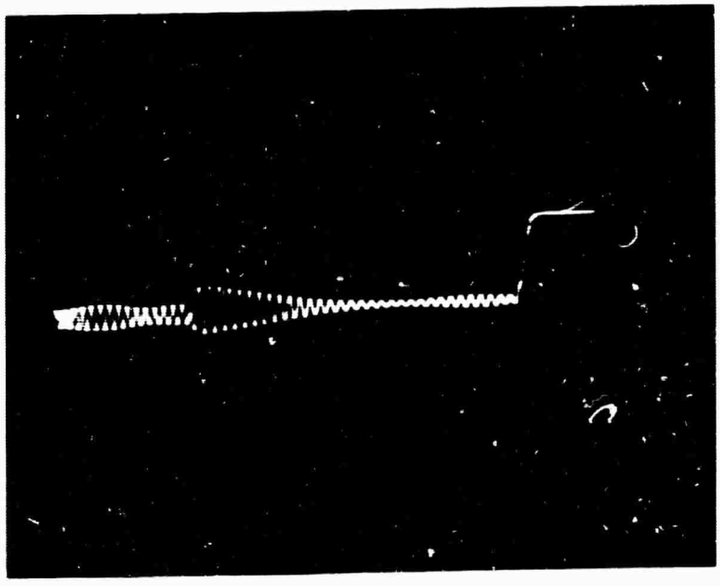

Electric Field Detector. Located 3 meters downstream of "Tee" section.

Sweep Time: 200 μs/cm.

Note: The cancellation and subsequent growth of the signal as the "filter" structure goes through the $\frac{\lambda_g}{4}$ condition.

Figure E-3.2